

博士論文

Study on Functional Design of Printable Electronic Circuits and Mechanical Devices

(印刷可能な電子回路および機械部品の機能設計に関する研究)

タ デウック トウン
Ta Duc Tung

指導教員: 川原 圭博 准教授

STUDY ON FUNCTIONAL DESIGN OF PRINTABLE ELECTRONIC CIRCUITS AND MECHANICAL DEVICES

TUNG D. TA

ABSTRACT

Digital fabrication has enabled the democratization of manufacturing on a large scale. The fact that powerful fabrication tools such as 3D printers, laser cutters, and inkjet printers are placed into the hands of end-users makes it possible for anyone to design, customize and fabricate almost anything. The digital fabrication which can be considered as a process of personalized fabrication has opened a whole new range of possibilities. Especially, users such as small companies, hobbyists, and researchers have been taking advantage of these tools to accelerate the design to production iteration.

However, the current digital fabrication tools are only focusing on the morphing of the object. How to fabricate a fully functional object is still questionable to researchers in many different fields. The integration of actuation and sensor components into those printed objects has not been fully explored yet. Without these input and output channels, the product of the digital fabrication process will be limited to being a static model. Adding active components to the fabricated object will enhance its functionality as well as its interaction with end-users. Adding these components in a single process with the morphing process will further revolutionize the impact of digital fabrication on making stuff, and magnify its adoption among a broader range of user base.

This dissertation will focus on reporting our exploration in the use of a variety of functional inks, including sintering-free silver nano-particle ink and ultra-violet (UV) cured resin, to embed rich featured functionality into printed objects. We will go from the 2D printing of electronic circuits with silver nano-particle ink, then 3D printing with the integration of electronic circuits in a single pass, through fabrication of printable sensors and actuators for soft-bodied robotics, to the printing of a

frictional anisotropic surface for fabricating soft-bodied robots.

In the 2D printing of electronic circuits using silver nano-particle ink, we propose and develop a Traveling Salesman Problem based autorouter to evenly distribute electric current to multiple light-emitting diodes (LEDs) wired by conductive ink printed traces. The problem of lighting up a bunch of LEDs is more troubling than it sounds. The intrinsic resistance of silver nano-particle ink makes it much more difficult to balance the brightness of all LEDs, even with an electronic circuits design expert. Our autorouter helps to automatically generate the conductive patterns to wire multiple LEDs, average their brightness without any additional resistors.

Moving from 2D to 3D printing, we challenge the problem of fabricating and integrating electronic circuits into 3D printed objects. We first realize the fabrication of double-sided electronic circuits with silver nano-particle ink on double-sided photo papers. The interconnections between two layers are attained by making via-holes with felting needles. The next step in the 3D printing field is to integrate electronic circuits into 3D printed objects in a single process. We combined the laminated object manufacturing (LOM) technique with our silver nano-particle ink inkjet printed electronic circuits to achieve this goal. Before printing, the 3D model will be sliced into multiple layers in a designing software. Embedded electronic circuits are decomposed and printed on paper with silver nano-particle ink. By stacking these papers one-by-one, we fulfill the goal of integrating electronic circuits into 3D printed objects.

Stepping on top of these building blocks, we explored the printability of sensors and actuators for rapid prototyping soft-bodied robots with an all-printed paper caterpillar robot (Paper Caterpillar) as an example. Our Paper Caterpillar consists of a plastic film with silver nano-particle ink printed heater on top of it. As the plastic film is a multiple layers structure, when heated up by the printed heater, the difference in the coefficient of thermal expansion of each layer makes the whole structure bend. By controlling the on-off of this heater, we are able to make it crawl forward. The bending of the plastic film will induce a change in the resistance of the printed heater, and we can use this change as a feedback of the bending angle. Thus, our robot is able to detect the alternation of its surrounding environment and switch its locomotion gaits to best fit the change of the environment.

In addition to printing electronic circuits, we also studied the fabrication of soft-bodied robots with different mechanical properties materials. Being inspired by the scales on the skin of a snake, we proposed a designing scheme to achieve an all-printed wriggle soft-bodied robot by computationally patterning high and low friction material to the ventral side of the robot. This patterning creates a frictional anisotropy underneath the robot. When generating a traveling wave along the body of the robot, we are able to make it undulate forward.

Going from 2D, through 3D, and approaching robotic printing, we are aiming at lifting the difficulty of digital fabrication and amplifying the functionality of the fabricated objects. We take this chance to vision a future where a user can easily print a fully functional object in just a single process. It is the future where anyone can make almost anything, and that thing is not only standing statically but actively interacting with the surrounding environment and humans.

ACKNOWLEDGMENTS

I am deeply grateful for the guidance and advice from Prof. Yoshihiro Kawahara. I have been learning so much from him about how to work, how to find balance, and how to have grit in research. I will be forever thankful for all the chances, all the challenges he is giving me. They are shaping me to be a better person. I would like to thank Prof. Tohru Asami for his warm welcome and thoughtful guidance. Without him, I will never have a chance to be in one of the best universities in the world as The University of Tokyo. Asami-sensei and Kawahara-sensei were not only my academic advisers but also my life coaches. Their passion, their wisdom, and their teaching are so profound that I feel so lucky to be their student.

I would like to show my warm gratitude to Takuya Umedachi-sensei for his mentoring. I have been always wanted to be a part of the robotics field. He was the one who gave me chances and showed me how to get into the robotics community. His passion in the robot field is enormous that I am so glad to be his mentee.

I am thankful to be a mentee of Masaaki Fukumoto-san in MSRA. I am blessed being under his mentoring during my internship to Microsoft Research Asia. His creativity, his perseverance, his enthusiasm are incomparable.

I am much obliged to Prof. Phan Duy Hung and Prof. Huynh Anh Dung, my former mentors at FPT University. They guided me through college life with so much support, guidance, and so many eye-opening lessons.

A thank will never be enough for the member of Asami and Kawahara Group. Thanks to Fujita-san for always supporting me in the lab. Her spirit is the thing that I always admire. Thanks to Tsushio-san, Kanai-san, Mizuno-san for the enormous effort. Their thoughtful supports are greatly valuable to me and every member in our lab.

I am indebted to all the students in AKG. Your warmness helps me overcome so many barriers being a foreigner. I especially thank Yuta Morisawa, Taeyoung Song, Masaru Takagi, Duong Minh Quan, Hiroshi Nishimoto, Yoshiaki Narusue, Ryo Shigeta, Yasumoto Shirahama, Ryosuke Kobayashi, Akihiro Nakamata, Kousuke Fujimoto, Shinoda Shiori, Naoki Uchida, Naoto Hayashi, Takaaki Sunaga, Takuya Sasatani for your generous hospitality. Thanks to Koya Narumi and

Fuminori Okuya for always being great co-authors and super thoughtful people in the lab. Thanks to Weiwei Jiang for helping me with the development of a tracking tool for my robots, and Jie Qi for helping me preparing my slide deck.

I am obliged to all Vietnamese in The University of Tokyo (Todai). Away from home, conversing in the mother tongue is always one of the most splendid things to have.

I am forever indebted to Panasonic Corp. for their generous funding to my studying in Japan. Without Panasonic Scholarship, there would be no Japan for me, no Todai for me, and even this dissertation would not exist. Thanks to Nguyen Ngoc Thuy, Iwaki-san, Sayuri-san, Koezuka-san, Matsuyoshi-san, Komori-san, Fukuda-san and all people in Panasonic Scholarship for giving me this life-changing opportunity. Thanks to Panasonic Scholarship Students, especially A. Hop, Mai, A. Cuong, C. Trang, A. Hiep for their warm friendship in Panasonic Scholarship group.

This research and my Ph.D. life are generously supported by The University of Tokyo Graduate Program for Social ICT Global Creative Leaders (GCL). Without this support, I could not carry my study as a Ph.D. student here.

A large part of this dissertation was supported by JST ERATO Grant Number JPMJER1501, Japan.

Lastly, I am forever grateful for the unlimited support from my family, my parents, my sisters. My deepest thanks to my wife – Thuy Hong, thanks to all of her support, encouragements, sacrifice, and most importantly – her love – that I have my courage to overcome whatever challenge that life might bring.

*This dissertation is dedicated to
my wife Vuong Thi Thuy Hong and
my daughter Ta Thi Hong Anh.*

CONTENTS

List of Figures	14
List of Tables	22
Acronyms	23
1 INTRODUCTION	25
1.1 Digital Fabrication	26
1.1.1 Form Shaping Digital Fabrication	26
1.1.2 Electronic Circuits Fabrication	28
1.2 Printing Fully Functional Objects	31
1.2.1 Challenge of 2D Printing of Electronic Circuits with Silver Ink	31
1.2.2 Challenge of 3D Printing of Fully Functional 3D Objects	33
1.2.3 Challenge of Printing Sensors and Actuators for Robotic Design	34
1.2.4 Challenge of Printing Mechanical Functionality for Robotic Design	36
1.3 Contributions	38
2 PRINTABLE 2-DIMENSIONAL APPLICATION DESIGN WITH SILVER NANO-PARTICLE INK	39
2.1 Introduction	40
2.2 Related Works	42
2.2.1 Printed Circuit Board Routing Algorithms	42
2.2.2 Tree Based Routing Algorithm	42
2.2.3 Design Assistant in Electronic Circuits Prototyping	43
2.3 Problem Formulation and Solution	44
2.3.1 Problem 1 - Routing	45
2.3.2 Problem 2 - Brightness Balancing	47
2.3.3 Improved routing	48
2.3.4 Multiple Color LEDs	49
2.4 Implementation	50
2.4.1 Adobe Illustrator Extension	50
2.4.2 Prevent Polar Cross	50
2.4.3 Eliminate the Excessively Narrow Conductive Traces	51
2.5 Experiment of Routing Multiple LEDs with TSP Auto-router	54
2.5.1 Brightness Balance Evaluation	54
2.5.2 TSP Routing Time Performance	56
2.5.3 Ink Consumption	56
2.6 Applications	58
2.6.1 Electronic Artwork with Multiple LEDs	58

2.6.2	Characters and Emojis with LEDs and Conductive Ink	58
2.6.3	Quickly Made Greeting Card	59
2.7	Discussion and Future Work	60
2.8	Conclusions	62
3	PRINTABLE 3-DIMENSIONAL FABRICATION WITH SILVER NANO-PARTICLE INK	63
3.1	Introduction: Limitations of 2D Printing Electronic Circuits	64
3.2	Via-hole for Double Sided Silver Nano-particle Ink Printed Circuits	65
3.2.1	Related Works	67
3.2.2	Approaches to Double Sided Flexible Circuit	68
3.3	Integration of Printed Electronic Circuit into 3D Printing	71
3.3.1	Introduction	72
3.3.2	Contributions and Benefits	73
3.3.3	Related Works	74
3.3.4	Overview: Printed Electronic Papercrafts	76
3.3.5	PEP Fabrication workflow and Techniques	78
3.3.6	PEP Functional Primitives	81
3.3.7	Software Design Interface	83
3.3.8	Applications	87
3.3.9	Limitations and Future Work	93
3.3.10	Summary	95
3.4	Conclusions	96
4	PRINTABLE SENSORS AND ACTUATORS FOR SOFT-BODIED ROBOTS	97
4.1	Introduction: Printable Soft-bodied Robots	99
4.2	Design and Fabrication of Instant Inkjet Actuator and Sensor	101
4.2.1	Design	101
4.2.2	Fabrication	102
4.3	Experiment	104
4.3.1	Actuation	104
4.3.2	Displacement and Curvature	105
4.3.3	Responsiveness	105
4.3.4	Sensing	105
4.3.5	Robustness	106
4.4	Application - Paper Caterpillar	107
4.5	Discussion and Future Works	113
4.6	Conclusions	114
5	PRINTABLE MECHANICAL FUNCTIONALITY FOR DESIGNING SOFT-BODIED ROBOTS	115
5.1	Introduction: Snake-like Soft-bodied Robot	117
5.2	Soft-bodied Robots Design with 3D Printer	119
5.2.1	Directional Friction	119

5.2.2	Parameters of Directional Friction	120
5.2.3	Soft-bodied Robot Assembly	121
5.2.4	Undulation Generation	121
5.3	Locomotion Model	124
5.4	Experiment on Locomotion	126
5.4.1	Experiment Setup	126
5.4.2	Experiment Result	127
5.5	Discussion	132
5.6	Conclusions	133
6	FUTURE WORKS	135
7	CONCLUSIONS	137
A	APPENDIX: GRADUATE PROGRAM FOR SOCIAL ICT GLOBAL CREATIVE LEADERS	141
A.1	Interdisciplinary Classes	141
A.2	Internships	141
A.3	Workshops	142
A.4	GCL Social Innovation Project	143
	PUBLICATIONS	144
	BIBLIOGRAPHY	149

LIST OF FIGURES

Figure 1	Subtractive manufacturing process removes unnecessary material to form the physical 3D object.	26
Figure 2	Additive manufacturing process adds layer-by-layer of material to form the physical 3D object.	27
Figure 3	Research included in this dissertation. We try to solve each challenge on the way to achieve printable functional objects fabrication.	31
Figure 4	Challenge of 2D printing of electronic circuits with silver nano-particle ink: Averaging brightness of multiple LEDs is very difficult even to an electrical expert. (a) Circuit wired by a traditional copper printed circuit board results in uneven distribution of current to each LED which in turn leads to overheating of LEDs. All LEDs should be green, but several overheated LEDs change color to yellow, orange, and red. (b) Silver nano-particle ink circuit which is routed by the autorouter in Eagle with trace width and clearance set to 1 mm. Some LEDs are very bright, a lot of LEDs are not turning on due to lacking of current. (c) Silver nano-particle ink circuit which is routed by our Traveling Salesman Problem-based autorouter evenly distributes electric current to all the LEDs, thus assures them to have the same brightness [111, 112].	32
Figure 5	Examples of Printed Electronic Papercrafts: (1) sculptural cube lamp; (2) moisture sensing flow-erpot (3) architectural model with simulated lighting; (4) smart toy armadillo with RFID tag; (5) loudspeaker [78].	33
Figure 6	Instant inkjet actuator and sensor consists of an electro-thermal actuator and a resistance based bending sensor which are instantly printed with silver nano-particle ink on a plastic film [114].	35
Figure 7	An example of the 2D anisotropic friction and its application in making a snake-like soft-bodied robot. The 2D anisotropic friction surface is easy to slide forward but difficult to slide backward or laterally [113].	36

Figure 8 Multiple LEDs are automatically routed to balance brightness. A total of 22 LEDs are placed to form the text "AB". Our algorithm resulted in better brightness balance for all the LEDs. 40

Figure 9 Pu Gong Ying Tu (Dandelion Painting) [89] ©Jie Qi 41

Figure 10 A naive approach to balance the LEDs brightness by dividing the LEDs into different layers and connecting them to the two parallel power lines using conductive traces with different width. This approach does not optimize the ink consumption and the routing space. Furthermore, it does not guarantee brightness balance when there are multiple LEDs on a same level branch. 45

Figure 11 Routing process flow of our algorithm 46

Figure 12 Genetic encoding used in our GA TSP solver implementation. n LEDs are put consecutively between anode and cathode power pads. For each generation, our GA TSP solver will shuffle the order of n LEDs to find the fittest route which will be the input for the next generation. 47

Figure 13 Equivalent circuit of multiple LEDs routed by our algorithm 48

Figure 14 Equivalent circuit of multiple color LEDs routed by our algorithm 49

Figure 15 Plug-in integrated into Adobe Illustrator 50

Figure 16 Rotation of LEDs to route the anode and cathode branches 51

Figure 17 Conversion of an excessively narrow conductive strip to its equivalent meander line. By proportionally increasing the width and length, the resistance between the end points A and B of the meander line in (b) is the same as that between the end points of the narrow strip in (a) 52

Figure 18 Meander lines of appropriate width are printed using conductive ink to achieve the desired resistances 52

Figure 19 Voltage drop and current through each LED when routed by our algorithm 53

Figure 20 Voltage drop and current through each LED when routed by the autorouter in Eagle 53

Figure 21 Mixture of 8 red LEDs and 14 blue LEDs are connected by conductive pattern generated by our algorithm 55

Figure 22	Time performance and approximation ratio of our TSP routing algorithm for different number of LEDs. Approximation ratio is calculated as ratio between the total length of the route found by our GA TSP router and the total length of the optimal route which is calculated by Concorde TSP Solver [6].	55
Figure 23	Evaluation of ink consumption based on the total area of the conductive patterns considering different number of LEDs. The power source is set to 20 V and 30 V before routing. For each case, we made 11 samples with the same number of LEDs under different distributions. The area of the conductive pattern is averaged based over these samples	56
Figure 24	Routing a large number of LEDs to create interactive lighting artworks. By controlling brightness of separated groups of LEDs, we can create a depth perspective in the pictures	58
Figure 25	Alphabet characters and emoji using LEDs and conductive ink	59
Figure 26	Lighting greeting card generator using a smartphone application	59
Figure 27	An example of Printed Electronic Papercrafts with embedded electronic circuits.	63
Figure 28	Examples of Printed Electronic Papercrafts: (1) sculptural cube lamp; (2) moisture sensing flow-erpot (3) architectural model with simulated lighting; (4) smart toy armadillo with RFID tag; (5) loudspeaker.	63
Figure 29	Via hole structure	66
Figure 30	Composite structure of paper and functional layers. Paper supports cutting, folding, and bending to construct 3D forms; craft techniques add images and colors. Functional layers embed actuation, sensing, display, and communication.	76
Figure 31	PEP design and fabrication process.	78
Figure 32	Extracting the rest of the printed object by using a tweezers and fixing damaged parts with craft supplies.	79
Figure 33	Two methods to connect multiple functional layers: (1) extending and bending conductive parts (2) carving channels and filling them with conductive material.	80

Figure 34	Embedding coils into 3D printed papercraft enables us to make actuators such as a heater (1) and speaker coil (2).	81
Figure 35	(1) Printed interdigitated capacitors sense the presence of water and humidity, and (2) human touch. (3) A printed resistor can also act as a bend sensor.	82
Figure 36	Structure of an electroluminescent sheet.	82
Figure 37	(1) Thin-film RFID tag and (2) wireless power transfer can be embedded.	83
Figure 38	Design of a cube lamp in the PEP editor.	85
Figure 39	Components in the PEP database.	86
Figure 40	Fabricating a cube lamp: (1) inserting a functional layer with two attached LEDs and printed conductive traces into a stack of paper; (2) sculpting the cube with the Mcor IRIS printer; (3) inside the printed cube lamp; (4) connecting to power to light LEDs.	87
Figure 41	Fabricating an architectural model: (1) inserting two electroluminescent sheets in a stack of paper; (2) 3D sculpting the model; (3) the resulting model; (4) painted in watercolor and equipped with electroluminescent layers.	88
Figure 42	Fabricating a photo frame: (1) a photo printed layer and an electroluminescent functional layer; (2) 3D sculpting a photo frame; (3) the resulting product; (4) lighting the functional layer displays the embedded photo.	89
Figure 43	Fabricating a flowerpot: (1) a water sensing layer with printed conductive traces is inserted into a stack of paper; (2) printing a flowerpot with the sensing layer on the bottom; (3) We decorated the printed pot with colored pens. The graph on the screen behind the plant shows soil moisture as we water the plant.	89
Figure 44	Fabricating a smart toy hedgehog: (1) attaching an RFID tag sticker to a sheet and inserting it into a stack of colored paper; (2) sculpting a toy; (3) a partner toy with an embedded RFID reader senses the RFID tag and plays a melody when it is within 10 cm.	90

Figure 45	Fabricating a multicolor cube lamp: (1) preparing a stack of paper with two functional layers with different color LEDs; (2) sculpting the form; (3) bending the upper functional layer and attaching it to the lower layer; (4) inside of the lamp; (5) when power is connected, LEDs on both layers light up.	91
Figure 46	Fabricating a speaker: (1) inserting two printed coil layers into a stack of paper; (2) sculpting a speaker with coils on different layers; (3) connecting coils by injecting conductive epoxy into cross-layer channels; (4) preparing a stack of paper; (5) sculpting a cone; (6) attaching it to the body; (7) the combined model; (8) connecting the coil to a melody circuit.	92
Figure 47	Fabricating a cup holder: (1) combining four functional layers of printed coils with a stack of paper; (2) sculpting five parts of the cup; (3) connecting the coils by injecting conductive epoxy into the cross-layer channels; (4) the applied thermochromic color without heat; (5) color changes when the power is connected by heat generation.	93
Figure 48	Designers must consider model orientation in the printer. Structure 1 is more fragile than 2: (1) horizontally attached sheets and (2) vertically attached sheets	94
Figure 49	Instant inkjet actuator and sensor consists of an electro-thermal actuator and a resistance based bending sensor which are instantly printed with silver nano-particle ink on a plastic film.	98
Figure 50	Structure of the instant inkjet actuator and sensor. The photo paper or plastic film film is bent due to the effect of the Joule heat generated by the silver nano-particle ink printed heater.	101
Figure 51	Three patterns of actuators and sensors are printed with silver nano-particle ink on the top of three substrates to evaluate the performance of the actuation as well as the sensory reading.	102

Figure 52	Bending actuation of the instant inkjet actuators with different patterns of silver nano-particle ink printed heaters. Thermography of each actuator show that the heater H_1 gives the most uniform heat distribution. For heater H_2 , there is an imbalance between top and bottom edge. Heater H_3 generates heat mostly in the middle and edges of the actuator.	103
Figure 53	Bending of the H_1 pattern in series from flat to max bending. Along with that are the changing of the temperature of the actuator during the bending phase.	104
Figure 54	Time response of actuators are measured by the time it takes for a actuator to go from resting to maximum bending state	108
Figure 55	By continuously reading the resistance of the conductive trace, we can infer the bending angle of the actuator based on the change of its resistance. The instant inkjet actuator and sensor is control by an Arduino Mega board to actuate and to read the resistance of the heater and to show it on a display behind. (Real actuation and sensor reading are included in the supplemental video).	109
Figure 56	Resistance of the silver nano-particle printed pattern changes accordingly to the change of the bending angle.	109
Figure 57	The actuator starts to deform unpredictably when the temperature is more than 120°C , and it burns itself when the temperature is more than 180°C at time $t = 14\text{s}$	110
Figure 58	The instant inkjet actuator and sensor performs stably through multiple times of bending and releasing.	110
Figure 59	The printable paper caterpillar with actuator and sensor is printed with silver nano-particle ink on white PET photo plastic film substrate.	111
Figure 60	The bending of the robot is represented by the resistance change of silver nano-particle ink printed actuator on the body of the robot.	112

Figure 61	2-segment soft-bodied wriggle robot is fabricated from elastic material. It travels based on the undulation generated by two motors which keep winding/unwinding four tendons. The ventral of the robot is patterned with the directional friction surface to support the lateral undulation locomotion.	116
Figure 62	Patterning of high and low friction material to achieve frictional anisotropy	119
Figure 63	Configuration of the directional friction patterns with different α and N . Dark areas have high friction whilst light color areas have low friction to the ground surface.	120
Figure 64	The wriggle soft-bodied robot is assembled from a $150 \text{ mm} \times 11 \text{ mm} \times 8.5 \text{ mm}$ beam and a directional friction surface at ventral side. Locomotive behavior of the robot will change according to the patterning of high/low friction material in the directional friction surface. Here we have 7 types of combination: $F_0, F_1, F_2, F_3, F_4, F_5, F_6$. In the Experiment part, we will add one more type, F_7 , which has flat ventral for comparison.	121
Figure 65	The wriggle soft-bodied robot is actuated by two motors put at two ends of the beam. Four tendons are attached to the motor and the center of the beam so that when motor M_1 winds tendon τ_0 , it will unwind tendon τ_2 . Same principle is applied for M_2, τ_1, τ_3	122
Figure 66	By timely winding and unwinding two motors, we are able to sequentially bend parts of the beam to form an undulation movement. T is period of the undulation, t is the time that a tendon is being wound, Δt is the time that two consecutive tendons are being wound.	123
Figure 67	The robot moves forward based on the traveling wave along its body. The traveling wave alternatively kicks the ground to push the robot forward. Poisson ratio of the elastic beam makes edges of the flat ventral beam lift up when bent. When the ventral side is patterned with directional friction regions, these regions will lift up and touch down the ground accordingly to the bending and relaxing of the beam.	125

Figure 68	8 robots with 8 different ventral surfaces named from F_0 to F_7 . $F_{0..4}$ have α and N as mentioned in Figure 63. F_5 and F_6 have same value of $\alpha = 90^\circ$ and $N = 2$ but are different in alignment to the orientation of the beam. F_7 is a flat ventral robot without directional friction surface.	126
Figure 69	Each robot is put onto a horizontal flat rigid glassy surface. We run the robot for 20s then measure its traveled distance. Each robot has markers so that we can analyze its locomotion using Kinovea.	127
Figure 70	Friction coefficient of ventral pattern on the experimental surfaces in forward direction μ_f , backward direction μ_b , and transverse direction μ_t . Reddish cells indicate high friction coefficient. Greenish cells indicate low friction coefficient.	128
Figure 71	Chord length of the curvature formed by a tendon in its maximum wound state and locomotion speed of robots on <i>White Board</i> surface. All 8 robots have the same beam structure and controlling mechanism so the chord length depend on the friction between ventral of the robot and the experimental surfaces. . .	129
Figure 72	Speed of each robots on different experimental surfaces. In case of <i>White Board</i> surface, F_2 and F_5 showed the best locomotion speed. In case of <i>Fabric</i> and <i>Paper</i> surface, F_2 , F_3 , and F_5 have the highest locomotion speed.	129
Figure 73	Trajectory of the robots when run for 20s on the experimental surface. On the XY plane of the experimental surfaces, each robot is placed along the X-axis so that one end of the robot is positioned at point (0,0). The robots are controlled to move on the same direction as the positive X-axis.	131
Figure 74	A Paper Caterpillar robot with its gripping legs	142
Figure 75	Three Paper Caterpillar robots in a race	143

LIST OF TABLES

Table 1	Parameters of the GA to solve the TSP	47
Table 2	General setting for the experiments	54
Table 3	Environment setup to evaluate time performance of the TSP routing algorithm	55
Table 4	Comparison of approaches to interconnection for double sided circuits	69
Table 5	Fabrication equipment and material	103
Table 6	Setup value of controlling parameters	127
Table 7	Comparison to other wriggle robots	132

ACRONYMS

CAD	Computer-Aided Design
CNC	Computer Numerical Control
CTE	Coefficient of Thermal Expansion
DC	Direct Current
DIY	do-it-yourself
FDM	Fused Deposition Modeling
GA	Genetic Algorithm
GCL	Graduate Program for Social ICT Global Creative Leaders
GDWS	Global Design Workshop
ICT	Information and Communications Technology
IPMC	Ionic Polymer-Metal Composite
LED	Light-Emitting Diode
LOM	Laminated Object Manufacturing
PCB	Printed Circuit Board
PEP	Printed Electronic Papercrafts
PET	Polyethylene Terephthalate
PWM	Pulse Width Modulation
SDL	Selective Deposition Laminating
SMA	Shape Memory Alloys
TSP	Traveling Salesman Problem
UV	Ultra-Violet
VLSI	Very Large Scale Integration
WPT	Wireless Power Transfer

INTRODUCTION

This chapter will give a brief introduction to the background of digital fabrication and rapid prototyping of electronic circuits, the two pillars that enabled the democratization of fabrication. This paradigm shift in maker movement empowers common users with powerful tools to design, make, and tweak. Thus, it helps to shorten the design-to-product cycle as well as to diversify the making task.

1.1 DIGITAL FABRICATION

Digital fabrication has been there since the dawn of computer era. Originally, digital fabrication is the action of auto-controlling a fabricator using computers. For a long time, these fabrication tools and controlling methods have been restricted in big industrial factories. The high entry bar in both financial investment and skill required has made it alien to general audiences until recent years. The development of low-cost computers and new materials has fuelled the spread of digital fabrication with 3D printing taking the lead, followed by other functional rapid prototyping methods.

1.1.1 Form Shaping Digital Fabrication

Traditional forming technologies such as casting and injection molding are mature and widely used in the industry. However, though these technologies are very good at large volumes manufacturing, they require big initial investment even with small volumes manufacturing. This is not preferable for rapid prototyping. That is where the digital fabrication takes place. The form-shaping digital fabrication aims at making the physical instance of a 3D designed model. The instantiation process can be classified into two categories: subtractive manufacturing and additive manufacturing.

1.1.1.1 Subtractive Manufacturing

A representative of subtractive manufacturing is the Computer Numerical Control Machining (CNC). Based on the 3D model, the milling drill will follow a computer generated tool-path to remove unnecessary material from an original block to form the physical 3D object (as shown in Figure 1). That is how it is called subtractive. The subtractive manufacturing can give high precision with excellent repeatability for fabrication in a wide range of materials. However, a sub-

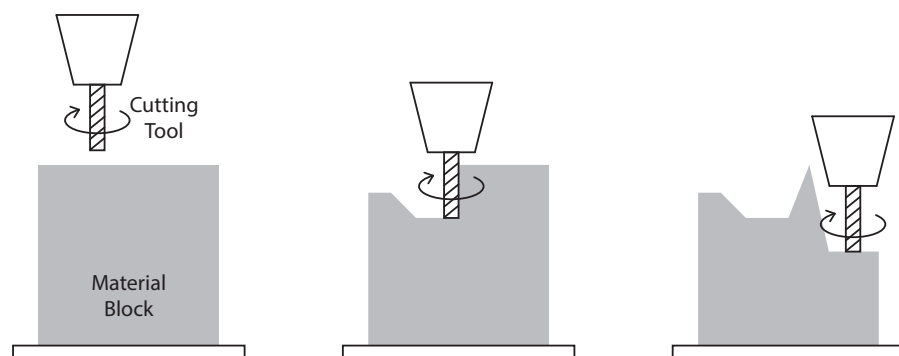


Figure 1: Subtractive manufacturing process removes unnecessary material to form the physical 3D object.

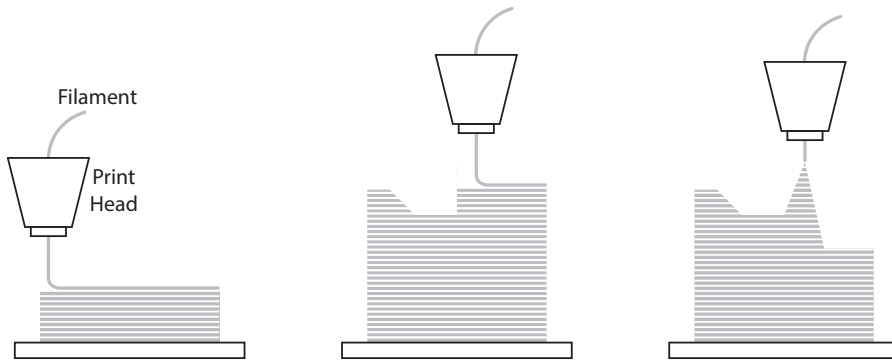


Figure 2: Additive manufacturing process adds layer-by-layer of material to form the physical 3D object.

tractive process will result in a large amount of material waste. Furthermore, the investment and maintenance cost is high.

1.1.1.2 Additive Manufacturing

The principle of additive manufacturing, or 3D printing, is to additively add layers of material to form the designed shape (as shown in Figure 2). The 3D design model will be triangulated and sliced to multiple layers. The 3D printer driver will use this information to deposit material layer-by-layer. There are several methods to deposit printing material such as Fused Deposition Modeling (FDM), Stereolithography (SLA), Digital Light Processing (DLP), Laminated Object Manufacturing (LOM), and Material Jetting. The diversity of the 3D printing methods gives users more flexible options to satisfy the goal, time, and cost requirements. Compared to subtractive process, an additive manufacturing process produces much less material waste. It is also capable of printing much more complex 3D object such as topology-optimized geometries which is drastically difficult to make with subtractive manufacturing or a traditional casting process.

One of the most valuable advantages of 3D printers is the competence to print multi-material. Those are materials of different characteristics such as transparent, rigid, soft, or biocompatible. This flexibility in printing material is a great enabler to design structures with built-in functionality. We will discuss this in more detail in Chapter 5.

Shape forming fabrication is improving more and more on its speed, cost, and printing accuracy. However, whether it is subtractive or additive manufacturing, the printed object is still lack of active functionality. The object cannot move, cannot sense, cannot communicate. How to breathe life into these static printed objects? This question will be discussed in Chapter 3.

1.1.2 *Electronic Circuits Fabrication*

Besides 3D printing for morphing the shape of a 3D object, fabrication of electronic circuits is also important in the maker movement. Following the flourish of 3D printers is the appearance of rapid prototyping tools for electronic circuits. New conductive materials such as conductive paste and conductive ink have enabled us to use existing printing methods to fabricate conductive patterns on a variety of substrates quickly. Thanks to that, the iteration speed of electronic circuits designing is significantly increased.

1.1.2.1 *Traditional Fabrication Processes*

Printed Circuit Board (PCB) holds and connects electronic components using conductive tracks. The tracks are typically made by copper. Common methods to fabricate the designed copper patterns include Etching and PCB Milling.

Etching

PCB Etching is a subtractive process which involves working with chemical substances to remove the unnecessary copper region to form a desired copper trace pattern. The process starts with a PCB copper foil which is a plate of a substrate (*e.g.* glass-reinforced epoxy composite) with a thin layer of copper at one or both sides. The foil will be masked and submerge into an etching solution. The unmasked region of copper will dissolve into the solution, leaving the desired copper trace pattern.

The etching process can produce high-quality PCB which is reliable, durable, and neat. However, it is messy due to the usage of toxic chemical substances. Disposal of these chemical substances also requires strict regulation.

PCB Milling

PCB Milling is also a subtractive process which the unnecessary copper region is selectively removed by drill bits and removal cutters in a CNC XY plotter. In a similar way to the CNC mentioned in Section 1.1.1.1, based on the board design data, a host controlling software will generate a tool-path to remove unwanted conductive material, leaving designed wiring patterns. This process is suitable for low volume manufacturing. Though it generates a lot of material waste, users can avoid working with toxic chemical substances. The disadvantage of the PCB milling is that it requires a huge investment in the milling machine as well as in maintaining the tool-set.

1.1.2.2 *Rapid Prototyping of Electronic Circuits with Conductive Inks*

Beside industrial-grade fabrication processes, there are other ways to rapid prototype electronic circuits which are beneficial to researchers and makers. Though the do-it-yourself (DIY) PCB etching can be counted as a rapid prototyping process, it suffers from the troubles caused by involving chemical substances usage and disposal. Instead, recent electronic circuits rapid prototyping tools are based on new development of conductive materials which can be printed easily on a variety of substrates. The methods discussed here are classified as additive electronic circuits fabrication processes because the conductive material is printed onto the substrate to directly form the wiring pattern.

Electrically Conductive Paste Silk-screening

A conductive paste is usually made from metal particles suspended in a sticky component which explains its name. The metal particles can be silver, copper, nickel, or graphite [97]. The particles, which are usually at μm -order size, are in contact to each other, thus establish conductivity. These conductive pastes are typically conductive at room temperature but it is preferable to cure them in high temperature to achieve the designed electrical and mechanical properties. Due to its high viscosity, the conductive paste is only suitable to be silk-screened which limits the resolution of the prints.

Sintering Silver Nano-particle Ink

Different from conductive paste, sintering silver nano-particle ink is a low viscosity ink with ligand-based coating nm-order size silver particles suspended in a solution to form an inkjettable colloidal [108]. The ligand-based coating of each silver particle is necessary to make it printable with inkjet nozzles. However, due to this coating layer on each particle, the whole solution is not conductive. After printing, the trace needs to be sintered in elevated temperature (typically, 150°C to 250°C) for several hours to remove the coating, coalesce the separating particle, and develop bulk metal patterns. Though the resolution of the print is better than conductive paste, the requirement of high-temperature sintering limits the substrates that can be used as well as reduces the speed of prototyping.

Sintering-free Silver Nano-particle Ink

Sintering-free or room temperature sintering silver nano-particle ink is also metal particle filled inkjettable ink which is used to printed conductive patterns [53]. What makes this ink special is its capability of developing bulk metal pattern at room temperature. The substrate that is used to print the sintering-free silver nano-particle ink is a microporous structure coated with chemical agent to break the bonding between the metal particle and its ligands, thus to coalesce the

metal particles and establish electrical conductivity [130]. This process is also regarded as chemical sintering. The sintering-free silver nano-particle ink made by Mitsubishi Paper Mills Inc. is one of the most marketed as it can be filled in almost any consumer graded inkjet printers to print conductive pattern on flexible substrates such as photo papers, transparent Polyethylene Terephthalate (PET) films, and white PET films. The conductivity is established instantly after printing. This approach is favorable to common users because it is low-cost, off-the-shelf, and fast. The applications of the sintering-free silver nano-particle ink in functional design digitally fabricated devices will be recurred throughout this dissertation and be deeply discussed in Chapter 2 and Chapter 4.

1.2 PRINTING FULLY FUNCTIONAL OBJECTS

Although the development of fabrication tools as mentioned in Section 1.1 above has made it much easier for novice users to fabricate electronic circuits as well as to print 3D objects, the learning curve is still very steep. Moreover, the fabricated objects are passive and required further manual assembling to be able to interact to the surrounding environment. Our goal is to make it possible to quickly fabricate functional objects. These objects should be able to move and actively interact with the environment. In order to achieve this goal, we need tackle it from both electrical and mechanical perspectives. The challenges include designing of electronic circuits, fabrication of 3D objects with electronic circuits embedded, printing of sensors and actuators, and designing of mechanical structures. Figure 3 shows the research in this dissertation that address the main challenges of achieving printable functional objects fabrication.

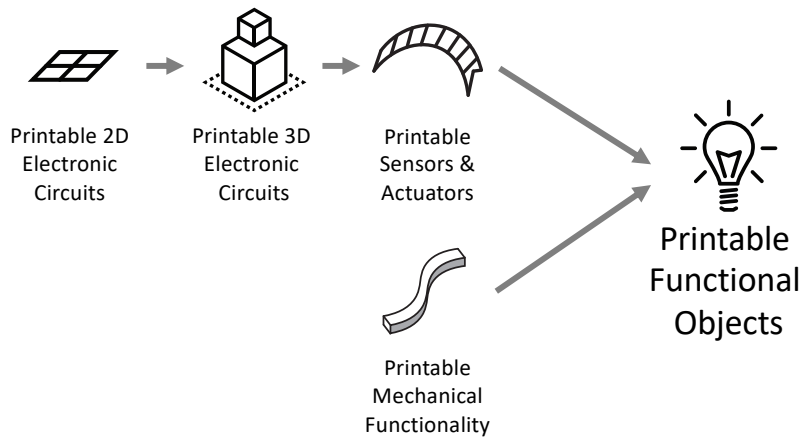


Figure 3: Research included in this dissertation. We try to solve each challenge on the way to achieve printable functional objects fabrication.

1.2.1 Challenge of 2D Printing of Electronic Circuits with Silver Ink

There should not be any doubt about the convenience that silver nanoparticle ink has brought to the rapid prototyping of electronic circuits. Fabrication of a well-designed flexible electronic circuits is just one click away from a normal user. However, the bottleneck lies in the term "well-designed". It is arduous for a common user to consider all the tricky and complicated behaviors of the electronic components. Though there are numerous tools that help to automatically design an electronic circuits (e.g. Eagle [22]), all of them ignore the resistance of the wiring as a typical PCB board is wired with copper which has negligible electrical resistivity. That is not the case of silver nano-

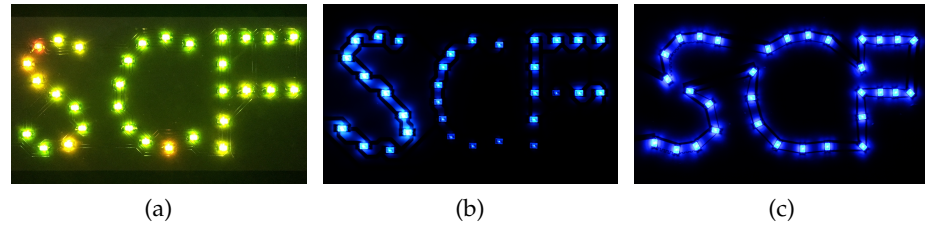


Figure 4: Challenge of 2D printing of electronic circuits with silver nano-particle ink: Averaging brightness of multiple LEDs is very difficult even to an electrical expert. (a) Circuit wired by a traditional copper printed circuit board results in uneven distribution of current to each LED which in turn leads to overheating of LEDs. All LEDs should be green, but several overheated LEDs change color to yellow, orange, and red. (b) Silver nano-particle ink circuit which is routed by the autorouter in Eagle with trace width and clearance set to 1 mm. Some LEDs are very bright, a lot of LEDs are not turning on due to lacking of current. (c) Silver nano-particle ink circuit which is routed by our Traveling Salesman Problem-based autorouter evenly distributes electric current to all the LEDs, thus assures them to have the same brightness [111, 112].

particle ink printed circuits. For example, the intrinsic resistance of silver nano-particle ink is insignificant in simple applications like driving one or two loads (*e.g.* one or two light-emit diodes (LEDs)). But it will cause trouble in more complex applications when the number of loads is increased (*e.g.* 20 LEDs). Figure 4 shows that averaging the brightness of multiple LEDs is difficult, even to an electrical expert. Tools to support designing interactive application with conductive ink, such as in [42, 91, 100], include an autorouter, but again, ignore the resistance of the conductive ink as the number of load those tools assume to route is small. ConductAR [75] tried to solve the problem using computer vision techniques to estimate the resistance of the drawn/printed conductive patterns. However, as an ad-hoc tool, it cannot generate circuits to connect multiple loads on demand.

In our approach, we address this challenge by developing an autorouter which will automatically generate a suitable circuit for wiring and evenly distributing electric current to all the loads. We focus on the routing of multiple LEDs as it is one of the most common application that designers and novice users want to make with conductive ink, yet hardly be able to fulfill. We achieve this by using genetic algorithm to find the Traveling Salesman Problem path through all the loads and adjusting the width of the conductive patterns to tune the resistance to each load. Our experiments show that the conductive pattern generated by our autorouter can drive multiple LEDs at the

same brightness and effectively reduce the amount of ink consumption. Chapter 2 will discuss our proposal in more detail.

1.2.2 Challenge of 3D Printing of Fully Functional 3D Objects

Rapid prototyping of 3D objects using 3D printers focus only on forming the geometric aspect of the objects. How can we provide active functions to the printed object? One of the most plausible answers is to electrify them.

Surfcuit [120] reported an approach of attaching electronic components on the surface of the 3D printed objects. Although this approach is simple and straightforward, it suffers from the requirement of manually wiring and assembling. Furthermore, it heavily affects the outlook of the objects. Pineal [58] proposed to place a smart watch or phone into the 3D objects. Through the embedded devices, users can define the interactive behaviors of the objects. From the same point of view, .Net Gadgeteer [123] suggested embedding a micro-controller kit into the 3D objects and let users program the kit to define new functions for the object. However, this approach is costly and may affect the form factor of the objects.

A more robust approach is to integrate electronic circuits by printing conductive materials at the same time with thermoplastic or UV-cured polymer materials as reported in Voxel8 [124], ChemCubed [16], Delfense [10], Flexibles [102], Capricate [103], and soft electronics printing [122]. However, these processes are not only expensive but also having low printing resolution.

Our approach takes advantage from the development of thin-film printed electronic, which has made it easier than ever to print electronic circuits [53] and components [38, 79, 80]. However, rather than forming 3D shapes by bending and folding of the thin sheets, we cut and stack normal paper and functional paper layer-by-layer to embed functions and make 3D shapes of the printed object simultaneously.

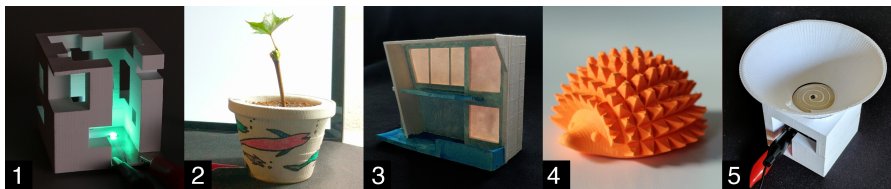


Figure 5: Examples of Printed Electronic Papercrafts: (1) sculptural cube lamp; (2) moisture sensing flowerpot (3) architectural model with simulated lighting; (4) smart toy armadillo with RFID tag; (5) loudspeaker [78].

We provide a plugin for a 3D modeling software (*i.e.* Autodesk Fusion 360) to support users in placing functional layers into the 3D model. Our analysis in Chapter 3 will show that our approach enables a unique design space where users can easily integrate displays, sensing, actuation, and communication into 3D printed objects (as shown in Figure 5).

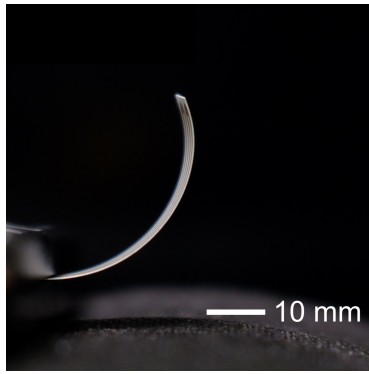
1.2.3 Challenge of Printing Sensors and Actuators for Robotic Design

Being able to embed electronic circuits into 3D printed objects opens a whole new designing space for creating interactive applications. However, can we make the object mechanically move, and at the same time, sense the environment to self-control its movement? This will further expand the designing space, especially for robotic designing. Streamlining and making the fabrication process of sensors and actuators for robotics printable is decidedly desirable for prototyping of soft-bodied robots. It will help to mitigate the non-compatibility between soft materials and rigid traditional sensors/actuators a problem which poses a serious challenge to designing of a fully compliant soft-bodied robot.

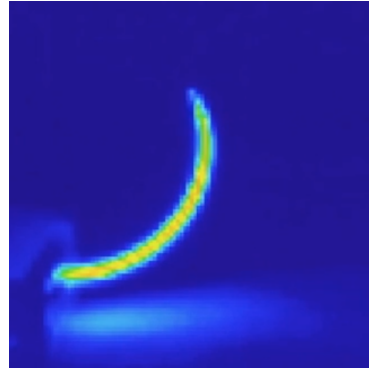
There are research that attempt to make printable pneumatic actuator [66, 76, 81] by printing a pouch and inflate/deflate it with a compressor. Although the pneumatic actuator is responsive and can provides multiple actuation, the compressor is bulky and constraint of tubes and valves. One can use shape memory alloys as in [118]. However, the shape memory alloys are not printable and normally need manual assembling.

From another standpoint, Amjadi *et al.* in [4], Arazoe *et al.* in [7], Hamedi *et al.* in [36], Kirigami robot [105], Hygrobot [106], and Printed Paper Actuator [125] tried to make printable thin-film actuators which enable the fabrication of self-compact printable soft-bodied robots. However, the processes are neither simple nor accessible to common users. Printed Paper Actuator takes a long time with a special printer to print, needs to be driven by a high voltage source, and as Kirigami robot, requires post-processing. Others can only be fabricated with expensive equipment which are out of reach of common users. Furthermore, except Printed Paper Actuator, these approaches do not have a built-in sensory functionality which makes it difficult to control the actuation due to the lacking of feedback information. Kamamichi *et al.* in [50] dealt with the sensor feedback problem by using ionic polymer-metal composite (IPMC) as an actuator and sensor for a snake-like robot. However, the IPMC is expensive and not printable.

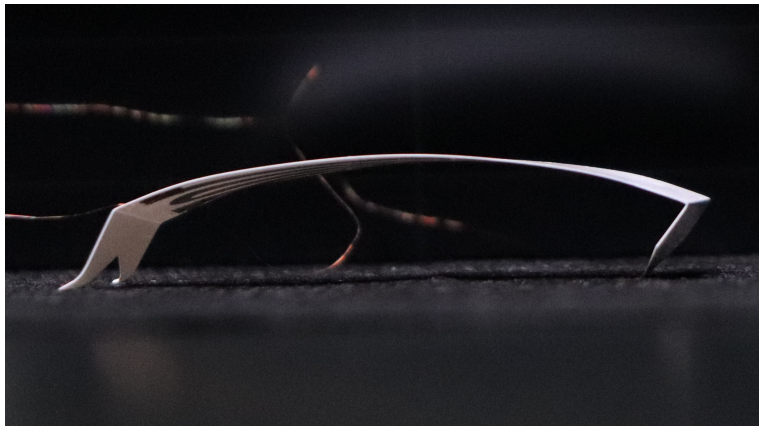
In our approach, we take advantage of the fact that a commonly



(a) Instant inkjet actuator and sensor.



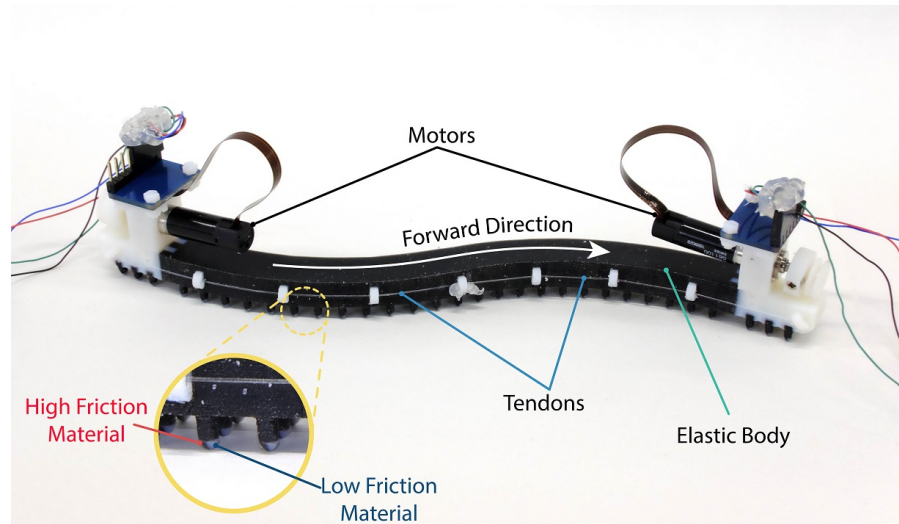
(b) The actuation is based on thermal expansion.



(c) An instant inkjet paper caterpillar which can inch forward and sense its body bending angle.

Figure 6: Instant inkjet actuator and sensor consists of an electro-thermal actuator and a resistance based bending sensor which are instantly printed with silver nano-particle ink on a plastic film [114].

available photo plastic film is a multilayer structure, in which, each layer has different coefficient of thermal expansion. By printing a resistance-based heater with silver nano-particle ink on top of the photo plastic film, we are able to actuate it by supplying a small electric current. Moreover, when the actuator bends, the resistance of the silver ink printed heater also change. Based on this change, we are able to infer the bending angle of the actuator. It is a printable sensor/actuator in a single printed pattern. Figure 6 shows the actuator at bending state. With this instantly printable sensor and actuator, we make a paper caterpillar which can crawl and sense its body bending angle. The design, fabrication, and evaluation of the sensor and actuator are covered in Chapter 4.



(d) A snake-like soft-bodied robot which uses the design of the 2D anisotropic friction to support serpentine locomotion gaits

Figure 7: An example of the 2D anisotropic friction and its application in making a snake-like soft-bodied robot. The 2D anisotropic friction surface is easy to slide forward but difficult to slide backward or laterally [113].

1.2.4 Challenge of Printing Mechanical Functionality for Robotic Design

Beside electrical functionality, another challenge we need to deal with is the design of mechanical functionality which decides the way a printed object mechanically interact with the environment. The mechanical functionality can include stiffness/softness [3, 49], elasticity/viscoelasticity [64, 94], or friction [34, 43, 63]. Among these characteristics, friction plays a important role in deciding movement of the printed objects. In attempt to make crawling robots such as caterpillar [119] or snake-like robots [40, 41, 60, 62, 82, 98], ventral side of the robot is engineered to be an anisotropic frictional surface - a surface with different friction coefficients in different directions. The most typical frictional anisotropy surface the one with passive wheels. However, attaching passive wheels to the body of a crawling robot make it bulky and lengthen the fabrication process. Though making of a anisotropic friction surface is reported in [34, 63], the fabrication processes are not easily accessible for a common user. A simpler model is to use tilted nails at the contacting surface. However,

it is not easy to scale and the nails are broken or bent over time.

In designing of a soft-bodied caterpillar-like robot [118], variable friction legs have been used to push the body of the caterpillar-like robot forward. Although this is an elegant technique for off-plane locomotion, it is 1-Dimensional anisotropic friction which limits the locomotion direction of the crawling robots. A 2-Dimensional anisotropic friction surface is preferable as it increase the number option in designing locomotion of a crawling robot.

Our proposal aims at simplify the fabrication process at the same time with achieving 2-Dimensional anisotropic friction. We use a multi-material 3D printer to selectively combine high and low friction material into designed patterns which give different configuration of the 2D anisotropic friction. We apply printable 2D anisotropic frictional surface in fabricating a printable snake-like soft-bodied robot. Figure 7 shows an example of the printable 2D anisotropic frictional surface and its application in supporting locomotion of a snake-like soft-bodied robot. Chapter 5 will discuss thoroughly the design, fabrication, and evaluation of the 2D anisotropic functional surface as well as the performance of the snake-like soft-bodied robot.

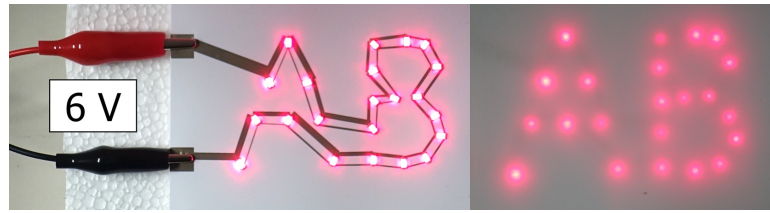
1.3 CONTRIBUTIONS

In this dissertation, we focus on (1) improving the usability of sintering-free silver nano-particle ink by developing tools to support users in working with conductive inks (in Chapter 2), (2) adding new functionality to 3D printed objects by scaling up conductive ink printing from 2D to 3D (in Chapter 3), (3) applying silver nano-particle ink in fabrication of printable sensors and actuators for soft-bodied robots (in Chapter 4), and (4) designing functionality for mechanical devices with multi-material 3D printers and its application in fabricating soft-bodied robots (in Chapter 5). Our contributions includes:

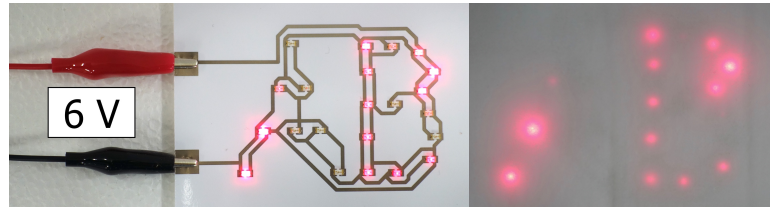
1. *Tools and algorithms:* We developed supporting tools and algorithms to help both novice and expert users in working with conductive ink. To be more specific, we developed an autorouter to auto-route and average the brightness of multiple light-emitting diodes.
2. *Fabrication method:* We scaled up the printing of electronic circuits from 2D to 3D and integrated the fabrication of electronic circuits into 3D printing. This research streamlined the morphing and functional designing of physical 3D objects into a single fabrication process.
3. *Design method:*
 - *Printable sensors and actuators:* We proposed the use of silver nano-particle ink to design and simultaneously print sensors and actuators for soft-bodied robots. This is one step closer to the all-printed robots.
 - *Printable frictional anisotropy body structure:* We explored the design of frictional anisotropy surfaces for effectively designing crawling wriggle soft-bodied robots with multi-material 3D printers. This research pushed the robotic fabrication field to the integration of printable functionality in body design and morphology.

PRINTABLE 2-DIMENSIONAL APPLICATION DESIGN WITH SILVER NANO-PARTICLE INK

Printable electronic circuits have received a big adoption from a variety of users such as researchers, hobbyists, designers, and children. The designers want to use electronic circuits along with graphic design yet focus on the creativity and aesthetics of the design. However, current technology requires them to take care of the discouraging electrical behaviors of the circuits. Taking the task of lighting up a bunch of Light-Emitting Diodes (LED) as an example, it sounds simple, but is posing significant challenges for inexperienced users. Given the non-negligible resistance of conductive ink, it is not straightforward to generate a pattern that lights up the LEDs evenly. Furthermore, a large number of LEDs makes it difficult and error-prone to wire them efficiently. It is possible to try existing autorouters in Computer Aided Design tools to automatically route these LEDs. However, being optimized to make circuits with highly conductive materials such as copper and gold, these autorouters ignore the intrinsic resistance of the conductive ink. In this chapter, we propose an LED autorouter which computationally generates a conductive pattern to balance brightness of multiple LEDs without the need of additional resistors. Our routing algorithm is based on the Traveling Salesman Problem to find the shortest cross-less path through the LEDs, thus minimize the ink consumption. It then adjusts resistances of the conductive patterns to regulate the current which flows through each LED.



(a) Routing by our algorithm to auto-route and adjust the resistance to LEDs so that they evenly light up



(b) Routing by the autorouter in Eagle with trace width and clearance set to 1 mm

Figure 8: Multiple LEDs are automatically routed to balance brightness. A total of 22 LEDs are placed to form the text “AB”. Our algorithm resulted in better brightness balance for all the LEDs.

2.1 INTRODUCTION

Sintering-free conductive ink [53], thanks to its easy accessibility, is being used by many groups of researchers, designers and hobbyists to design and rapidly fabricate interactive applications. Conductive ink filled pens [11, 19, 20] are low-cost and convenient solutions for hand-drawing of working electronic circuits. For more complicated conductive patterns, the conductive ink can be put into an inkjet printer to quickly print the conductive patterns. Researchers take advantage of this to rapidly prototype HCI-related applications such as Extension Sticker [52], Inkantatory paper [117] and touch interfaces [32, 51]. Besides, designers also use conductive inkjet ink to create interactive lighting applications with LEDs as in [109]. Problems arise here when the number of LEDs increases. Wiring multiple LEDs is complicated and tedious. Furthermore, intrinsic resistance of the conductive inkjet ink makes the resistance of the printed pattern non-negligible, thus, causes an uneven lighting up of the LEDs as shown in Figure 8b.

An example of art-works with LEDs is “Pu Gong Ying Tu (Dandelion Painting)” [89] (Figure 9). Here, a lot of LEDs were placed behind a painting to bring in interactivity with the subject of the picture. It was manually designed with copper tape and a large number of LEDs. As shown in Figure 9b, the copper tape-based electronic circuit behind the picture is complicated and would take a lot of time to wire it manually. Using conductive ink to print the printable digital design of the circuit will obviously simplify the labor of making



(a) Front side showing the painting and LEDs lit up from behind. ©Jie Qi



(b) Back side having electronic circuits to power the LEDs. ©Jie Qi

Figure 9: Pu Gong Ying Tu (Dandelion Painting) [89] ©Jie Qi

and replicating this work. Some conductive ink existed at the time of the project, but the author of this work would not have done it using conductive ink due to the complication of designing a cross-less wiring pattern. Moreover, using conductive ink instead of copper would require a thorough consideration to overcome the troubles caused by the resistance of the conductive ink.

In this section, we propose the implementation of an autorouter as an extension of, but not limited to, Adobe Illustrator to support designing LED-based applications with conductive inkjet ink. Our contributions include:

- A Traveling Salesman Problem (TSP) based routing algorithm to search for the shortest cross-less 2D conductive pattern that will evenly light up multiple LEDs, and minimize the ink consumption. The generated circuit can be printed on a single-sided sheet of paper to regulate the current through the LEDs without additional ballast resistors.
- An integrated tool to design with LEDs and conductive ink. Users can drag and drop LEDs as well as a power source to the desired position before letting the autorouter wire them all appropriately.

2.2 RELATED WORKS

2.2.1 Printed Circuit Board Routing Algorithms

Printed Circuit Board (PCB) and high-density circuits routing have been well studied with many efficient algorithms which can be put into two large group as follows:

Grid-based: Grid-based routing in PCB originated from Dijkstra search [21] and is considered as a class of A* search. It assumes that all components are aligned and routed on a rectangular grid. Algorithms in this group aimed at routing the electronic nets and minimizing the total Manhattan-length of all the routing traces. Subgroup in grid-based routing algorithms are maze routers [59] [35], line search algorithms [39, 70], and the Steiner tree grid-based algorithm [1].

Gridless: In contrast to grid-based algorithms, algorithms in the gridless routing group such as in [27, 57, 101] route the electronic nets without the assumption of any grid. Width and angle of the routing traces can be dynamically changed during routing process to meet routing requirements.

Grid-based and gridless routing algorithms are implemented in Electronic Design Automation tools (e.g., Eagle [22]) to mitigate the burden in designing electronic circuits. In these autorouters, due to the high conductivity of the bulk metal used to wire, the dimension of these metal patterns are normally put aside as long as the circuit is routable. However, this is not applicable in case of using conductive inkjet ink because of the non-negligible intrinsic resistance in the conductive ink. Ignorance of this resistance leads to generation of conductive patterns that cannot light up multiple LEDs evenly as shown in Figure 8b.

2.2.2 Tree Based Routing Algorithm

In addition to A* search based algorithms, routing problems can be addressed with tree-based algorithms. Zero-skew clock routing is a typical problem in designing high-performance synchronous Very Large Scale Integration (VLSI) systems. In these systems, it is crucial to assure that the arrival times of a clock signal from a clock source to synchronous elements are the same. This can be analogized to our problem of LEDs brightness balancing in terms of providing the same current to all the LEDs in the circuit. Among different approaches to the zero-skew clock distribution problem such as in [15, 92, 116], clock trees based algorithm [69] is widely used. However, a tree-based approach will not be a good solution to our LEDs brightness problem.

The reason is that a tree-based algorithm will require multiple layers for routing. Although there are ways to fabricate double-sided circuits with conductive ink such as in [115] [5], they complicate the fabrication process significantly and make it difficult to optimize the ink consumption. Routing and balancing brightness of the LEDs in a single-layer circuit are more desirable.

2.2.3 *Design Assistant in Electronic Circuits Prototyping*

Since the emergence of consumer grade conductive inks, there are many tools to assist designing with these new materials. Circuit Stickers [42], Ellustrate [61], PaperPulse [91] and Midas [100] each proposed a development tool based on A* search and Lee's algorithm [59] to support/automate the wiring of electronic components with conductive inks/pastes. However, these tools neither are fully automated nor consider the resistance of the conductive ink which as we mentioned above, severely affects the performance of the printed electronic circuits.

To deal with troubles caused by the resistance of the conductive ink, ConductAR [75] used computer vision techniques to estimate the resistance of hand-drawn or printed conductive ink patterns. Thus, it suggests an optimized trace width to each path of the circuits. However, it is an ad-hoc tool that cannot generate 2D paths to connect multiple LEDs on demand.

2.3 PROBLEM FORMULATION AND SOLUTION

In its normal working zone, the brightness of an LED is roughly proportional to the current that flows through it. Therefore, in order to achieve an even lighting up of multiple LEDs, the circuit needs to assure that all the LEDs get the same amount of current. This can be guaranteed by chaining all LEDs serially and regulating the current by a ballast resistor. However, this approach requires a high voltage of the power source as the number of LEDs increases. In this case, a more reasonable approach is to put all the LEDs in parallel to the power source and regulate the current through each LED with ballast resistors. In a parallel schematic, these ballast resistors play a very important role in regulating and protecting the LEDs. Without them, due to the LEDs' vicious loop of heating - increasing forward current, all the LEDs will be sequentially over-current and burn-out. As mentioned above, the existing autorouters assume that resistance of the metal pattern is negligible and additional ballast resistors will be added to regulate the LEDs. Given the non-negligible intrinsic resistance of conductive ink, the first assumption does not hold. The second assumption about additional ballast resistors is discouraging. Adding rigid ballast resistors leads to the needs of calculating value of each resistor as well as the labor of attaching all of them to the circuit. Hence, we lose the advantage of using conductive inkjet printing technology. Instead, by means of computational design, the conductive inkjet ink can be used to act as a printable ballast resistor for each LED. We can take advantage from the apparent disadvantage of the conductive inkjet ink (i.e., high intrinsic resistance) and turn it into our favor.

A naive solution to averaging brightness of the LEDs could be rectilinearly connecting the power source to each LED as shown in Figure 10. Apparently, this approach does not minimize the amount of ink consumed as well as the routing space. Furthermore, if there are multiple LEDs on a same level branch, it is difficult to assure that all these LEDs will light up.

In our proposal, to balance the brightness of the LEDs, we aim to solve the following two challenges:

- *Routing*: To find the shortest cross-less path that connects all the LEDs to the power source, thus, minimizes the conductive ink consumption.
- *Brightness Balancing*: To assure that each LED receives the same amount of current so that they have the same brightness.

For simplicity, in solving these two challenges, we will assume that all the LEDs have the same dimension.

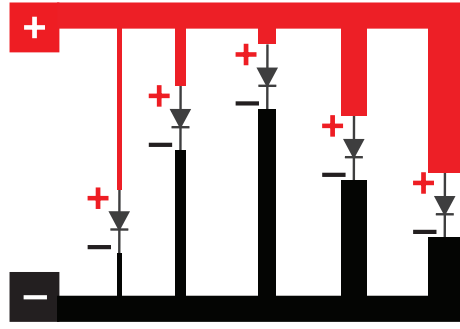


Figure 10: A naive approach to balance the LEDs brightness by dividing the LEDs into different layers and connecting them to the two parallel power lines using conductive traces with different width. This approach does not optimize the ink consumption and the routing space. Furthermore, it does not guarantee brightness balance when there are multiple LEDs on a same level branch.

2.3.1 Problem 1 - Routing

Problem statement: Given a group of n LEDs ($L_i, i = 1, 2, \dots, n$), and the two poles of a power source (L_0, L_{n+1} respectively denoting anode and cathode) as shown in Figure 11a, find a route that connects the LEDs in parallel to the power source and minimizes the ink consumption.

Solution: For the goal of minimizing the amount of conductive ink consumed, we will find the shortest path to connect all the LEDs in parallel to the power source. Although this can be achieved by using the A* search algorithms, they are optimized to search for the shortest path between two points on a grid. A* search algorithms do not search for the shortest path through multiple points (i.e. LEDs). Building the Minimum Steiner Tree of all LEDs and the power source is the best solution to minimize the total length of connections [13]. Nevertheless, it is not feasible to route the two separated anode net and cathode net on a single layer circuit. To deal with the routing problem, we propose to solve the Euclidean-metric Traveling Salesman Problem corresponding to the set of LEDs and power source poles. L_0 and L_{n+1} act as the fixed starting and ending points of the TSP path. The TSP path will go from L_0 , through all LEDs L_i , to L_{n+1} . Because searching for the TSP path is a NP-Complete problem [83], it is more practical to approximate the shortest path using heuristic algorithms such as Christofides' algorithm [18], the simulated annealing algorithm [29] and the genetic algorithms(GAs) [33]. We implement the TSP solver using the genetic algorithm because it is flexible in the evaluation of the best route.

In a GA based TSP solver, an *individual* is a candidate for the shortest

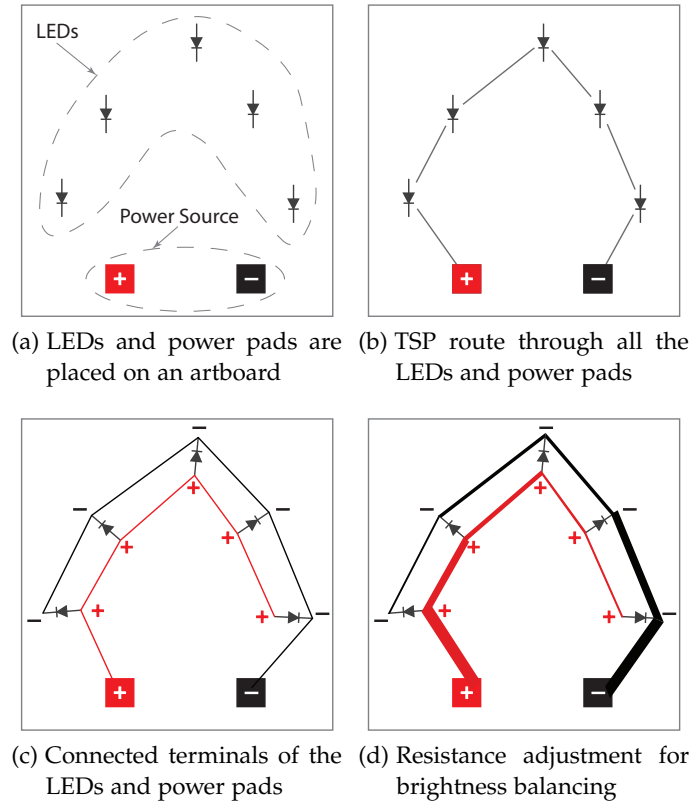


Figure 11: Routing process flow of our algorithm

path through all the LEDs. It will be encoded as the array shown in Figure 12. In this encoding, the starting and ending points are always fixed at the head and tail of the array. Only the order of the elements in range of 1st to nth ($L_{i=1,2,\dots,n}$) are alterable. For every generation of the GA, we generate a *population* of $p = 50$ *individuals* by evolving from the *population* of the previous generation. Evolution through generations involves running *crossover*, *mutate*, and *selection* operations on the current population. To evaluate each *individual*, we define a *fitness* function as the reciprocal of the total length of the corresponding tour [85]. At each generation, we extract the fittest *individual* (i.e., the one with the highest *fitness*) for seeding the next generation. We stop the TSP solver when there is not better *individual* for $\text{converge_threshold} = 10n$ consecutive generations, or when the evolution reaches $\text{MAX_GENERATION} = 100n$ generations. Choosing of these thresholds is done through empirical experiments. Detail parameters of the GA TSP solver are listed in Table 1. After stopping the GA evolution, we use 2-opt algorithm [88] to eliminate all the crossing edges, if any, in the path generated by the GA to make it the shortest path as shown in Figure 11b. Finally, after rotating each LED to an appropriate angle as described in section 2.4.2, our algorithm connects all the LEDs along the found TSP path as shown in Figure 11c.

Table 1: Parameters of the GA to solve the TSP

Population Size	$p = 50$
Mutation Rate	0.015
Mutation Scheme	Ordered Changing [77]
Crossover Scheme	Two-point Crossover [77]
Selection Scheme	Tournament [30]
Tour Size	5
Fitness	Reciprocal of Tour Length
Number of Generations	MAX_GENERATION = 100n
Convergence Threshold	converge_threshold = 10n

Convergence Threshold: the maximum number of consecutive generations that have the same fitness value

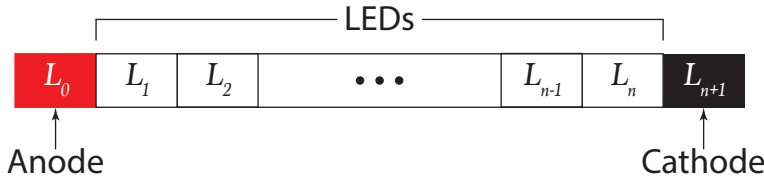


Figure 12: Genetic encoding used in our GA TSP solver implementation. n LEDs are put consecutively between anode and cathode power pads. For each generation, our GA TSP solver will shuffle the order of n LEDs to find the fittest route which will be the input for the next generation.

2.3.2 Problem 2 - Brightness Balancing

The goal of lighting up all the LEDs evenly is achievable when each LED receives the same amount of current. This is fulfilled by adjusting the resistance from the power source to each LED. Because we put all the LEDs in parallel to the power source, the topology as in Figure 11c has an equivalent circuit as shown in Figure 13.

In case that the electronic circuit consists of the same color LEDs, all the LEDs have the same magnitude of forward current I_F and forward voltage V_F . The brightness balancing problem can be stated as follows:

Problem statement: Given a set of n LEDs that are connected to a V_0 power source as shown in Figure 13, find all the resistances $R_i, i = 0, 1, 2, \dots, 2n - 1$ that regulate the current through each LED to the common forward current I_F .

Solution: The equivalent circuit in Figure 13 is just a bunch of LEDs that are put in parallel to the power source. Values of the resistors

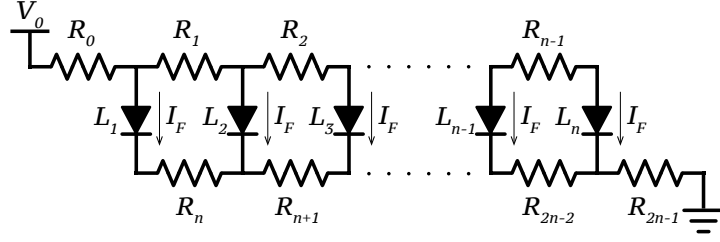


Figure 13: Equivalent circuit of multiple LEDs routed by our algorithm

are retrieved by using the nodal analysis on the equivalent circuit. In order to balance the currents through the single color LEDs (i.e., $I_i = I_F, i = 1, 2, \dots, n$), the resistances must satisfy the following two equations:

$$\begin{cases} (n-i)R_i = iR_{n-1+i}, & (1) \\ R_0 + R_{2n-1} = \frac{V_0 - V_F - I_F \sum_{i=1}^{n-1} (n-i)R_i}{nI_F} & (2) \end{cases}$$

Because there are many sets of resistances R_i , we assume that $R_i = R_{2n-1-i}$ where $i = 0, 1, \dots, n-1$. Once the user chooses the input voltage V_0 , our algorithm will calculate the values of all the resistances $R_{i=0,1,\dots,2n-1}$.

Conductive Patterns As Printable Resistors: once the values of all the resistors are derived from the procedure above, we can print these resistors with the conductive ink. For an $l \times w$ conductive strip, the resistance between two ends is $R = R_s \frac{l}{w}$ where R_s is the sheet resistance of the conductive inkjet ink. With R as derived above, R_s fixed to each type of the conductive inkjet ink, and l as the distance between two consecutive LEDs on the TSP path, we can easily calculate the width w of each conductive segments. Figure 8a and Figure 11d show an output of our routing algorithm.

2.3.3 Improved routing

Our routing algorithm consists of two steps as follows:

- *Step 1:* Find TSP path from the anode of the power source, through all LEDs, to the cathode of the power source. Then connect them so that the LEDs are put in parallel to the power source.
- *Step 2:* Solve the equivalent circuit to get the resistance of all the resistors. Then print these resistors using conductive inkjet ink.

However, taking advantage of GA, we can improve the routing algorithm by combining these two steps into one. Instead of searching for the TSP route, we search for the path that minimizes ink consumption. In order to implement this, we replace the distance based

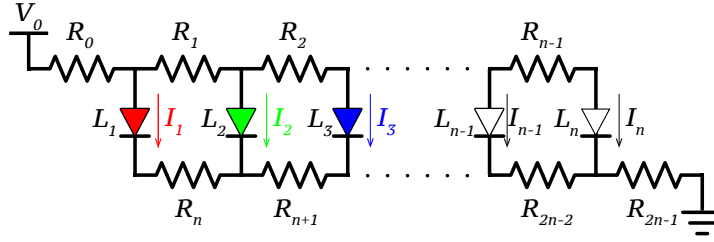


Figure 14: Equivalent circuit of multiple color LEDs routed by our algorithm

fitness function of our GA implementation with a printed area based *fitness* function. The printed area based *fitness* function is defined as reciprocal of the printed area. At each generation of GA, we do as *Step 2* above and then calculate the printed area. Smaller printed area routes will be selected to the next generation.

2.3.4 Multiple Color LEDs

In section 2.3.2, we solved the problem of brightness balancing for single color LEDs. That is, all the LEDs in a circuit are the same color which results in the same requirement of forward voltage and forward current. It is possible to solve the problem in a circuit which have different color LEDs. In that case, depends on its color, each LED has different requirements of forward voltage and forward current. The problem can be stated as follows:

Problem: Let forward voltage and forward current through LED L_i , $i = 1, 2, \dots, n$ be V_i and I_i , voltage of the power source be V_0 . Knowing the order of LEDs which should be connected in parallel to the power source, generate conductive inkjet patterns so that the voltage drop on each LED L_i is V_i .

The circuit of multiple color LEDs put in parallel to the power source has an equivalent circuit as in Figure 14. With known V_0 , V_i , I_i , the resistors are solvable using the nodal analysis. Let $I_{a,b} = \sum_{i=a}^b I_i$, all the LEDs L_i will get its required amount of current when the resistors satisfy the following equations:

$$\begin{cases} I_{i+1,n} R_i = I_{1,i} R_{n-1+i} + V_i - V_{i+1}, & (3) \\ I_{1,n} R_0 + \sum_{i=1}^{n-1} I_{i+1,n} R_i + I_{1,n} R_{2n-1} = V_0 - V_n & (4) \end{cases}$$

Among many sets of resistances that satisfy the equation system above, we can choose the one that minimizes the area of the conductive pattern. We assign larger resistances to conductive segments which have longer length, thus overall reduce the width of the pattern.

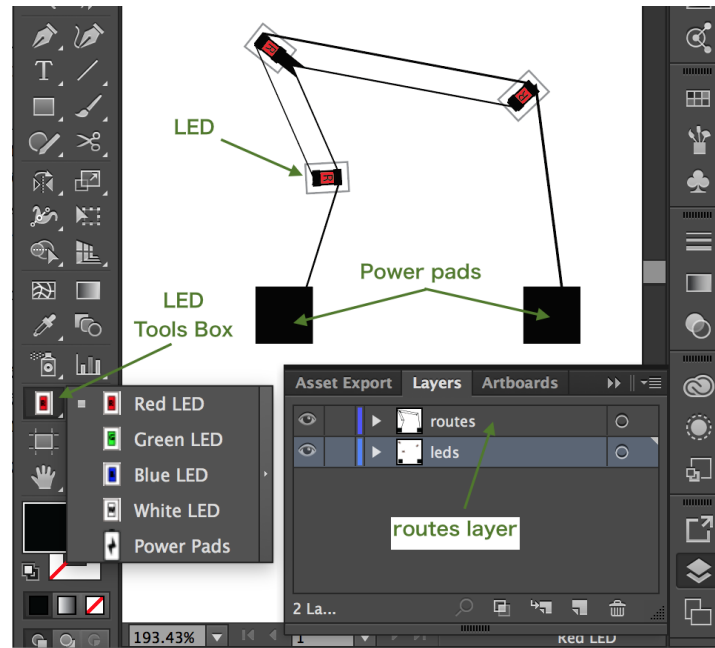


Figure 15: Plug-in integrated into Adobe Illustrator

2.4 IMPLEMENTATION

We implement the aforementioned algorithm as a plugin of Adobe Illustrator ¹.

2.4.1 Adobe Illustrator Extension

Integrating our autorouter into a commonly used design software as Adobe Illustrator keeps the user from the struggle of learning a completely new tool (Figure 15). Electronic components like LEDs and the power source footprint are arranged into the toolbox of Adobe Illustrator. Our auto-routing script will route all the LEDs and the power source then generate a ready-to-print conductive pattern to be printed with conductive inkjet ink. Finally, the user will attach real LEDs to the print and drive them with a real power source.

2.4.2 Prevent Polar Cross

During discussion of routing, to simplify the implementation of the TSP solver, we assume that the LEDs and power source poles are points on a 2D plane. However, we need to put the dimension of each component into consideration when we route them together. From Figure 13, we see that the circuit comprises two branches which are the anode branch made up of $R_{i=0,1,\dots,n-1}$ and the cathode branch made up of $R_{i=n,n+1,\dots,2n-1}$. In order to prevent these two polar

¹ Source code is stored here: <https://github.com/tatung/LightTrace>

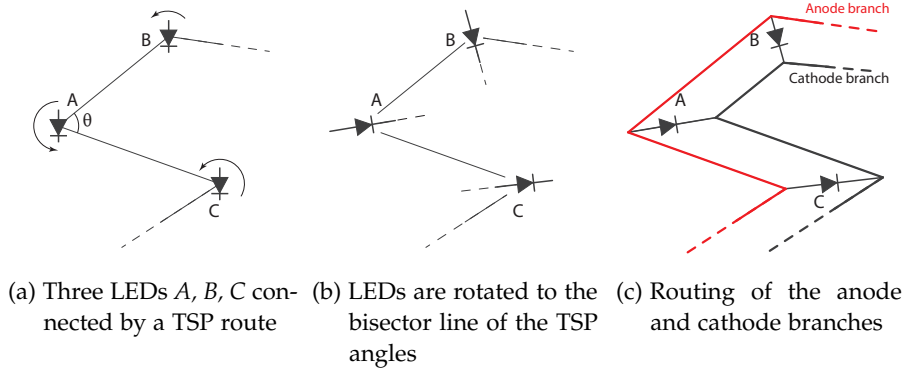
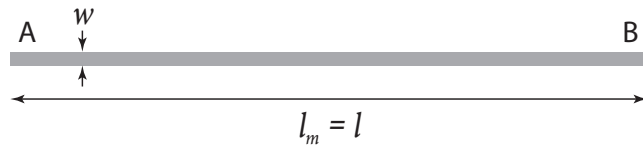


Figure 16: Rotation of LEDs to route the anode and cathode branches

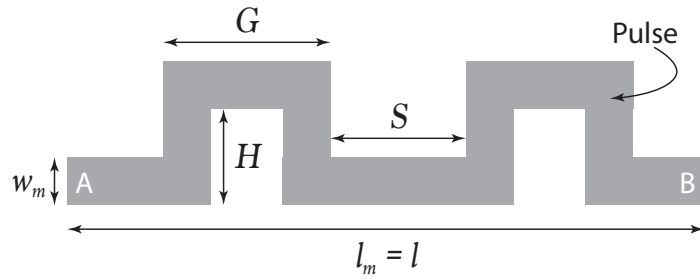
branches from crossing each other, we rotate each LED around its center to an appropriate angle. Considering the case of three LEDs as shown in Figure 16a, the directional axis of an LED is defined as the vector from the center point of its anode to the center point of its cathode. We define TSP angle θ of an LED as the angle formed by the two edges of the TSP route at the corresponding LED. For each LED, we align its directional axis to the bisector line of the TSP angle θ as in Figure 16b and then if necessary, we reverse the directional axis of the LED to eliminate the twist (if any) of the anode and cathode TSP edge (Figure 16c). This equals to switching position of anode and cathode terminal of the corresponding LED.

2.4.3 Eliminate the Excessively Narrow Conductive Traces

The width of a conductive segment in our TSP routing depends on the required resistance and the length of the conductive segment. Besides, it is also influenced by the characteristic of the conductive inkjet ink and the printing technology. The minimum tolerable width $W_{\text{threshold}}$ is defined as the narrowest conductive trace that is printable. Any trace with the width $w < W_{\text{threshold}}$ is either highly resistant or not conductive at all. This usually happens when the required resistance R is high whilst the distance l between two ends of the conductive segment is small. In order to solve this, we need to eliminate the excessively narrow conductive traces by converting them into electrically equivalent meander lines. The electrically equivalent meander line need to have the same end-to-end distance as the original narrow trace, wider width than the original width of the narrow trace, and the same end-to-end resistance as the original narrow trace (Figure 17). An example of this conversion is shown in Figure 18.



(a) An excessively narrow strip has a very high resistance or is not conductive at all



(b) Equivalent meander line having the same end-point distance but that is longer and wider

Figure 17: Conversion of an excessively narrow conductive strip to its equivalent meander line. By proportionally increasing the width and length, the resistance between the end points A and B of the meander line in (b) is the same as that between the end points of the narrow strip in (a)

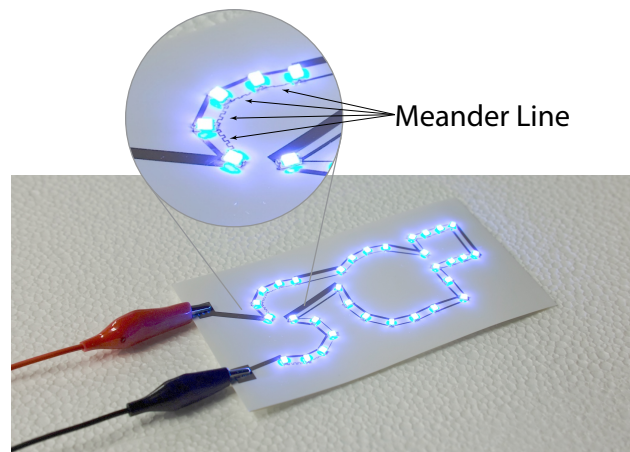


Figure 18: Meander lines of appropriate width are printed using conductive ink to achieve the desired resistances

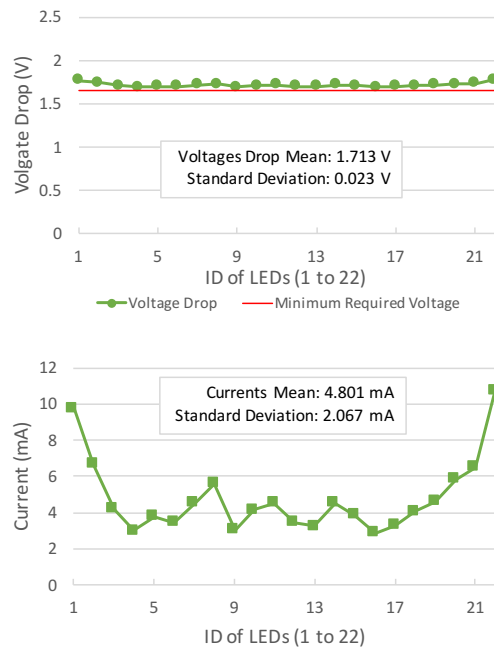


Figure 19: Voltage drop and current through each LED when routed by our algorithm

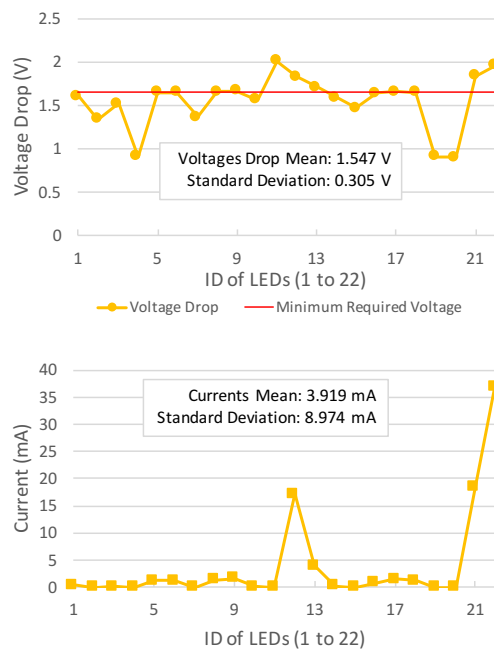


Figure 20: Voltage drop and current through each LED when routed by the autorouter in Eagle

2.5 EXPERIMENT OF ROUTING MULTIPLE LEDS WITH TSP AUTO-ROUTER

Settings for all the experiments in this section are listed in Table 2.

Table 2: General setting for the experiments

Substrate	NB – RC – 3GR120 [71]
Red LED	LTST – C150CKT [95]
Blue LED	LTST – C150TBKT [96]
Conductive Ink	NBSIJ – MU01 [72]
Inkjet Printer	Epson PX – S160T
Sheet Resistance R_s	0.13 Ω/\square (ohm-per-square)

2.5.1 Brightness Balance Evaluation

To evaluate the performance of our algorithm in balancing brightness of multiple LEDs, we placed 22 red LEDs to form the text “AB”, and then connected them using printed conductive inkjet ink as shown in Figure 8. We use our algorithm and the autorouter in Eagle respectively to generate the conductive pattern in Figure 8a and Figure 8b. In the case of using Eagle, trace width and clearance are set to 1 mm. The circuits are driven by a 6 V regulated DC power supply (TEXIO PA36 – 3B [110]). We use a digital tester (Hozan DT – 124 [45]) to measure the voltage drop on each LED.

As evidently shown in Figure 8, our TSP router outperformed the autorouter in Eagle in terms of brightness balancing. A closer look at the voltage drops on each LED (Figure 19 and Figure 20) shows that our TSP router give a much better distribution of the voltage drop on each LED. All of them are stable and larger than the minimum required voltage (i.e., above the red line). Due to the instability in printing resistor using conductive ink, especially when printing narrow traces, which are located in the two ends of the circuit due to the constraint in Equation 1, the voltage drop on the first and last LEDs are slightly higher than the others. This difference, along with the non-linearity of the I-V characteristic of the LED, makes the currents flow through these two LEDs higher than the other LEDs. However, this deviation in current is acceptable as the brightness difference it causes is ignorable for human eyes (as shown in Figure 8a). In contrast, the autorouter in Eagle showed difficulty in providing stable voltage drops to each LED. Most of the LEDs, in this case, have the voltage drop less than the minimum required voltage which resulted in the uneven lighting of the LEDs.

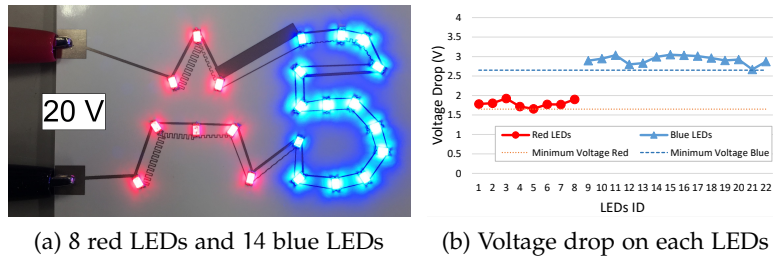


Figure 21: Mixture of 8 red LEDs and 14 blue LEDs are connected by conductive pattern generated by our algorithm

Experiment with multiple color LEDs (8 red LEDs and 14 blue LEDs) as in Figure 21 shows that our routing algorithm works well in case of circuits with different color LEDs. Voltage drop on the same color LEDs are stable and above minimum voltage requirement for each color. However, due to mixing the different color of LEDs, the input voltage needs to be higher compared to the case of single color LEDs.

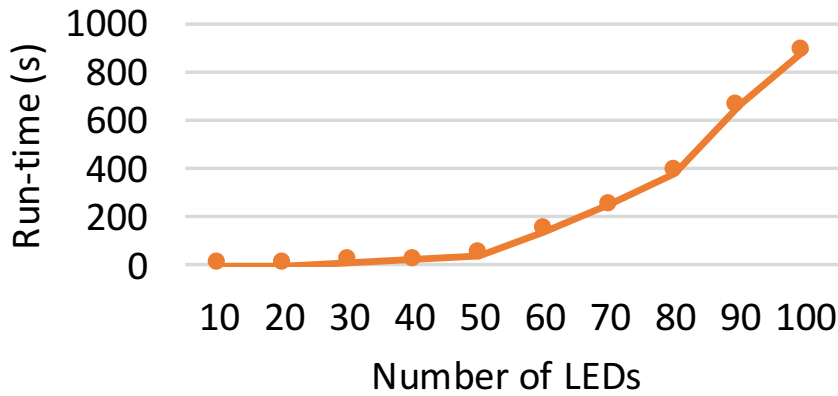


Figure 22: Time performance and approximation ratio of our TSP routing algorithm for different number of LEDs. Approximation ratio is calculated as ratio between the total length of the route found by our GA TSP router and the total length of the optimal route which is calculated by Concorde TSP Solver [6].

Table 3: Environment setup to evaluate time performance of the TSP routing algorithm

Operating System	Mac OS X Sierra 10.12.2
Processor	2.7 GHz Intel Core i5
Memory	8 GB 1867 MHz DDR3
Adobe Illustrator	CC 2017

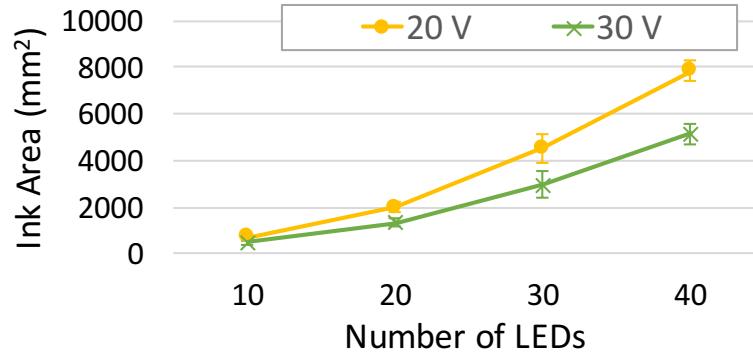


Figure 23: Evaluation of ink consumption based on the total area of the conductive patterns considering different number of LEDs. The power source is set to 20 V and 30 V before routing. For each case, we made 11 samples with the same number of LEDs under different distributions. The area of the conductive pattern is averaged based over these samples

2.5.2 TSP Routing Time Performance

Performance of our TSP router is also evaluated in terms of running time. With the experimental environment setup as in Table 3, we ran it with different number of LEDs and then measure the routing time in each case.

The experiment results in Figure 22 shows that our TSP routing algorithm can route up to 60 LEDs in a convenient time frame using a commodity laptop. However, it starts to struggle when the number of LEDs increases more. This can be improved partially by introducing heuristic fine-tuning or dynamic programming into the search for the TSP path.

In addition to running time evaluation, we also evaluate the approximation ratio of our GA TSP solver with difference numbers of LEDs. The approximation ratio here is defined as the ratio between the total length of the route found by our GA TSP solver and the total length of the optimal route which is calculated by Concorde TSP Solver [6]. As shown in Figure 22, we can achieve reasonable approximation of the TSP route with the highest ratio in the case of 100 LEDs is about 1.6. That means in this scenario, the route found by our GA TSP solver is only 1.6 times longer than the optimal one.

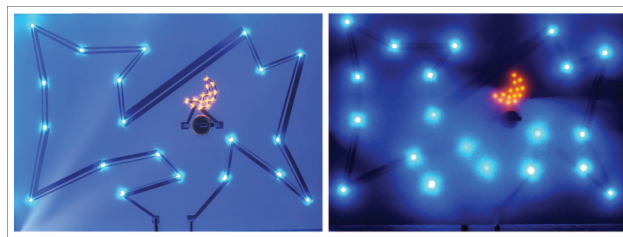
2.5.3 Ink Consumption

Assuming that conductive inkjet printing will always print the conductive ink with the same thickness, we evaluate the ink consumption by measuring the area of the conductive pattern. We do not acknowl-

edge of any tool that helps to route and balance brightness of multiple LEDs. Therefore, we conducted the experiment by comparing printing area in case of different numbers of LEDs and different of input voltages. We distributed multiple LEDs uniformly on an A4-sized artboard. Input voltage is set to 20 V and 30 V for each case. As shown in Figure 23, increasing number of the LEDs requirement more conductive ink to route all of the LEDs. However, it is possible to reduce the ink consumption by increasing the input voltage.



(a) Fireflies



(b) Moon and stars

Figure 24: Routing a large number of LEDs to create interactive lighting artworks. By controlling brightness of separated groups of LEDs, we can create a depth perspective in the pictures

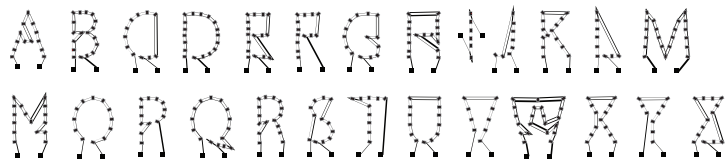
2.6 APPLICATIONS

2.6.1 *Electronic Artwork with Multiple LEDs*

With our plugin, users can automatically route a large number of LEDs and print the circuit quickly with conductive inkjet printing (Figure 24). It is also possible to mix multiple types of LEDs in a single artwork by stacking altogether transparent Polyethylene Terephthalate (PET) films with different types of LEDs routed on each layer.

2.6.2 *Characters and Emojis with LEDs and Conductive Ink*

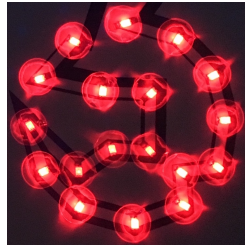
Characters and emojis help to convey information efficiently. They are often used in designing interactive applications with LEDs. Using our plugin, instead of manually connecting each LED, users can easily generate conductive patterns of all characters in the alphabet table (Figure 25a) or emojis such as the smiling or frowning face (Figure 25).



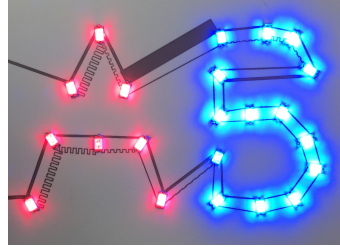
(a) Routing of all characters in the alphabet



(b) Smiling face



(c) Frowning face



(d) Text sign using LEDs

Figure 25: Alphabet characters and emoji using LEDs and conductive ink

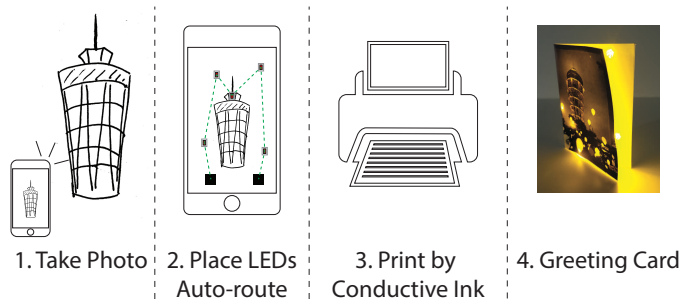


Figure 26: Lighting greeting card generator using a smartphone application

2.6.3 Quickly Made Greeting Card

Although our algorithm is originally implemented in Adobe Illustrator, it is possible to port the algorithm to other platforms which are more familiar to beginners. Figure 26 shows a proposal of a smartphone app that lets users generate LED-based greeting cards by taking a photo, placing LED and route with our TSP router. The generated conductive pattern is ready to print and assemble.

2.7 DISCUSSION AND FUTURE WORK

Our TSP router helps to generate conductive patterns that wires and regulates the current through each LED to assure that they light up evenly. Besides, we can expand this routing algorithm to other 2-terminal components such as sensors, actuators and paper speakers. We can also port it to other popular Computer-Aided Design (CAD) platforms such as Fritzing and KiCAD.

However, our TSP router is still having several issues that should be investigated more in future:

- *Routing time*: Our autorouter can route up to 60 LEDs in a short time. However, in the case that an user would like to light up 1000 LEDs or more to fill a whole wall or ceiling, a faster algorithm to solve the TSP is necessary.
- *GA Parameters Tuning*: Genetic algorithm is a heuristic algorithm so it is critical to choose the parameters properly. Although we find that the default parameters (result from empirical experiment) in Table 1 is working well in most of the experimental cases, tuning GA parameter will help to improve the performance of the GA TSP solver. In the future, we want to develop our router so that it can dynamically change the parameter based on the number of LEDs and other user-defined constraints.
- *Power Source Placement*: Our current algorithm requires users to place the power pads before routing. This is simple in most of the cases. However, when the number of LEDs increases or the art work is more complicated, it might be challenging for users to decide position of the power pads properly. In addition, current algorithm allow only one power source for the whole circuit which leads to high voltage requirement when the number of LEDs increases. In the future, our autorouter will suggest the number of power sources and the position of each power pad so that the routed circuit meets user-defined constraints (such as time, ink consumption, required voltage of the power source, and aesthetic).
- *Scalability Evaluation*: To assess the scalability of our autorouter, we want to investigate the performance of the router in terms of the number of LEDs, the voltage of the power source, the sheet resistance of the conductive ink, total space that all LEDs occupy, and LEDs distribution.
- *Overlapping*: In our current implementation, we eliminate the crossing edge before brightness balancing using 2-opt algorithm while temporarily ignore the width of the conductive trace. This

approach assure that the TSP route do not have any crossing edge. However, in extreme cases where the routing area is strictly limited by the wiring space or the density of the LEDs distribution, there is a possibility that an anode branch might overlap with a cathode branch causing circuit shorting. This can be prevent by increasing the voltage of the power source. In the future, it is possible to search for a non-overlapping pattern of the TSP routed circuit by either checking for overlapping during TSP search or adjusting the width of the overlapping segments while still assure that the Equation 1 and 2 are satisfied.

- *Power consumption optimization:* The conductive pattern area, resistances, and power source voltage have a tight relationship. Based on this relationship, we may find the adequate trade-off between resistance and power source voltage required to drive multiple LEDs.

2.8 CONCLUSIONS

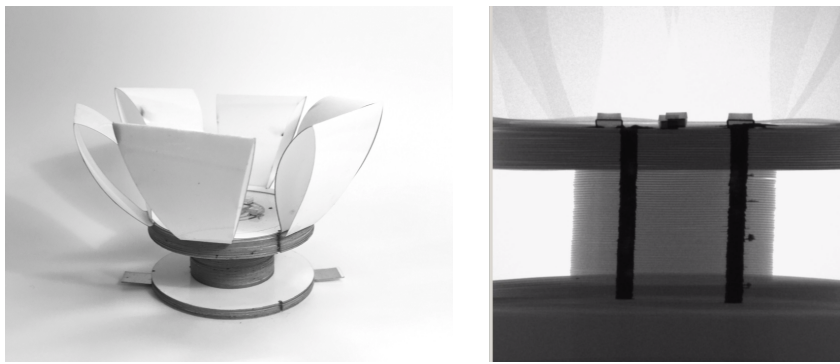
In this section, we addressed the hassle of wiring and balancing brightness of multiple LEDs (single and multiple colors). We proposed an autorouter based on traveling salesman problem and resistance adjustment of the conductive pattern as a designing tool for creating interactive applications with LEDs and conductive inkjet ink. We took advantage of the apparent disadvantage of the conductive ink (i.e., high resistance) to eliminate rigid ballast resistors which are inherently necessary to regulate the LEDs. Besides the deep integration into Adobe Illustrator, our extension provides:

- A tool for arranging and designing with LEDs
- An autorouter based on the traveling salesman problem to find the shortest cross-less path to connect multiple LEDs on a single-layer sheet of paper
- A mechanism of adjusting the width of the conductive patterns to control the resistance to each LED, hence allowing to control the brightness of each LED without the need of additional resistors.

In this research, we aim to support inexperienced users in working with electronic circuits, especially working with conductive inkjet ink and multiple LEDs. Our plugin allows users to focus on creative designing instead of struggling with complicated electronic circuits.

PRINTABLE 3-DIMENSIONAL FABRICATION WITH SILVER NANO-PARTICLE INK

In this chapter, we will add another dimension to the printing of electronic circuits with silver nano-particle ink. In other word, we will scale it from 2D to 3D printing. We will start with fabricating of double sided Instant Inkjet Circuits with via-holes as interconnections between two layers. Build on top of these techniques, we will stack multiple layers of printed circuits to form 3D objects with embedded electrical functionality.



(a) A simple lamp made by stacking papers and silver ink printed circuits. (b) A CT-Scan image of the lamp reveals the vertical interconnections which were made by filling the inner tubes with conductive paste.

Figure 27: An example of Printed Electronic Papercrafts with embedded electronic circuits.

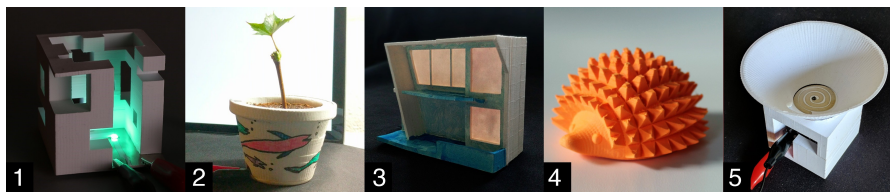


Figure 28: Examples of Printed Electronic Papercrafts: (1) sculptural cube lamp; (2) moisture sensing flowerpot (3) architectural model with simulated lighting; (4) smart toy armadillo with RFID tag; (5) loudspeaker.

3.1 INTRODUCTION: LIMITATIONS OF 2D PRINTING ELECTRONIC CIRCUITS

The rapid prototyping of flexible electronic circuits with silver nano-particle ink has made the process accessible to a wide range of audiences. With one click, users can print a working electronic circuits on a photo paper. However, it is limited to 2D electronic circuits. There exist circuits which cannot be route in a single plane (*e.g.*, LEDs array). Though it is possible to print the circuits in two separate photo papers and attach them back-to-back, establishing the interconnections between the two layers is always a big challenge. These interconnections should be reliable, small in size, high in conductivity, and easy to fabricate. Our proposal, as discussed in Section 3.2, is to poke a hole on a double sided photo paper and fill it with silver nano-particle ink to establish interconnection between the two layers.

Another challenge that is not a 2D print electronic circuit problem but can be tackled with 2D printing is the fabrication of fully functional 3D objects. Orthodox 3D printers only focus on the shape forming of the objects. Therefore, the printed objects are static without any active functionality. In order to bring in active functions such as actuating, sensing, displaying, and communicating, users have to take an extra step of adding electronic components to the printed object. We want to streamline the process by embedding the functionality into the printing process so that the object will be functional object immediately coming out of the printer. The detail process and evaluation is discussed in Section 3.3.

3.2 VIA-HOLE FOR DOUBLE SIDED SILVER NANO-PARTICLE INK PRINTED CIRCUITS

Instant Inkjet Circuits by silver nano-particle ink realized home-brew electric circuit fabrication. However, current method can support only single-layered patterns, and conventional inter-layer connection methods are not suitable. In this section, we will evaluate various easy-to-use inter-layer connection methods by making via holes, especially the ones made by different drilling mechanisms. We show that the felting needle is the best candidate as it can establish good conductivity immediately after nano-particle ink is printed into the hole, without using any curing process. This section will briefly review the key-points of the via-hole for double sided silver nano-particle ink printed circuits. More detail is discussed in [115].

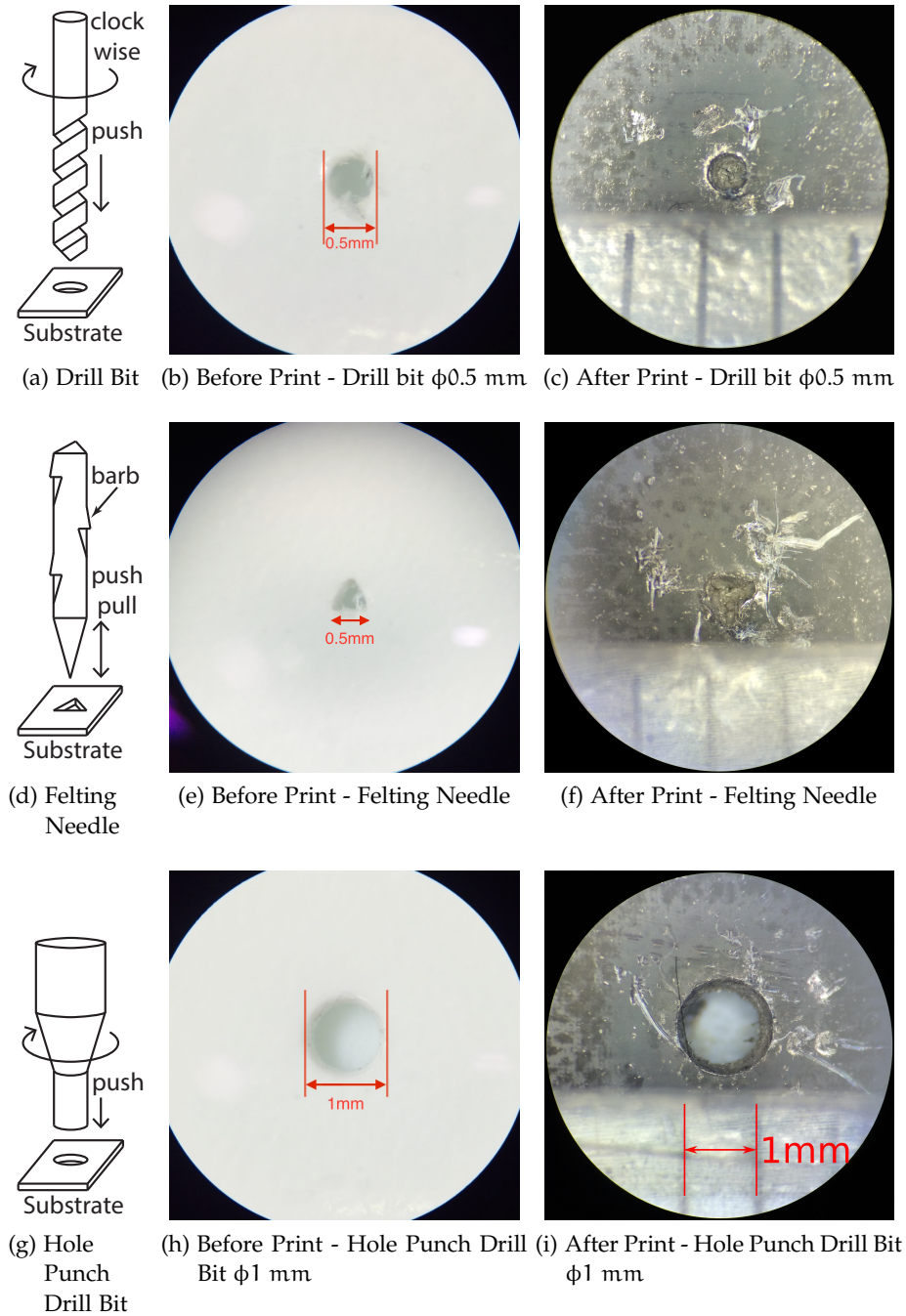


Figure 29: Via hole structure

3.2.1 *Related Works*

3.2.1.1 *Electro-plating PCB vias*

For traditional PCBs, in order to fabricate multi-layered circuits, different electronic nets are formed on separated layers and they are connected using via holes. These via holes are made by drilling tiny holes on the surface of the PCB and filling them with a highly conductive material (typically, copper). A widely used method to fill these holes is electro-plating. Drilled PCB via holes will be rinsed and electroplated in an electrolytes composed of copper sulfate and sulfuric acid, so that conductive material will stick to the inner wall of the drilling holes [129]. Although this method has the advantages of low cost and simple operation, it involves in working with chemical substances which are hazardous and difficult to be used in the rapid prototyping with flexible substrates like paper or film.

3.2.1.2 *Conductive adhesive*

Another approach to filling a via hole without involving in chemistry process is to fill it with conductive adhesives [55, 56]. In this method, tiny holes will be drilled in PCB substrate and a squeegee will pass through this surface, fill the drilled holes with the conductive adhesive. This can make via holes with resistance as low as 0.3Ω . However, due to the use of the conductive adhesive, the whole sample needs to be cured in a high temperature during at least 30 minutes. This is troublesome and time consuming.

3.2.1.3 *Silver nano-particle ink and sintering*

Emergence of new conductive materials at nano size has enabled us to fabricate a conductive pattern more conveniently. Along with this, laser beam has also been investigated and applied to drill via holes on a PCB substrate [28]. By printing silver nano particle ink on an array of laser drilled micro size holes, we can have an interconnection "microvia" structure on the flexible substrate [26]. In this method, after laser drilling and silver nano particle ink inkjet printing, hole array was cured at high temperature for at least 2 hours. This step is important to make the filled holes become conductive. The use of the laser cutter to drill tiny holes is a barrier for this method to approach normal users (to whom possession of a laser cutter is not common). And again, the silver nano particle ink used in this method required thermal sintering, which is not always a convenient way to conduct. Moreover, high temperature curing might affect characteristic of some flexible substrates.

3.2.1.4 *Silver nano-particle ink and rivet*

In another attempt to make double sided circuit with silver nanoparticle ink, a copper rivet has been used to connect 2 circuits in the front and the back sides of paper substrate [5]. Although this method can help to establish vertical interconnection between 2 circuits, the resistance of the connection is still high at 1.45 Ω . Moreover, using rivet requires the applying of silver epoxy to guarantee the contact between copper rivet and printed silver nano-particle ink. This is neither time efficient nor robust.

In our approach, we focus on implementing double sided circuit with a via hole in Instant Inkjet Circuits. The uniqueness of Instant Inkjet Circuits is that it uses silver nano particle ink which does not require thermal sintering or curing after printing. Printed pattern will be chemically sintered at room temperature and become conductive as soon as coming out from the printer. Chemical sintering at room temperature relies on the contact of the silver nano particle ink and special coating layer on the surface of the printed substrate. Our work would be trying to preserve sintering-free characteristic of Instant Inkjet Circuits while making interconnection in double sided circuit. Based on this, we aim at bringing an automatic printing circuit maker to every hobbyist's hand. Toxic materials (chemical substances like strong acids), harmful conditions (like high temperature, high power laser, etc.) should be avoided. We plan to realize an easy-to-use desktop sized system with low electrical power consumption which allows to reduce production cost and turnaround time. Entry level solution might be a low cost special pen to manually make double sided circuit interconnections. A final solution should be a full-automatic system with a specially designed computer-aided design software to print double sided circuits.

3.2.2 *Approaches to Double Sided Flexible Circuit*

3.2.2.1 *Office Supplies Approach*

One of the simplest ways to make interconnections for double sided circuits in Instant Inkjet Circuits is to use office supplies, tools like a stapler (with metal pins) or a crush-style needle-less stapler.

A stapler with metal pins

This was the first option that we have thought of when we tried to make interconnections between 2 sides of paper substrate. We simply made this connection with a metal pin from a stapler. A quick measurement showed that the resistance of an interconnection made by stapling is 6.3 Ω . However, this interconnection is not durable due to the loosening by time at contacting point between the metal pin

and silver nano particle ink. After 3 months, the resistance of the same sample was increased to ten-mega-ohm order. Moreover, with a normal stapler, we can only make the interconnections which are not too far from the substrate edge due to the size of the stapler.

Crush-Style Needle-less Stapler

A crush-style needle-less stapler is one kind of staples that does not have any metal pin. It uses pressure to press separated paper together [37]. At the place of pressing, 2 sides of the paper will be crushed and entangled so that when filled with the silver nano particle ink, this entanglement will help to bind the ink from both sides of the paper. The resistance of the interconnection made by the crushing stapler, as our observation, is more stable than the metal pin stapler's interconnection. The resistance of the interconnection increased from less than 3Ω right after painted with silver ink to 15Ω after 3 months. However, it also bears the limitation of the stapler size. We can only make the crushing interconnections at places where are closed to the edge of the substrate.

3.2.2.2 *Via-hole Approach*

As mentioned above, via hole has been long used as a solution for interconnection in the multi-layered circuit. It is natural to think of using via holes in the Instant Inkjet Circuits. By comparing approaches to make interconnection for double sided circuits (Table 4), we can see that drilling via hole should be selected as its superior over other methods. A stapler or a crush-style needle-less stapler results in large interconnection footprints and cannot make interconnection, far from the edge of the substrate. In contrast, a laser drill gives small footprint and flexibility in the positioning of the interconnection, however, it consumes a huge amount of energy and is difficult to miniaturize the apparatus. Standing out from these, drilling via hole mechanically can safely make small footprint and is flexible in positioning of interconnection without consuming energy.

The challenge is how to not only optimize the via hole quality, but

Table 4: Comparison of approaches to interconnection for double sided circuits

Approach	Footprint	Position	Energy	Danger
Stapler	Large	Near Edge	No	No
Crush	Large	Near Edge	No	No
Laser	Small	Any	Huge	Yes
Via Hole Drill	Small	Any	No	No

also retain the sintering-free characteristic of the Instant Inkjet Circuits. Coating layer on the substrate acts an important role in making the printed pattern conductive. It is necessary to have this coating layer in both edge and inner wall of the via hole. To achieve this goal, drilling operation is evaluated and optimized. We will focus on evaluating differences of the via holes made by different hole openers (drill bits, hole punch drill bits, and felting needles).

Detail of the experiment can be found in [115]. According to the our experiment, holes that are opened by a felting needle and filled with silver nano-particle ink are conductive immediately after printing with resistance $R = 0.56 \Omega$. Footprint of the hole is small and flat which makes it suitable for stacking multiple double sided circuits to fabricate even more complex multiple layered circuits.

3.3 INTEGRATION OF PRINTED ELECTRONIC CIRCUIT INTO 3D PRINTING

We present PEP (Printed Electronic Papercrafts), a set of design and fabrication techniques to integrate electronic based interactivities into printed papercrafts via 3D sculpting. We explore the design space of PEP, integrating four functions into 3D paper products: actuation, sensing, display, and communication, leveraging the expressive and technical opportunities enabled by paper-like functional layers with a stack of paper. We outline a seven-step workflow, introduce a design tool we developed as an add-on to an existing CAD environment, and demonstrate example applications that combine the electronic enabled functionality, the capability of 3D sculpting, and the unique creative affordances by the materiality of paper.

3.3.1 Introduction

Paper is a good medium for prototyping in many fields, including artistic and craft practice, scale models in architectural design, low-cost rapid prototyping for manufacturing, to name a few. Compared with the plastics used in stereo-lithography and fused deposition modeling, paper is inexpensive, lightweight, ubiquitous, and environmentally friendly, and easily affords creative expression. Unlike plastic we can fold, bend, or cut paper; and draw, paint, or print on it. And as electronic components become smaller, thinner, and lighter they can be attached and embedded in products made of paper. We can draw or print circuits on paper and in place of soldering, we can glue or tape electronic components.

While traditional papercrafts commonly cut, bend, and fold paper in its natural sheet form, cutting and laminating many sheets together creates solid objects similar to what 3D printing methods produce. As this selective deposition laminating (SDL) method involves removing material from each sheet before gluing cut sheets together, we refer to the process as '3D sculpting'. In the PEP project we integrate electronics into sculpted papercraft and ask: What unique expressive and technical possibilities might this combination enable?

Sculpting electronic papercrafts is a powerful technique that opens a new creative space in rapid prototyping of interactive products. Figure 27 and Figure 28 show several examples made using PEP techniques: Printed conductive layers embedded into 3D sculpted papercrafts, for instance, can light a lamp (Figure 28-1), sense moisture (Figure 28-2), or amplify sound (Figure 28-5). Electroluminescent layers (Figure 28-3) and RFID tags (Figure 28-4) can be fastened to paper and embedded into the product. We stack paper and insert functional layers with printed conductive traces, cut the paper to form 3D objects, extend circuits by bending sheets or carving vertical channels on the conductive printed parts and decorate the resulting objects with craft supplies.

The PEP (Printing Electronic Papercrafts) project comprises a software editor and a set of fabrication techniques. The editor enables a designer to select a 3D model from a database, embed functional layers of electronics into the model, and modify its structure to connect functional layers into a single circuit. Our fabrication techniques support design and engineering to embed actuation, sensing, display, and communication into sculpted 3D products.

3.3.2 Contributions and Benefits

The main contributions of this work are:

- Design techniques and process to creating 3D electronic devices from a stack of paper;
- A design platform add-on to an existing CAD environment, with a database of tested and parametric electrical and geometric components;
- Primitives that demonstrate the integration of four functions into 3D paper objects: actuation, sensing, display, and communication;
- Examples that show how PEP software and fabrication techniques generate new expressive possibilities.

Advantages of 3D Sculpting Paper

Our paper manufacturing techniques have several advantages over existing multi-material 3D printing processes that can print electronic products such as thermoplastic based Voxel8 [124] and photocurable resin based ChemCubed [16].

1. Paper is widely available, accessible and affordable and we integrate it with thin film electronic components. The main material we use in PEP is common office copy paper, which is ubiquitous and recyclable. Likewise, thin film electronic components, which we combine with plain paper, are widely available, accessible and affordable. Benefitting from the recent development of thin film- and paper-based electronic printing technology, PEP enables designers to deploy a larger variety of functional components, from simple resistive heating coil (Figure 47) to RFID tags (Figure 44).
2. 3D electronic papercrafts are robust. Embedding electronic parts in a PEP object produces more durable products than other approaches. For instance, Voxel8 [124] is a commercial 3D electronic printer that integrates fused deposition modeling (FDM) and conductive paste extrusion. According to the Voxel8 design guidelines, the silver shrinkage buffer is 40%. Therefore, the connections of the circuit inside a Voxel8 printed object tend to break due to differential thermal shrinkage between the non-conductive thermoplastic and the conductive silver paste. We use silver nanoparticle ink to print conductive traces on functional layers, which minimizes thermal movement.
3. 3D papercraft leverages the unique material properties and aesthetics of paper. An engaging medium enables continuous experimentation, which yields a variety of outcomes [67]. Paper's

unique materiality, which encourages diverse expressive exploration, explains why traditionally many creators prototype with paper. By augmenting paper prototypes with functional behaviors PEP can be a compelling medium for interaction designers. For instance, Figure 41 shows an architectural model 3D sculpted with embedded electroluminescent layers and painted in watercolor. Novices with little or no experience in 3D design or electronics can also employ it as a quick way to embed rich features into 3D printed objects.

3.3.3 *Related Works*

3.3.3.1 *2D and 3D Printing of Electronics*

Traditionally, prototyping of electronic circuits has been done by subtractive techniques such as etching or milling. Recently, however, the development of printable conductive material has enabled an alternative prototyping approach that leverages additive manufacturing processes. One popular approach is 2D inkjet printed circuits [31, 32, 53]. Recent work also highlights the combination of automated pick-and-place and elastomeric conductor extrusion for sheet-like electronic material [122].

The emergence of multi-material 3D printing suggests integrating electronic circuit into 3D printed objects. Voxel8 [124] implements this by printing conductive paste at the same time as thermoplastic materials. However, the resolution of electronic circuit printing is low, and the difference in thermal expansion of conductive paste and thermoplastic results in broken connections inside the 3D printed structure. The ChemCubed process [16] uses inkjet printing to deposit silver nanoparticle ink along with a UV-cured polymer. However, the printed object requires sintering to make the electronic pattern conductive, and the machine is expensive.

3.3.3.2 *Integrating Interaction into 2D and 3D Printing*

Several efforts integrate interaction in 3D printing for rapid prototyping of interactive physical objects. For example, Pineal [58] allows a user to integrate a smart watch or phone into 3D models. The user can specify high-level behaviors of the interactive 3D printed objects through a specialized design tool and programming environment. Similarly, .NET Gadgeteer [123] also provides a means for rapid prototyping of the interactive behavior embedded into the 3D printed objects. However, integrating interaction with a micro-controller or a smart watch or phone can be costly and require adopting a particular toolkit. In contrast, our approach using embedded electric circuits is more inexpensive and affordable. As circuit design may require users

to make lower level decisions, we provide a database of designs and a novice design tool to support the design process.

Similar to our approach, SurfCuit [120] integrates circuits into 3D printed objects. Whereas SurfCuit installs a circuit on top of a surface of a printed object, PEP embeds the circuit into 3D printed papercrafts. Recently, several works have explored the embedded approach to integrate interaction. This includes 3D printed objects that can sense deformation [10, 103] or touch [102] using carbon doped thermoplastic. Taking an inspiration from these works, we expand the design space of embedded interaction not only in sensing, but also in actuation, display, and communication.

Multi-layered material fabrication with different material properties in the composite is prepared by conductive inkjet printing or screen printing. These material composites are used for actuation [38], display [79], and sensing [80]. Or, using both additive and subtractive methods via a laser cutter, rigid, bendable, and flexible properties are embedded into the composite [87]. Whereas previous works developed “smart” sheets and used them to create 3D shapes by bending and folding, instead we sculpt a volume of a stack of paper. Our application examples demonstrate that our different approach enables a unique design space.

To employ soft and flexible materials for 3D printing, researchers have experimented with needle felted yarn [48], fabric [86], and textiles [93]. Whereas previous work used only additive manufacturing, our effort, which combines additive and subtractive methods adds another material, paper, into the list of nontraditional, soft, and flexible materials for 3D printing.

3.3.3.3 *Electronic Papercrafts*

Researchers have demonstrated design and fabrication techniques to integrate electronic and computing components with various forms of papercrafts such as a pop-up book [90], an invitation card and a headphone [107], a robot, a speaker, and a lamp [99]. To empower the creation of electronic papercrafts, conductive connection methods employing craft supplies, such as conductive tape, pen [20, 25], paint [10] and stickers [17, 42] have been developed and some have become inexpensive off-the-shelf products.

PEP explores the combination of electronics and papercrafts to enable a new creative space, and focuses on such integration by digital fabrication, in particular 3D sculpting, whereas previous work investigated embedding electronics into paper mostly by handcrafting techniques.

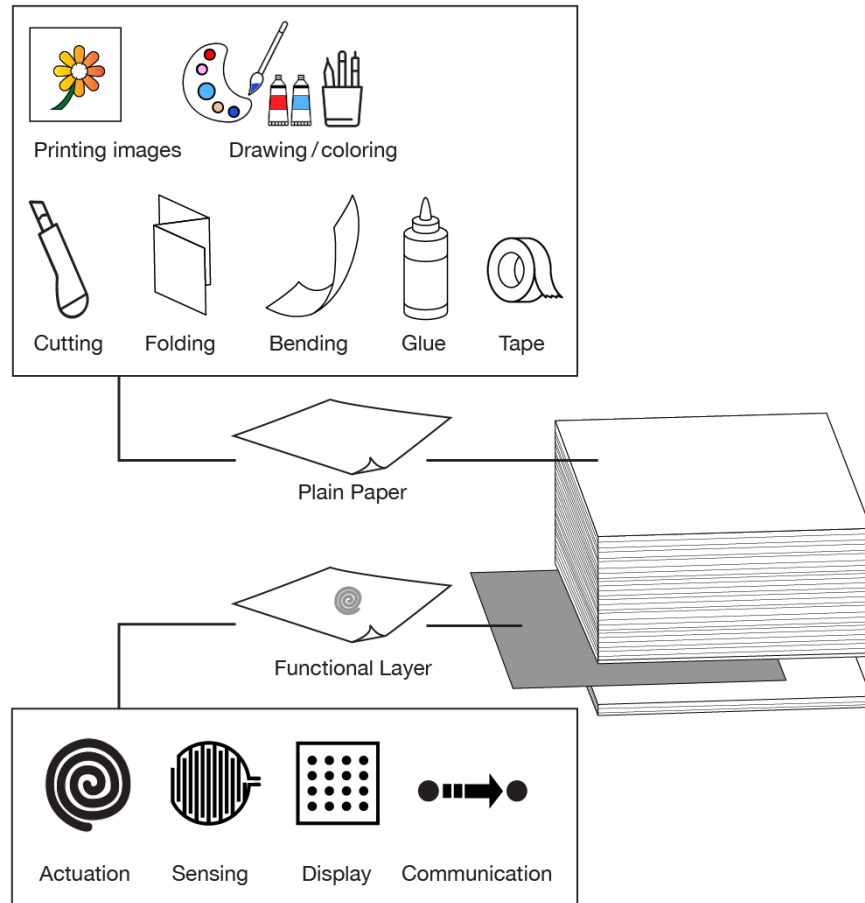


Figure 30: Composite structure of paper and functional layers. Paper supports cutting, folding, and bending to construct 3D forms; craft techniques add images and colors. Functional layers embed actuation, sensing, display, and communication.

3.3.4 Overview: Printed Electronic Papercrafts

PEP is a body of techniques to integrate interaction into printed papercrafts via 3D sculpting. We explore the design space of PEP in four functional aspects: actuation, sensing, display, and communication. When we insert these functional layers into a stack of plain paper, we can form 3D products that also embed interactive functionality. Each sheet of paper is thin, flat, and flexible; we stack many sheets to create volumetric solids while retaining the affordances of paper. Hence, integrating a stack of plain paper with paper-like functional layers can provide new expressive and technical opportunities for human-computer interfaces and applications (See Figure 30).

In order to sculpt a product from a stack of paper, we use Mcor's IRIS printer [68]. This printer applies glue to the layer on the build platform, advances a sheet from the paper tray and attaches it to the

stack on the build platform, cuts a slice of the 3D form in the top sheet, and repeats this process. It produces a volumetric object using the stack of paper and embeds functional layers within the object.

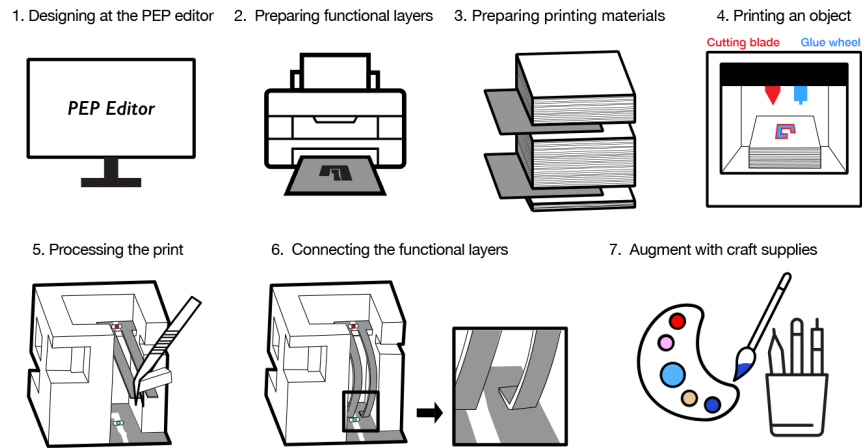


Figure 31: PEP design and fabrication process.

3.3.5 PEP Fabrication workflow and Techniques

Figure 31 shows how we use the PEP techniques to create a printed electronic papercraft. We design with the PEP editor, develop functional layers, compose a stack of paper with the functional layers, print 3D products, connect the functional layers, and decorate the product using craft supplies.

Step 1: Design the 3D Form in the PEP Editor

We use the PEP editor add-on in Autodesk's Fusion 360 [9], a widely-used existing CAD application. We can design a new 3D model or import one from our library. Then, selecting a surface in the model brings us to the next step: choosing a functional component to apply, and adjusting parameters or positions of the imported components. Once the design process is completed, we can download the functional layers as PDF files and the 3D model as an STL or OBJ file.

Step 2: Prepare Functional Layers

The functional layer can be prepared with different processes such as inkjet printing, silkscreen printing or simply attaching thin-film electronic components to paper.

Inkjet printing: We print conductive patterns with silver nanoparticle ink using a commodity inkjet printer. The printed silver ink can serve as wiring traces for LEDs, capacitive or resistive sensing, and coils for RFID tags or sound production. Passive components such as resistors, capacitors, and inductors can be designed and printed directly with silver nanoparticle ink.

Silkscreen printing: Some materials cannot be inkjet printed; these we prepare by hand. We used silkscreen printing to

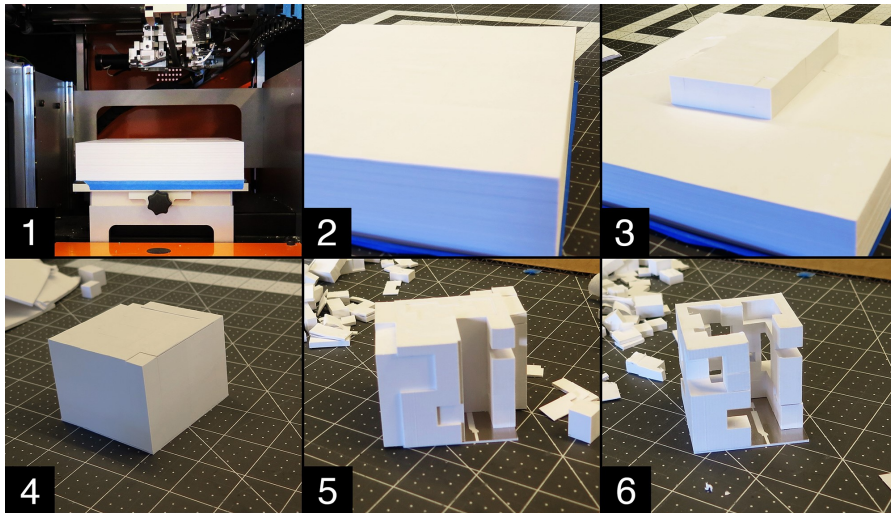


Figure 32: Extracting the rest of the printed object by using a tweezers and fixing damaged parts with craft supplies.

make cuttable electroluminescent sheets for lighting applications.

Attaching: Many electronic components are becoming smaller, thinner, lighter and commercially available. We can attach them to a paper sheet with glue, paint, or tape. The printer grabs, stacks and glues the sheet along with its electronic component: an RFID tag, bend sensor, or any thin-film electronic component.

Step 3: Prepare Printing Materials

Now we prepare the input stack of paper, inserting the functional layers at positions indicated by the PEP editor. The Mcor IRIS printer calculates the number of sheets, counting 0.1 mm per sheet; 100 sheets will produce a 10 mm height object.

Step 4: Sculpt a 3D Model

Now we load the 3D modeling file into the Mcor application and set the position and orientation of the imported model for sculpting. Essential here is to place the 3D model with functional layers horizontal. The build size is $9.39 \times 6.89 \times 5.9$ inches (using US letter size) or $256 \times 169 \times 150$ mm (using A4 size paper).

Step 5: Post-Process the Print

When the Mcor printer is finished, we unload the platform and extract the sculpted product. We use tweezers to remove small bits of waste material (See Figure 32).

As the product comprises many attached layers of thin sheets, it is easier to remove parts in the horizontal direction than vertical.

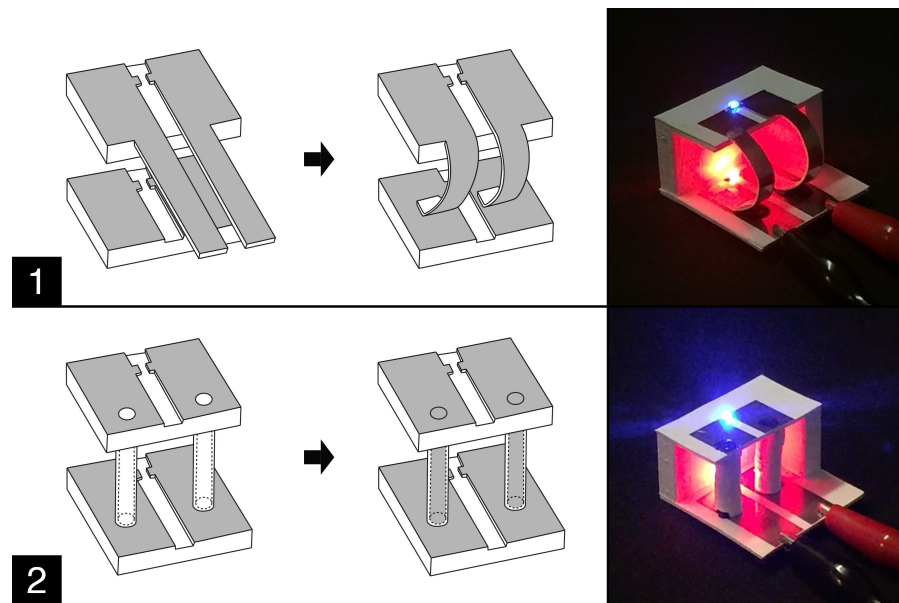


Figure 33: Two methods to connect multiple functional layers: (1) extending and bending conductive parts (2) carving channels and filling them with conductive material.

Removal is also more likely to damage horizontally attached parts than vertically attached ones (See Figure 48). Damaged parts can be repaired using a knife, glue and tape. At this stage, we also fix any connections in the functional layers that were damaged while printing.

Step 6: Connect Functional Layers

We can connect multiple conductive layers into one circuit by either (1) extending a printed circuit layer and bending it to connect with another layer, or (2) filling vertical channels with conductive adhesive (Figure 33). We can choose either method in the PEP editor, and the editor adjusts the model. For bending, the thickness of the extended parts is 0.2 mm, which employs two sheets of paper in order to support smooth bending. For carving the channels, we made the outer diameter 5 mm and the internal hole diameter 3 mm.

Step 7: Augment with Craft Supplies

The unique materiality of paper products enables various expressive explorations. We can decorate and color using craft supplies such as pens, watercolor, and acrylic paint. Especially as the PEP techniques add electronics into papercrafts, it opens another expressive exploratory space. For instance, we can integrate heat-generation in the printed object and add changing colors using thermochromic pigment (Figure 47).

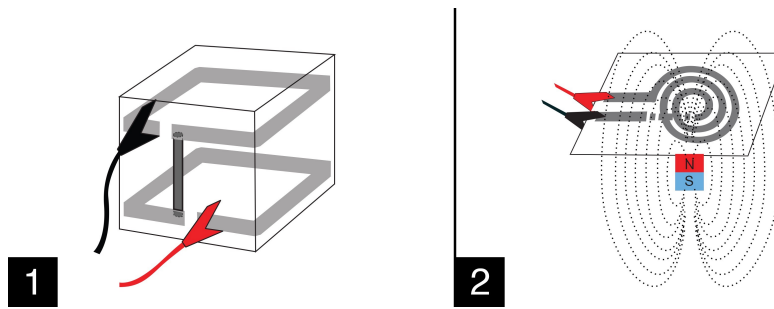


Figure 34: Embedding coils into 3D printed papercraft enables us to make actuators such as a heater (1) and speaker coil (2).

3.3.6 PEP Functional Primitives

We developed four types of functional primitives: actuation, sensing, display, and communication.

3.3.6.1 Actuation Primitive

Stacking conductive printed patterns during the crafting process enables us to embed actuators into the 3D printed papercraft. We introduce two simple actuators that can be embedded by printing a coil with silver nanoparticle ink.

Heater: A heater can be embedded into the 3D printed product by stacking a conductive ink meander printed resistor between sheets of plain paper. To distribute the heat more evenly in the 3D structure, several silver nanoparticle ink printed coils can be stacked on successive sheets of plain paper. We connect conductive traces on the different layers with conductive epoxy [23] to form a single larger coil-type heater (Figure 34). When a suitable voltage is applied, the conductive pattern generates enough heat to change the color of thermochromic ink or actuate a phase change pouch motor [74].

Sound Amplification Coil: A printed coil actuates a vibration membrane when embedded into a 3D printed papercraft. When we place the printed object into a magnetic field and connect a signal to the coil, depending on the amplitude of the signal, the magnetic force between the magnet and the coil causes the paper to vibrate and produce sound as a speaker [84].

3.3.6.2 Sensing Primitive

Users can embed various sensors into 3D sculpting electronic papercrafts so that the printed product recognizes changes in its surroundings. We can use existing thin-film sensors or design custom sensors and print them with silver nanoparticle ink.

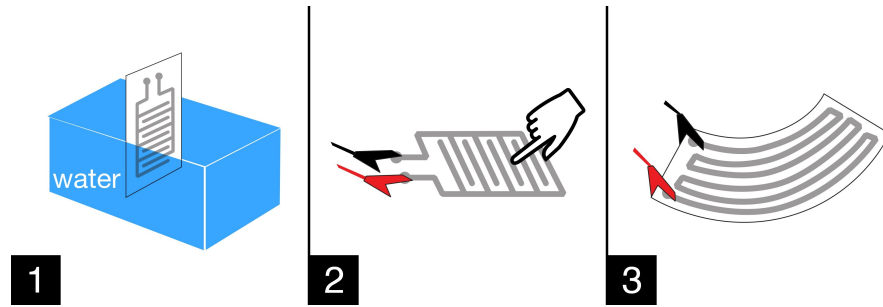


Figure 35: (1) Printed interdigitated capacitors sense the presence of water and humidity, and (2) human touch. (3) A printed resistor can also act as a bend sensor.

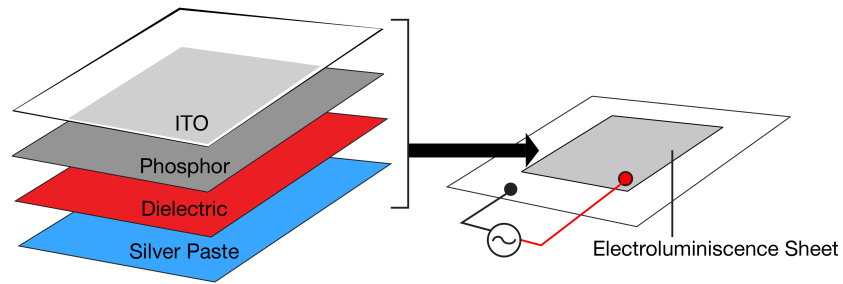


Figure 36: Structure of an electroluminescent sheet.

Capacitive Sensing: Figure 35 shows our printed capacitive sensor, an interdigitated capacitor. It can sense moisture and also functions as a touch sensor, providing an input channel for users to interact with the finished product.

Resistive Sensing: A silver nanoparticle ink printed pattern will change its resistance responding to an external stimulus. The resistance of a long ‘wire’ of silver nanoparticle ink changes when we bend the printed substrate. The resistance returns to the initial value when the substrate is no longer bent. Using this property, we can print a bend sensor with silver nanoparticle ink [121].

3.3.6.3 Display Primitive

Electronic components embedded into a 3D printed product can function as output for the model.

LED: An LED is among the most commonly used elements to display information. After sculpting the product, LEDs can be attached to printed traces using conductive glue.

Electroluminescence: Electroluminescent (light emitting) sheets can be fabricated by silkscreening [79]. We sequentially silkscreened phosphor, dielectric and silver paste layers on top of an indium tin oxide

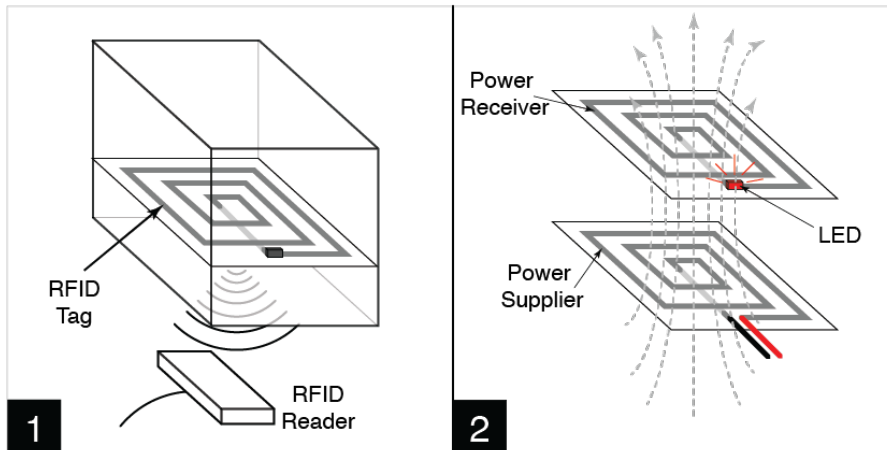


Figure 37: (1) Thin-film RFID tag and (2) wireless power transfer can be embedded.

(ITO) sheet [24] to make an electroluminescent sheet (see Figure 36). This produces a more subtle lighting effect than LEDs.

3.3.6.4 Communication Primitive

A communication primitive enables 3D printed papercraft objects to interact with other devices.

Radio-frequency identification (RFID): RFID tags, especially thin-film ones, are common in everyday applications such as tracking or advertising. With PEP fabrication, we can easily embed thin-film RFID tags in the stack of plain paper to make the 3D printed papercraft identifiable by an RFID reader (as shown in Figure 37–1).

Wireless Power Transfer (WPT): With the same mechanism of embedding thin film coils into the 3D printed papercraft, we can eliminate a battery or the need for a wired power source. Receiving coils for WPT can be printed with silver nanoparticle ink, see Figure 37–2, (though efficiency will suffer due to the high resistance of the printed pattern - about $0.2 \Omega/\square$). The silver printing can be strengthened by electroless (chemical) plating on thin-film to obtain low resistance coils [25].

3.3.7 Software Design Interface

We learned through initial prototyping of manual design and fabrication that PEP prototyping requires three different tasks: (1) designing functional layers, (2) integrating functional layers into 3D models, and (3) supporting the fabrication process, specifically file exports, precise measurements, and manual configuration of these parts. We found that the design workflow can be tedious and time consuming, which inhibits free design exploration. So, to enable users to easily design

and fabricate PEP objects, we developed a software tool specifically designed to support end-to-end design of PEP prototypes. The tool introduces two main components: a database for functional components and an interactive editor. The database of functional paper circuits enables a designer to browse and select desired functions without creating from scratch, while allowing the designer to modify the circuit. The interactive editor enables the designer to integrate functional components into an existing 3D model. The editor also provides instructions for fabrication.

To show how our design tool supports the design workflow, Figure 38 shows a step-by-step walk-through:

1. Load a 3D model. Select a function layer component from the database and a surface for the functional layer (Figure 38-1).
2. Apply the functional layer to the selected surface of the model and customize the design of functions (Figure 38-2).
3. More than one functional layer can be applied. Users can connect multiple functional layers to combine them in one circuit (Figure 38-3).
4. Once the user finishes the design process, they can export the functional layers as PDF files well as the 3D model as OBJ/STL files (Figure 38-4).

For the design and integration of functional layers into 3D models, we developed an interactive editor, specialized for the design of PEP products. Most designers prefer to continue using the design software with which they are familiar rather adopting an entirely new editor. Therefore, we decided to provide our software tool as an add-on to a commonly used 3D CAD tool, Autodesk Fusion 360.

In order to integrate functionality into a 3D model, a user selects components to be applied. As designing reliable electronic functional components can be difficult for designers who lack a technical background, we provide a database of functional components, including circuits for LEDs, switches, capacitive and resistive sensors, and coils. Each functional component is described parametrically, enabling a user to modify and extend designs without sacrificing functionality. The components are designed as two-dimensional sketches. The database is an online repository that designers can browse and select designs from to import into their models. Designers can customize components within the PEP editor as well as design functional components from scratch and add them to the component database. Next, the user selects a face of an existing 3D model to apply a functional layer. Currently, the designer can only apply a functional layer to horizontal or vertical surfaces. When a vertical surface is selected, the

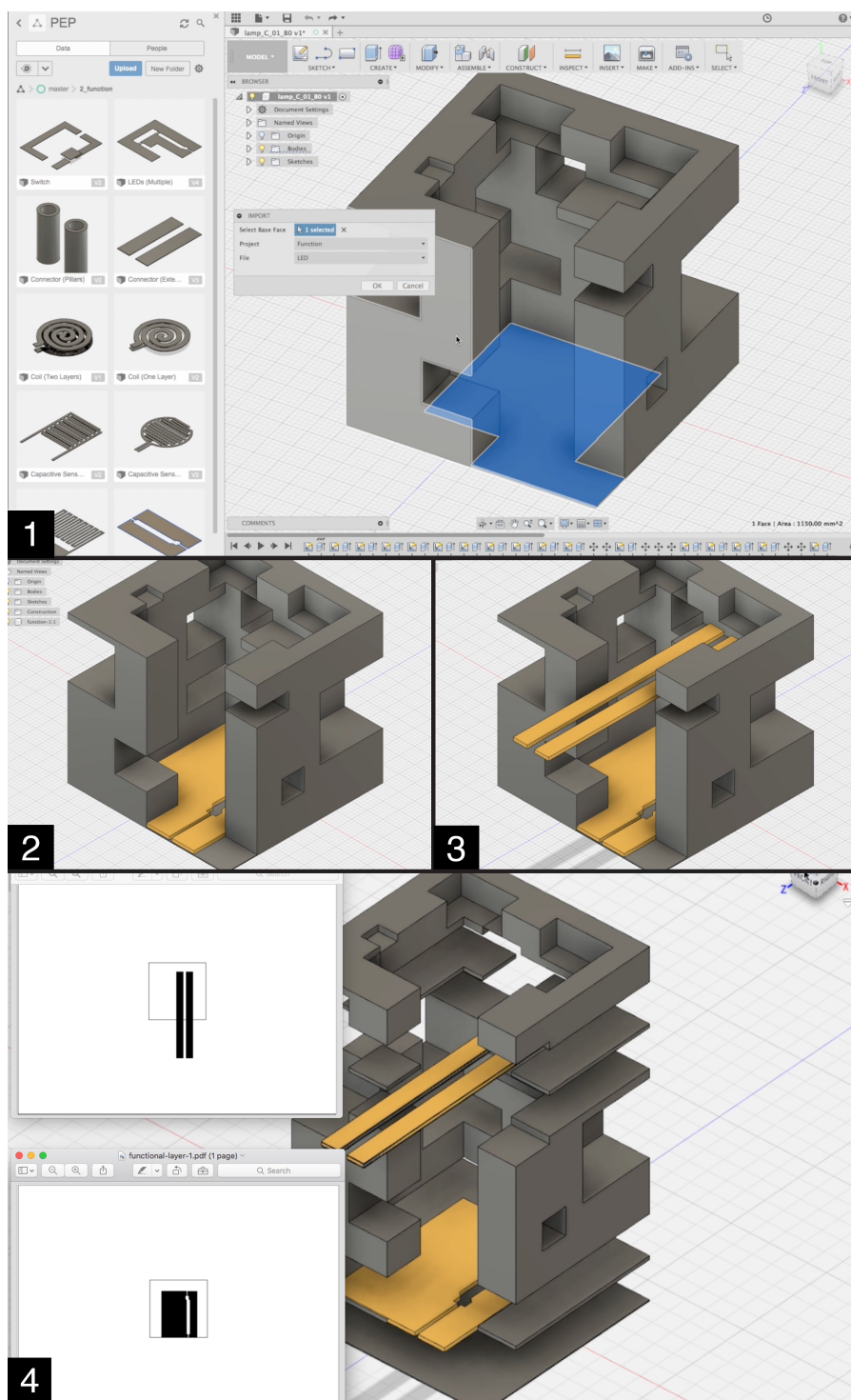


Figure 38: Design of a cube lamp in the PEP editor.

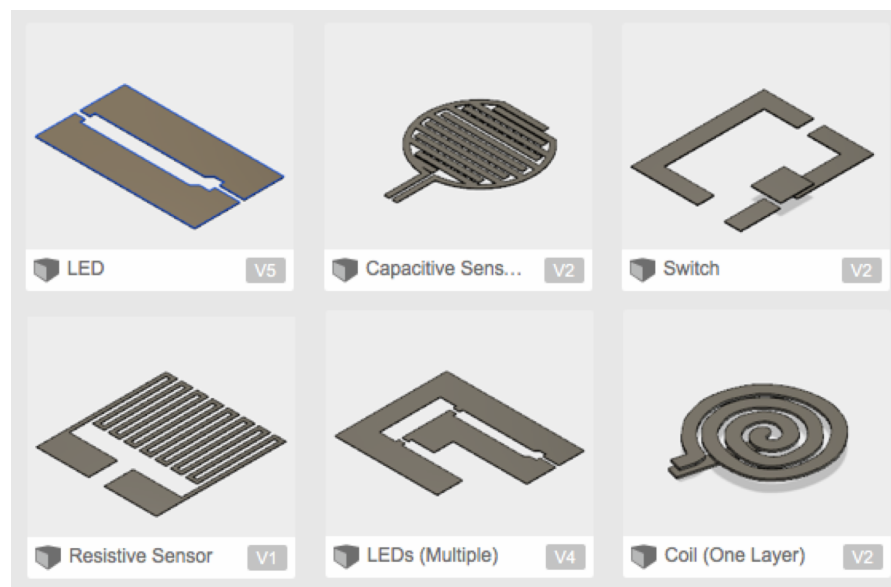


Figure 39: Components in the PEP database.

system automatically rotates the model.

Once the designer selects a face, the editor automatically inserts the functional layer into the selected horizontal or vertical surface. The user can interactively change the design and parameters of inserted layers by direct manipulation. To add layers the designer repeats the workflow outlined above. To connect layers, the user can choose from two methods: connecting with a conductive channel or pillar or bending the sheets with conductive traces.

After completing the design, the designer exports the functional layers and the modified 3D model as PDF files and STL/OBJ files respectively. To support the following fabrication stage, the software provides guidelines, such as where in the paper stack to insert the functional layer(s) and the horizontal offset of the printed circuit.

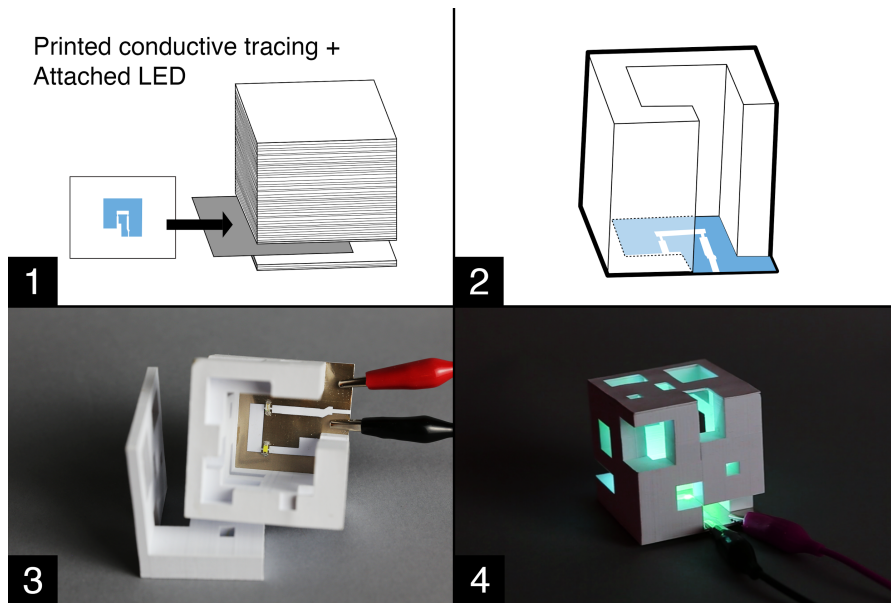


Figure 40: Fabricating a cube lamp: (1) inserting a functional layer with two attached LEDs and printed conductive traces into a stack of paper; (2) sculpting the cube with the Mcor IRIS printer; (3) inside the printed cube lamp; (4) connecting to power to light LEDs.

3.3.8 Applications

To illustrate the breadth of possibilities of the PEP editor and fabrication techniques, we built eight prototypes for functional layer integration: four display examples using LEDs and electroluminescent sheets; a sensing example using a moisture sensor; and communication using a RFID tag, and a sound actuation example using printed coils and a heat generating coil. Three of these prototypes also illustrate connected multi-layered functional embedding.

3.3.8.1 Simple Functional Layer Implementation

Cube lamp

A sculpted 50 mm cube lamp demonstrates a printed electronic papercraft with a display primitive, LEDs. It is sculpted from a stack of paper with one functional layer made by printing conductive traces on paper and attaching two LEDs with conductive glue. The LEDs light up when power is connected.

Architectural model

Architects develop and communicate design ideas with architectural models, and paper is often used to make these models. This application shows how printed electronic papercraft using another display primitive, electroluminescent sheets, can be used in architectural model-making. We attached electroluminescent sheets to ‘carrier’ sheets of paper, inserted them into a paper stack, sculpted the

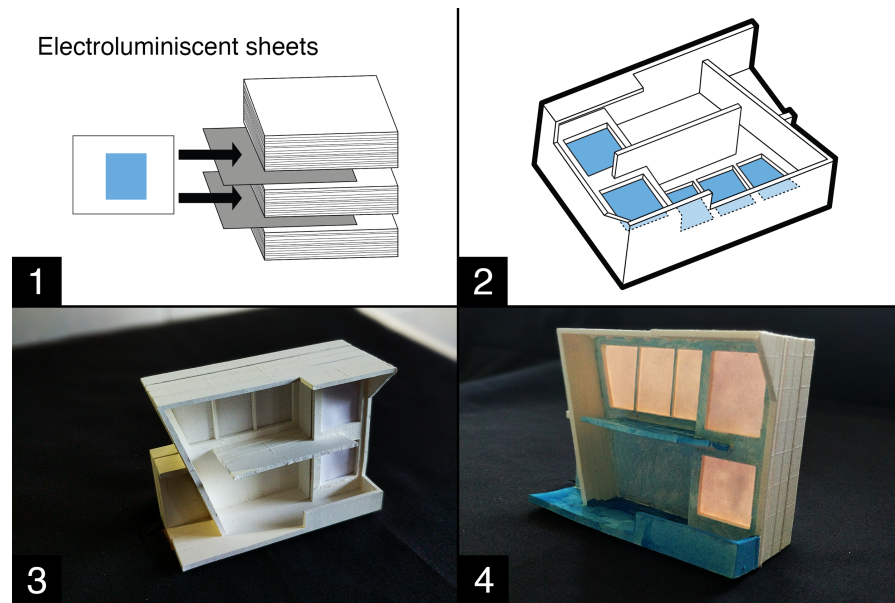


Figure 41: Fabricating an architectural model: (1) inserting two electroluminescent sheets in a stack of paper; (2) 3D sculpting the model; (3) the resulting model; (4) painted in watercolor and equipped with electroluminescent layers.

architectural model, and painted the model with watercolors. When power is connected the windows in front of the electroluminescent sheets light up.

Photo frame We can also use an electroluminescent sheet to print a photo frame that illuminates a photo when the surroundings are dark. We included a photo-printed paper sheet and an electroluminescent functional layer in a stack of paper and 3D sculpted a photo frame. When the photo frame is in a dark room, it lights the functional layer to make the embedded photo visible. This application demonstrates another use of an electroluminescent sheet and combines an image printed paper sheet in 3D sculpting electronic papercrafts.

Water sensing flowerpot

This flowerpot application demonstrates integration of a sensing primitive into the printing. We produced the functional layer by printing conductive traces, inserted it into a stack of paper, and sculpted a flowerpot. We decorated the pot with colored pens and sealed the inside and outside with two thin layers of Mod Podge [73]. Then we connected the sensing layer to an Arduino microcontroller programmed with capacitive sensing [8] code, showing users when to water the plant. The flowerpot example shows how paper's physical properties can be augmented. Although paper is sometimes seen as a 'weak' medium, depending on design and fabrication we can strengthen paper with post processing techniques.

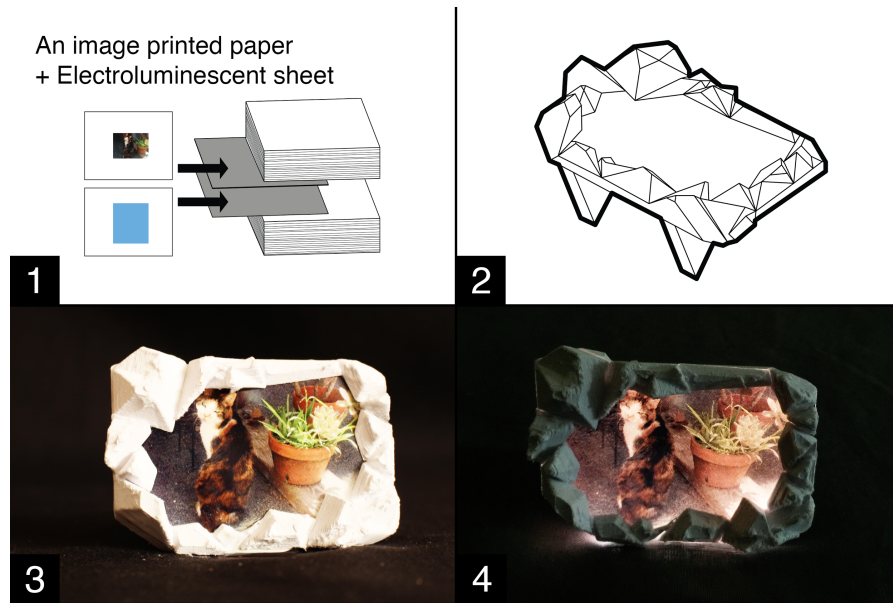


Figure 42: Fabricating a photo frame: (1) a photo printed layer and an electroluminescent functional layer; (2) 3D sculpting a photo frame; (3) the resulting product; (4) lighting the functional layer displays the embedded photo.

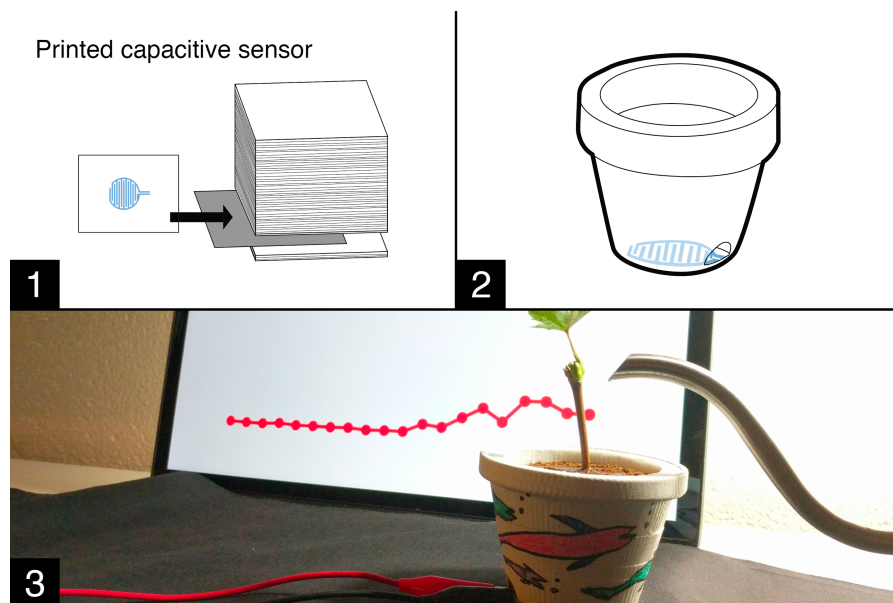


Figure 43: Fabricating a flowerpot: (1) a water sensing layer with printed conductive traces is inserted into a stack of paper; (2) printing a flowerpot with the sensing layer on the bottom; (3) We decorated the printed pot with colored pens. The graph on the screen behind the plant shows soil moisture as we water the plant.

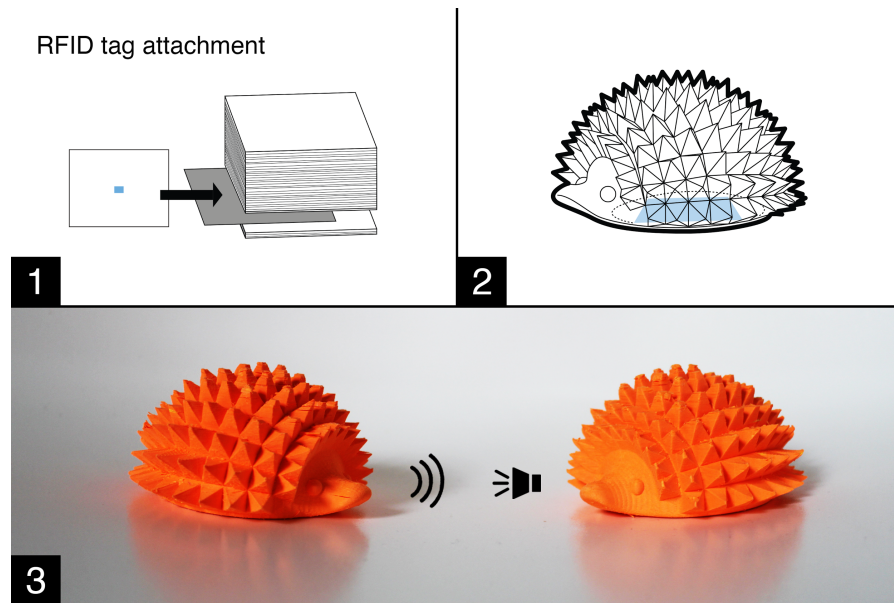


Figure 44: Fabricating a smart toy hedgehog: (1) attaching an RFID tag sticker to a sheet and inserting it into a stack of colored paper; (2) sculpting a toy; (3) a partner toy with an embedded RFID reader senses the RFID tag and plays a melody when it is within 10 cm.

Smart toy

Many electronic components are thin, flat and cuttable, and some can be attached as a sticker without soldering. We made a 'smart toy' hedgehog, inserting into a stack of colored paper one functional layer with an RFID tag sticker. When we place the toy near a partner toy (with an embedded the RFID controller [2] and Arduino micro-controller), the partner toy plays a melody on its buzzer.

3.3.8.2 *Connected, Multiple-Layered Function Implementation*

Multicolor cube lamp

We extended the sculpted cube lamp presented earlier to make a lamp with LEDs on different layers. This application demonstrates a method of connecting circuits on different layers by extending and bending the printed conductive traces. We started from the same cube model as the one-color cube lamp. Then, in the PEP editor we added another functional layer and selected the connection method to automatically extend the conductive traces of the upper functional layer. During fabrication, we prepared two functional layers with display primitives: red LEDs for one layer and green ones for the other. We inserted these into a stack of paper, which we used to sculpt a cube lamp. Next we connected the extended conductive traces on

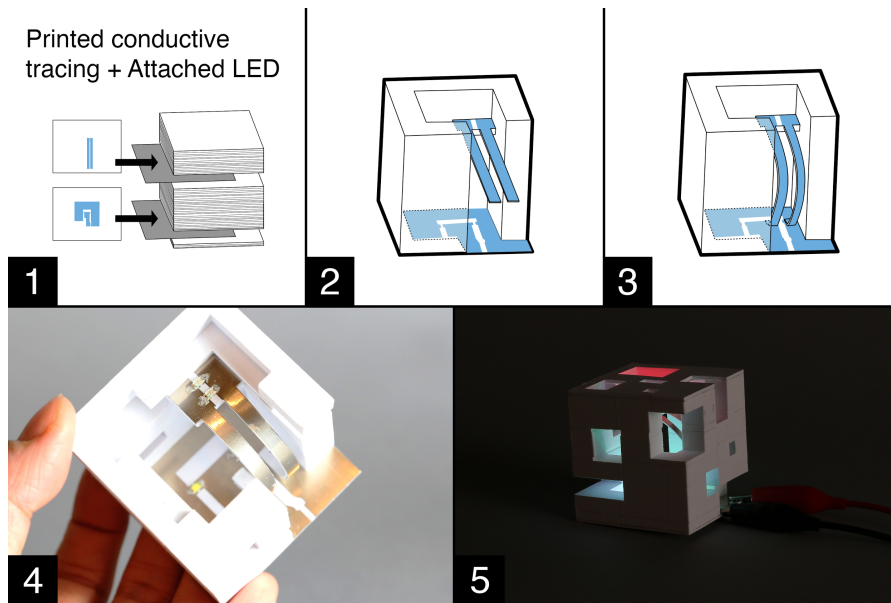


Figure 45: Fabricating a multicolor cube lamp: (1) preparing a stack of paper with two functional layers with different color LEDs; (2) sculpting the form; (3) bending the upper functional layer and attaching it to the lower layer; (4) inside of the lamp; (5) when power is connected, LEDs on both layers light up.

the upper functional layer to the lower layer by bending and attaching them with conductive glue. When power is connected, this bicolor lamp lights red LEDs on the upper layer and green LEDs on the lower layer.

Loudspeaker

This speaker application demonstrates another actuation primitive, a sound amplifying (voice) coil, and a connection method, filling vertical channels with conductive glue. We started by preparing two printed coil layers (a single three-winding coil produces too weak a sound) and a stack of paper for 3D sculpting. After sculpting the form, we connected the coils on two layers with conductive epoxy. In order to reduce resistance of the printed coil by thickening the conductive traces, we printed the coils several times on each sheet. After attaching the coils on different layers, we connected each terminal of the coil to a melody circuit and placed a magnet below.

Color-change cup holder

A cup holder demonstrates a heat generating coil application with thermochromic color change pigments. We developed a cup model in five parts, planning to embed four layers of coils between the parts. Then we printed four coil layers with a stack of paper and 3D sculpted all parts. Using the printed parts, we assembled the parts from the bottom using paper glue and connected the coils with

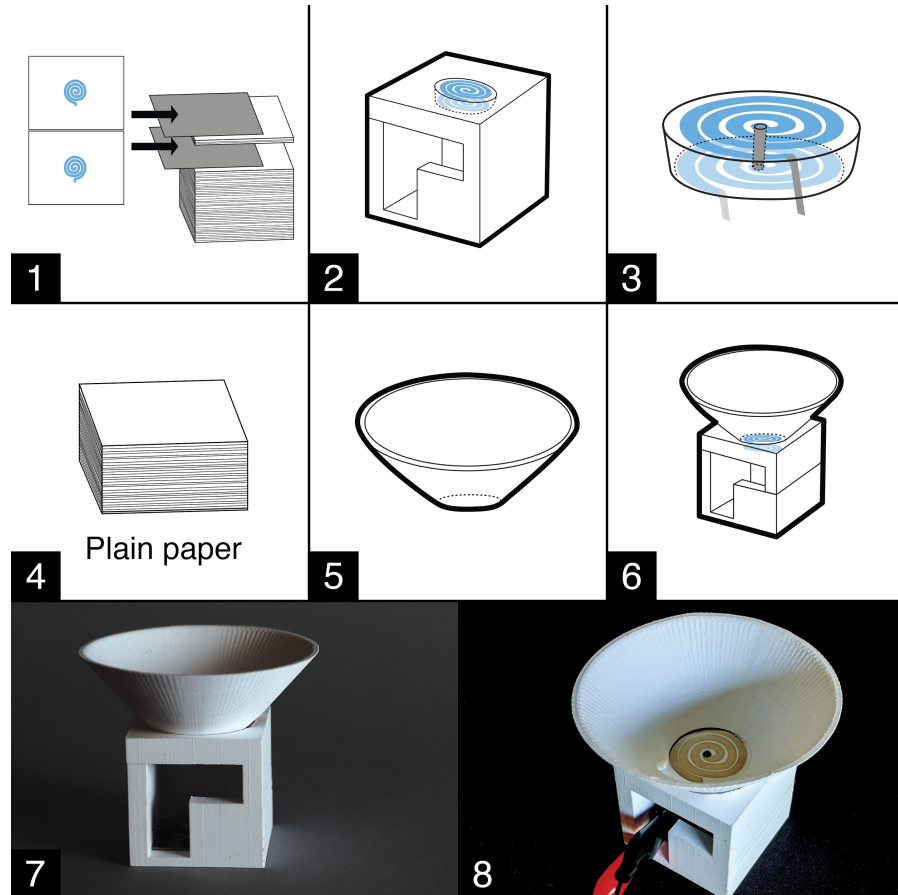


Figure 46: Fabricating a speaker: (1) inserting two printed coil layers into a stack of paper; (2) sculpting a speaker with coils on different layers; (3) connecting coils by injecting conductive epoxy into cross-layer channels; (4) preparing a stack of paper; (5) sculpting a cone; (6) attaching it to the body; (7) the combined model; (8) connecting the coil to a melody circuit.

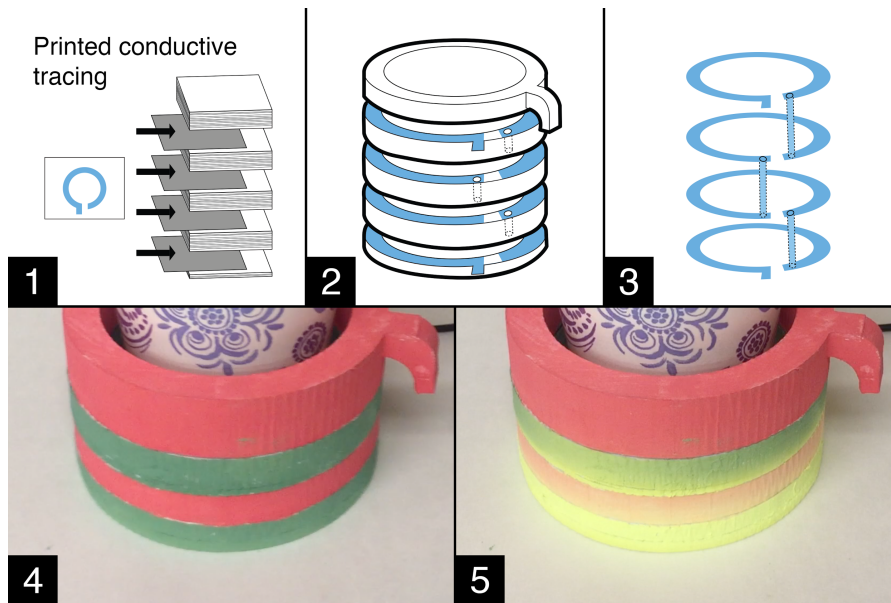


Figure 47: Fabricating a cup holder: (1) combining four functional layers of printed coils with a stack of paper; (2) sculpting five parts of the cup; (3) connecting the coils by injecting conductive epoxy into the cross-layer channels; (4) the applied thermochromic color without heat; (5) color changes when the power is connected by heat generation.

conductive epoxy. Once the cup holder was dried and cured, we painted thermochromic pigments and connected power to see the color changes. The coil resistance was 80Ω and we connected to 12 V , therefore the power dissipation was just 1.8 W , enough to produce color changes but not to make the surface too hot.

3.3.9 Limitations and Future Work

Our PEP techniques have unique limitations; this leads us to propose a call for future work:

- The Mcor IRIS printer for 3D sculpting constrains the size, thickness (weight), and texture (slipperiness) of material. We can only load US letter (or A4) paper under 20lb weight; otherwise the printer fails to transport sheets from the stack to the build platform. If the material is too slippery (e.g., OHP film) the printer fails to grab sheets or properly adhere layers; even one poorly attached layer impacts the accuracy of cutting and attaching successive sheets. Therefore, we glue electroluminescent sheets to a 'carrier' sheet of paper. Future printers may resolve these technical issues. To enhance the affordances of

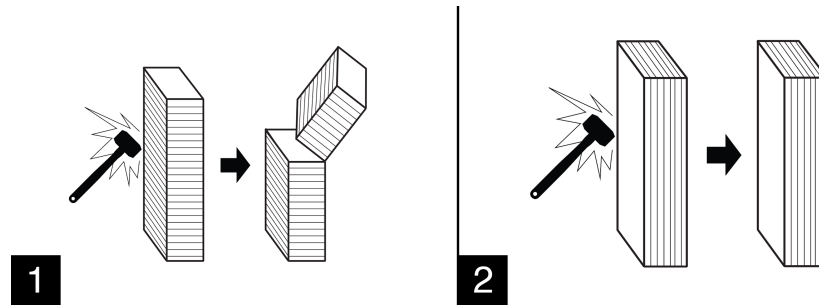


Figure 48: Designers must consider model orientation in the printer. Structure 1 is more fragile than 2: (1) horizontally attached sheets and (2) vertically attached sheets

PEP techniques, these two constraints need to be addressed in the next version of the printer development.

- Printed electronic papercrafts can be fragile depending on the design and placement of the model on the build platform. The printer creates 3D objects by gluing and cutting many flat sheets of paper. Therefore, a product that includes thin and long vertical parts (approximately less than 3 mm) is fragile. Likewise, we cannot bend or fold printed parts if the attached paper sheets are placed vertically.
- Our actuation primitives include only examples of heat and sound actuation. In the future, we can obtain mechanical actuation by adding thin film actuators such as actuated paper hinge that can be inkjet printed as for example in Foldio [80].
- Regarding the density of conductive layers, currently we support only single-sided conductive layers, so paper thickness governs density. In the future, we can adopt the double-sided conductive layer by via-hole techniques [115]. This can help to increase the density of conductive layers stacked into the model; two facing layers must be insulated by non-conductive coating.
- Although the PEP editor indicates where to embed functional layers in the stack of paper, we must count the number of layers to insert functional layers at the right position, which can be tedious and inaccurate. A counting error results in misplacing functional layers. We plan to address this by modifying the PEP editor to connect it to a printer to count the number of paper in forming the paper stack.

3.3.10 *Summary*

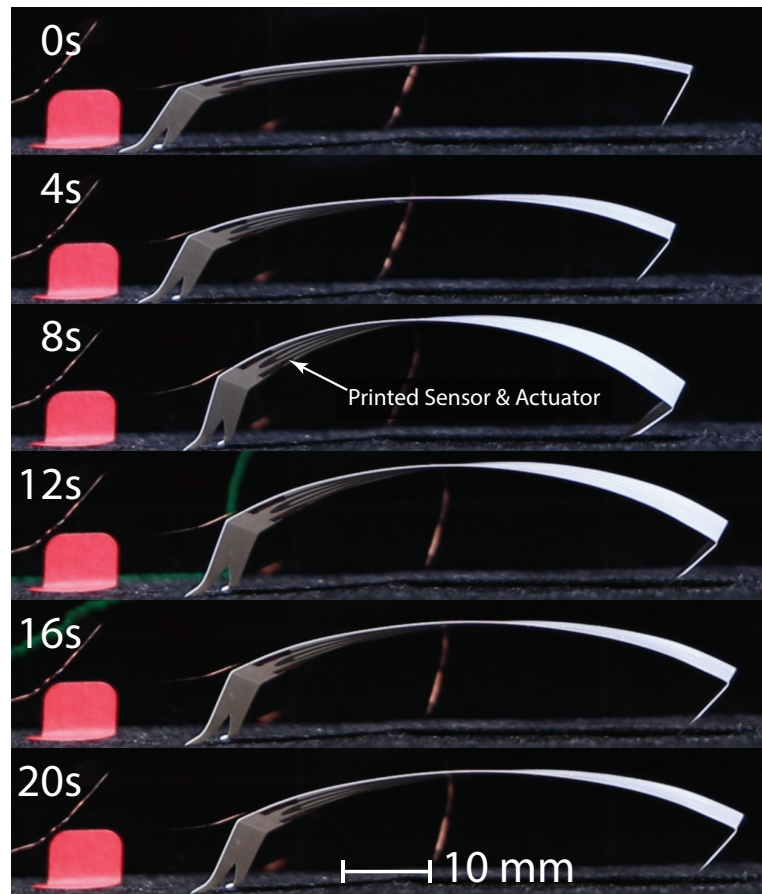
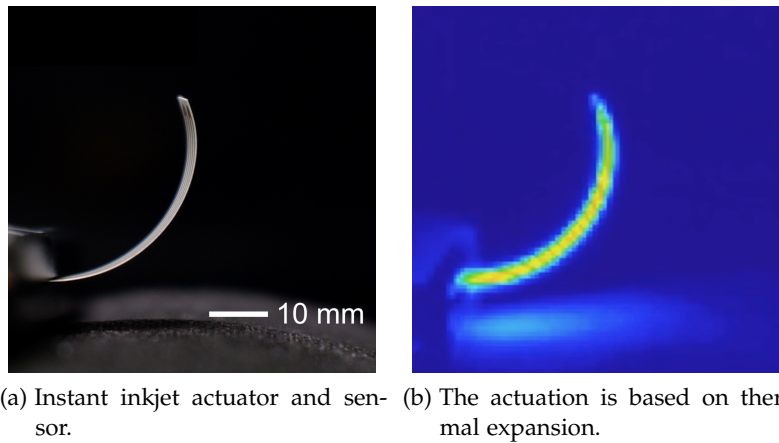
We introduced printed electronic papercrafts by 3D sculpting. Leveraging electronically enhanced papercrafts with 3D sculpting can enable new creative possibilities and we presented a set of fabrication techniques with a design editor to afford such prototyping using today's technology. By inserting functional layers into a stack of plain paper, we can develop interactive 3D paper prototypes by cutting and gluing sheets of paper. Our software supports designing the integration process with a set of functionality (actuation, sensing, display, and communication). We believe the unique affordances of paper prototypes can be further extended, and in this section we explored and demonstrated what's possible today by combining paper with electronic components and leveraging such combination with 3D sculpting.

3.4 CONCLUSIONS

In this chapter, we addressed the challenge of scaling electronic circuit printing from 2D to 3D. Double sided silver nano-particle ink printed electronic circuits with via-holes help to route complex circuits which cannot be routed in a single plane. Based on this technique, we proposed PEP, a method to print/fabricate 3D objects with functional layers embedded. These functional layers could be actuators, sensors, communication, and display modules. An object printed by PEP is not static anymore. It can be designed to actively interact with human and surrounded environment.

PRINTABLE SENSORS AND ACTUATORS FOR SOFT-BODIED ROBOTS

Soft-bodied robots are getting attention from researchers as its potential in designing compliant and adaptive robots. However, soft-bodied robots also pose many challenges not only in non-linear controlling but also in design and fabrication. Especially, the non-compatibility between soft materials and rigid sensors/actuators makes it more difficult to design a fully compliant soft-bodied robot. In this chapter, we propose an all-printed sensor and actuator for designing soft-bodied robots by printing silver nano-particle ink on top of a flexible plastic film. We can print bending sensors and thermal based actuators instantly with home-commodity inkjet printers without any pre/post-processing. We exemplify the application of this fabrication method with an all-printed paper caterpillar robots which can inch forward and sense its body bending angle.



(c) An instant inkjet paper caterpillar which can inch forward and sense its body bending angle.

Figure 49: Instant inkjet actuator and sensor consists of an electro-thermal actuator and a resistance based bending sensor which are instantly printed with silver nano-particle ink on a plastic film.

4.1 INTRODUCTION: PRINTABLE SOFT-BODIED ROBOTS

A printable, lightweight, and self-compact actuator is desirable for the rapid prototyping of soft-bodied robots, self-folding structures, or origami robots. A typical actuator for fabrication soft-bodied robot is pneumatic actuator such as in [76], [81], and [66]. However, the biggest drawbacks of pneumatic actuators are its large compressor and the constraint of guiding tubes and valves. Another more elegant approach is to use shape memory alloys such as in [118]. Again, this option is not printable and requires tedious preparation of shape memory alloys.

Standing out from these, thin film actuators demonstrate significant potential in the fabrication of compliant body robots. They enable the design of self-assembled structures which will be a key to high-level environment adaptive robots. Besides, a self-compact and printable thin film actuator is a crucial factor for mass production and self-deployment task. Kirigami robot [105] proposed an electro-thermal paper actuator to fabricate paper-based robots. However, its fabrication method requires the manual application of additional material such as polyurethane to the surface of the substrate. Printed Paper Actuator [125] use the reversible expansion of a conductive thermoplastic in the 3D printer to print paper-based actuators. Using 3D printing will consume more time than just 2D printing. Moreover, the conductive thermoplastic needs to be activated at high voltage to start expanding and contracting.

In the field of making new materials, such as in [36] and [4], the performance is promising. However, the fabrication process is neither simple nor accessible to a typical user. The actuator in [7] and Hygrobot in [106] tried to make a passive humidity paper actuator. They have the advantage of not requiring active energy from any artificial sources but utilizing the humidity gradient of the environment to actuate the actuator. This is its strong point but also its weakness. The actuator heavily depends on the randomness of the surrounding environment. In contrast, the tiny robot in [47] is controllable to move in different locomotion gaits. Unfortunately, the robot needs to be confined in a magnetic field which requires big and bulky equipment to generate and control.

In this chapter, we propose an all-printed electro-thermal paper actuator and bending sensor which can be printed instantly with silver nano-particle ink by a home-commodity inkjet printer without any pre/post-processing. We take advantage of the difference in coefficient of thermal expansion (CTE) between layers in photo plastic film to bend the plastic film with heat generated by the silver nano-particle

ink printed heater. When the temperature of the film decreases, it will return to the flat resting form. The bending of the film will change the resistance of the printed conductive trace. By measuring these changes, we can detect the bending angle of the actuation.

Our contributions include:

- Design of an instant inkjet paper actuator and sensor which can be printed quickly with any home-commodity inkjet printer and does not require any pre/post-processing.
- Characterization of the performance of the printed bending actuator and bending sensor with different types of substrate. Especially, we observe that the resistance change of the bending sensor is different from expectation. In other words, the silver ink pattern is less conductive when bending inwardly.
- An application of the inkjet actuator and sensor in making an all-printed inching worm which inches forward and senses its body bending angle.

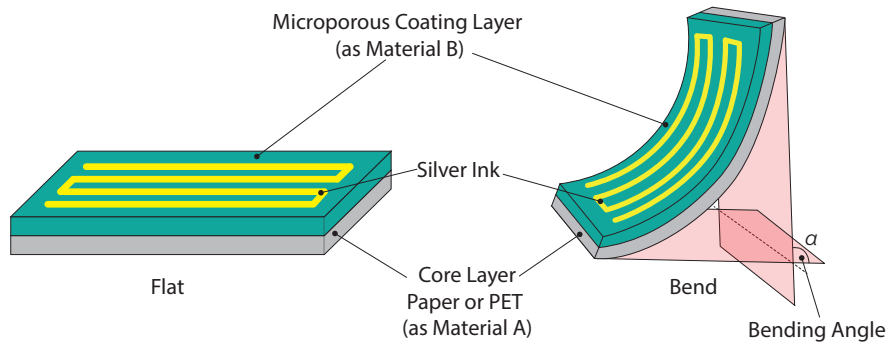


Figure 50: Structure of the instant inkjet actuator and sensor. The photo paper or plastic film is bent due to the effect of the Joule heat generated by the silver nano-particle ink printed heater.

4.2 DESIGN AND FABRICATION OF INSTANT INKJET ACTUATOR AND SENSOR

4.2.1 Design

4.2.1.1 Instant Inkjet Actuators

A thermal based uni-directional thin film actuator is a stack of at least two different materials (Material A and Material B) which have different CTE. When the whole structure is heated up, the difference in expansion ratio is converted into the bending motion of the thin film. This electro-thermal actuator is usually used in thermostat and Material A and B are respectively steel and brass [127]. In our approach, we use Instant Inkjet Circuits [53] to print an electrically-driven heater on the top of a resin coated photo paper, a transparent Polyethylene Terephthalate (PET) photo film, and a white PET photo film. The advantage of using a photo plastic film or photo paper is that they have multilayer structure [71] which consists of a core layer (wood free pulp or PET) as Material A and a porous coating layer as Material B (Figure 50). These two layers have different CTE, thus it will bend there is a change in its temperature. By printing a heater on top of the substrate, we can control the change of the temperature of the film. (Figure 50). The silver nano-particle ink printed heater can be designed so that the heat is distributed evenly across the film or concentrated on particular region of the film, thus enables us to design different bending direction.

4.2.1.2 Instant Inkjet Bending Sensors

Among many types of bending sensors, the most common one is resistance based bending sensors. It is a strip type resistor made from a special material which will change its conductivity when the strip is bent. Silver nano-particle ink also demonstrates resistance changes when the printed pattern is mechanically deformed. Flexy [121] took

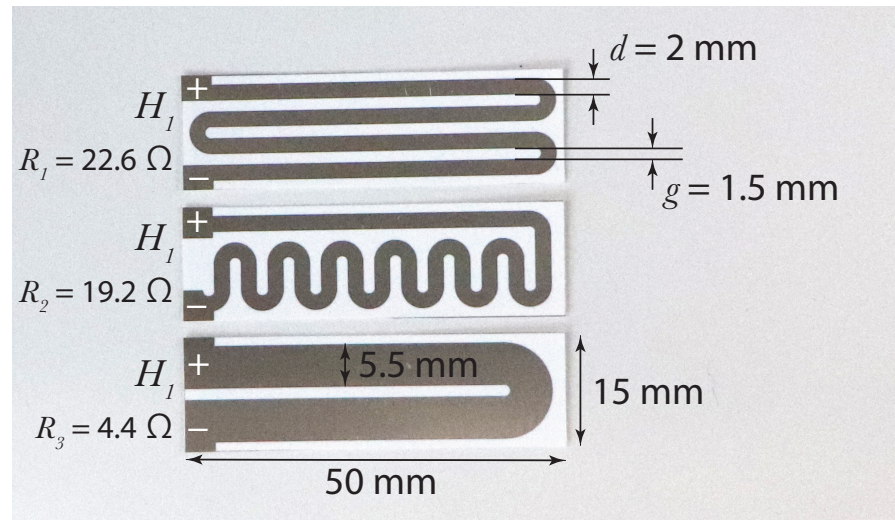


Figure 51: Three patterns of actuators and sensors are printed with silver nano-particle ink on the top of three substrates to evaluate the performance of the actuation as well as the sensory reading.

advantage of this characteristic to make a printable bending sensor from silver nano-particle ink print. We also adopt this design to make our bending sensor. However, Flexy is only working when the sensor temperature is kept at the room temperature. In our case where the temperature of the sensor will be high due to the heat generated by the actuator, the behavior of the silver ink pattern changes drastically.

At room temperature, the silver ink printed pattern will increase its resistance when it is bent outward (printed pattern is in the outside of the bending form), and vice versa. However, under a high temperature, as mentioned in the designing of the instant inkjet actuator, the heat will expand the substrate. Due to the difference in CTE, this expansion will, at the same time, bends the substrate and also breaks the links between silver nano-particles printed on the surface of the substrate, thus increasing the resistance of the printed pattern in total. We will base on this behavior to induce the bending angle from the resistance change of the silver nano-particle. In other words, our bending sensor is also the pattern which acts as a heater in the part of instant inkjet actuator. By keeping reading the variation of the resistance, we can detect the bending angle without any additional components or wiring.

4.2.2 Fabrication

Heater pattern is designed with common vector design software's (such as Adobe Illustrator or Inkscape). We print silver nano-particle ink heaters (as shown in Figure 51) onto a resin coated photo paper, a transparent PET photo plastic film, and white PET photo plastic film

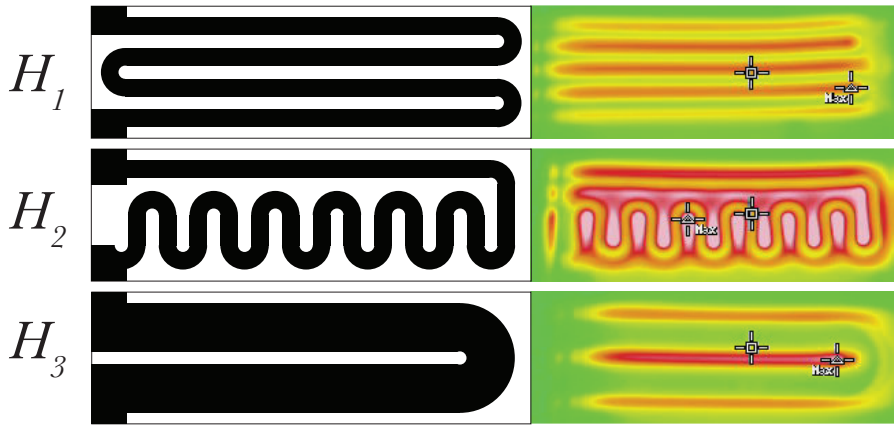


Figure 52: Bending actuation of the instant inkjet actuators with different patterns of silver nano-particle ink printed heaters. Thermography of each actuator show that the heater H_1 gives the most uniform heat distribution. For heater H_2 , there is an imbalance between top and bottom edge. Heater H_3 generates heat mostly in the middle and edges of the actuator.

(as listed in Table 5) to make electro-thermal actuators.

By printing silver nano-particle ink with home-commodity inkjet printers, each actuator can be made in just a few seconds. Except cutting the actuator from the print, which can be automated using cutting plotters or laser cutters, there is not any manual assembling.

Table 5: Fabrication equipment and material

Resin coated paper	NB – RC – 3GR120 [71]
Transparent PET film	NB – TP – 3GU100 [71]
White PET film	NB – WF – 3GF100 [71]
Inkjet Printer	EPSON PX – S160T [104]
Silver nano-particle ink	NBSIJ – MU01 [72]

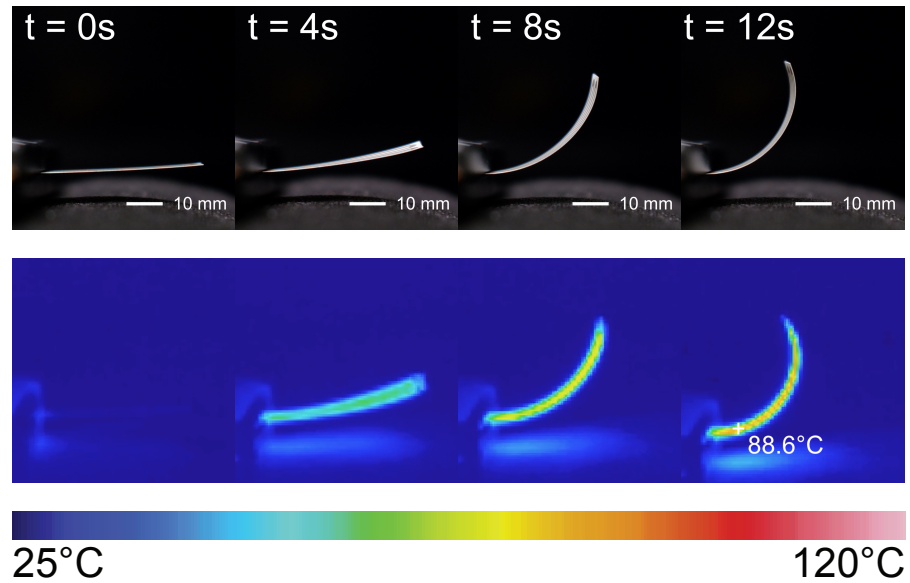


Figure 53: Bending of the H_1 pattern in series from flat to max bending. Along with that are the changing of the temperature of the actuator during the bending phase.

4.3 EXPERIMENT

During conducting experiments, we observe that the pattern printed on resin coated photo papers (NB – RC – 3GR120) and transparent PET photo plastic films (NB – TP – 3GU100) show inferior performances. The substrate is burnt and cannot bend effectively. Therefore, in this part, we will focus on the actuators printed on white PET photo plastic films (NB – WF – 3GF100).

4.3.1 Actuation

For each experiment, we fabricate actuators with a size of $W \times L = 1.5 \text{ cm} \times 5 \text{ cm}$. The actuators are actuated by heaters with different patterns of silver nano-particle ink printed as shown in Figure 51.

All actuators are put in room temperature (25°C) and driven by a stable direct current (DC) power supply (AD – 8722D). An output voltage is set to 9 V for all experiments (except actuator H_3 which is set to 2 V because the resistance of H_3 is 4.4Ω so it produces too much heat under 9 V which burns itself immediately). This setup accounts for the current flow through each heater H_1 , H_2 , and H_3 is $I_1 = 0.39 \text{ A}$, $I_2 = 0.46 \text{ A}$, and $I_3 = 0.45 \text{ A}$. These are empirical numbers which will not burn the actuator instantly. Actuation are recorded simultaneously by a normal camera (Sony Handycam

FDR – AX55¹) and a thermal camera (U5855A TrueIR Thermal Imager²). All recorded footage is analyzed with Kinovea³.

4.3.2 Displacement and Curvature

Displacement δ of each actuator is normalized by dividing the real displacement ΔH by the length L of the actuators as $\delta = \frac{\Delta H}{L}$. In measuring the bending curve, we assume that the curve is an arc of a circular, which means for each pattern H_i , the curvature of the bending actuation is $\kappa_i = \frac{1}{R_i}$ along the length of the actuators, where t is the instant time stamp. Based on this assumption, we calculate the curvature of the actuator when it bends at maximum. Result of the measurement is shown in Fig 54.

We attach each actuator to a fixed clamp and measure the displacement and curvature of the actuator at the maximum bending state. As shown in Figure 52, all three types of silver nano-particle ink printed heaters can generate enough Joule heat to bend the instant inkjet actuator. However, the H_1 heater pattern gives the most uniform heat distribution across the actuator surface and is the one which gives the largest displacement. Figure 53 shows the bending movement of the H_1 pattern actuator.

4.3.3 Responsiveness

Time response of each type of the actuators is evaluated by measuring the total time it takes for the actuator to bend from resting state to the maximum bending state.

As shown in Figure 54a, the actuator H_1 responses quickly and achieve maximum bending state in 7s. The slowest actuator is H_3 . The reason is that the heat generated by heater H_3 is only staying in the middle and edge region of the film. Therefore, the actuator can only bend slowly to a small displacement. H_2 is the fastest among the three actuators. However, its displacement is less than that of H_1 due to the imbalance in heat distribution on the H_2 actuator.

4.3.4 Sensing

From the result of the actuation experiment, we choose pattern H_1 as the actuator heater. In order to determine the bending angle of the active actuator, we measure the resistance of the pattern (KEYSIGHT

¹ <http://sony.jp>

² <https://www.keysight.com/>

³ <https://www.kinovea.org/>

34461A Digit Multimeter⁴) while applying a 9 V DC voltage to the printed patterns. When activated, the actuator body curls to the printing surface which makes it bend inwardly. Different from our expectation, the resistance of the conductive trace does not decrease but increases along with the increment of the bending angle (as shown in Figure 55 and Figure 56). This can be explained based on the cracking of the conductive pattern when the printing substrate undergoes thermal expansion due to the heat from the heater. Even though the inward bending will bring the silver nano-particles closer together, the thermal expansion acts more actively in separating the coalescence of the silver nano-particles. These two factors deduce the conductivity of the pattern. The bending angle of the actuator is calculated using Kinovea to find the relationship between the bending angle and resistance as shown in Figure 56.

4.3.5 Robustness

We evaluate the robustness of the instant inkjet actuator and sensor in terms of temperature robustness and resilience robustness.

4.3.5.1 Temperature

According to the specification document of the white PET photo plastic film, the substrate and the silver ink printed pattern can sustain a temperature of at most 120°C. We evaluate the temperature robustness of the actuator by continuously let a current of 0.5 A flow through the heater until the actuator burns itself. We find that, after 14s, the actuator is heated up to more than 180°C and gets burnt. The silver nano-particle ink printed heater is cracked and finally becomes non-conductive after 44s. Snapshots of the experiment are shown in Figure 57.

4.3.5.2 Resilience

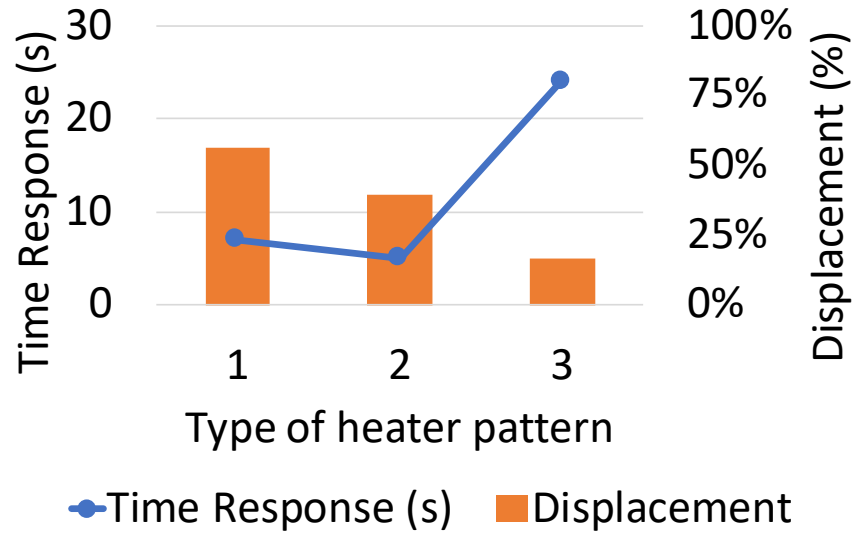
In order to evaluate the resilience of the instant inkjet actuator and sensor, we actuate it for 8 min which accounts for 24 cycles of bending/releasing with period $T = 20$ s (12s actuating under current $I_a = 0.5$ A, 8s releasing under current $I_r = 0.07$ A). As shown in Figure 58, the bending angle is changing stably through multiple times of bending. Along with the bending angle, the resistance of the heater also changes accordingly. This result shows that the instant inkjet actuator and sensor is durable both in terms of actuator and in terms of sensor.

4.4 APPLICATION - PAPER CATERPILLAR

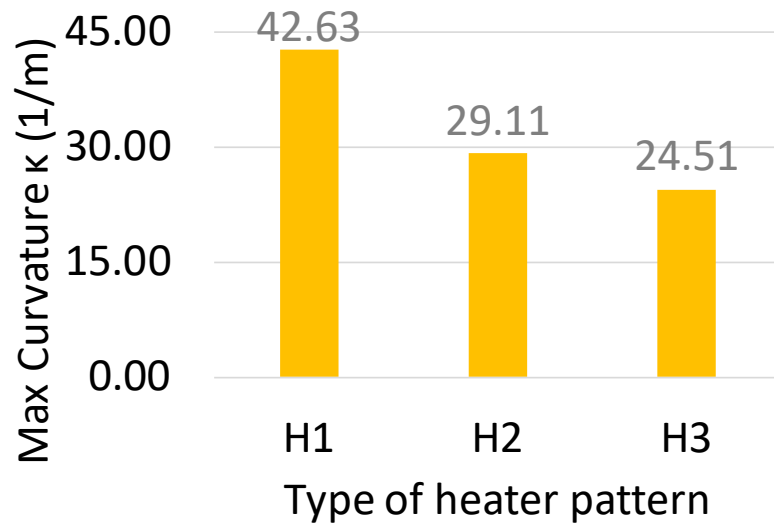
Caterpillars are getting more attention from soft-bodied robotics researchers because of its simple yet flexible enough body structure to generate and switch between locomotion gaits. In this chapter, as an application of the all-printed actuator and sensor, we make a simple version of a caterpillar which mimics its inching locomotion gait.

The paper caterpillar is designed as shown in Figure 59 and printed with silver nano-particle ink on a white PET photo plastic film. Head and tail of the robot are folded to form tiny hooks to realize frictional anisotropy along the body of the robot. The fabrication time of one robot includes less than a few second of printing and less than 5min of attaching the robot to the controlling circuit.

We control the robot using an Arduino board to switch the voltage connected to the robot between 9 V and 2 V. When only the 9 V line is on, the robot will bend, when only the 2 V line is on, the robot will release. The bend-release cycle will make the robot inch forward. During the releasing phase, the robot can be connected to 0 V instead of 2 V to make the releasing time shorter. However, because we use a voltage divider to measure the resistance of the actuator in real time, 2 V is just enough to not heat up the actuator too much yet provides acceptable resolution of the resistance measurement reading as shown in Figure 60. Snapshots of the locomotion of the robot are shown in Figure 49c. The robot was inching forward under the speed of about 10 m/s, which is equivalent to 1% body length per second. This is a slow speed locomotion, but we can improve by better designing of the frictional anisotropy between the gripping legs and the ground. Optimization of the ratio between activating/deactivating time of the actuator will also help to speed up the robot.



(a) Displacement and time response of each actuator



(b) Curvature at maximum bending state of each actuator

Figure 54: Time response of actuators are measured by the time it takes for a actuator to go from resting to maximum bending state

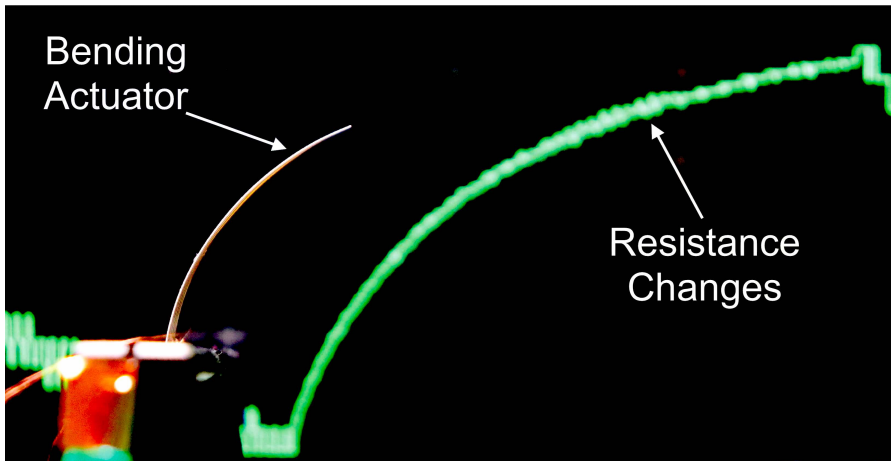


Figure 55: By continuously reading the resistance of the conductive trace, we can infer the bending angle of the actuator based on the change of its resistance. The instant inkjet actuator and sensor is control by an Arduino Mega board to actuate and to read the resistance of the heater and to show it on a display behind. (Real actuation and sensor reading are included in the supplemental video).

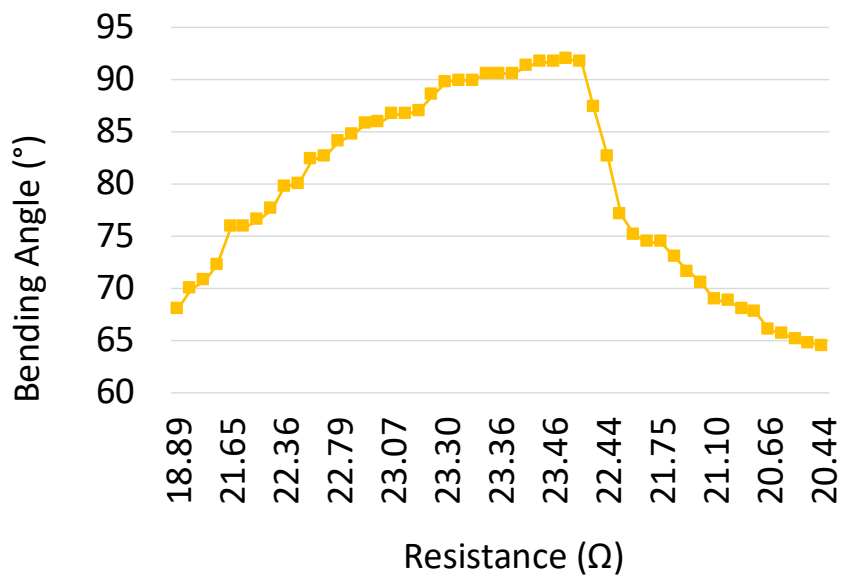


Figure 56: Resistance of the silver nano-particle printed pattern changes accordingly to the change of the bending angle.

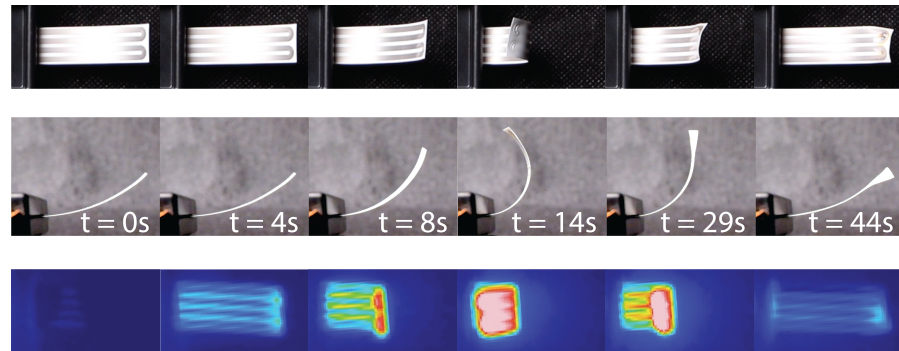


Figure 57: The actuator starts to deform unpredictably when the temperature is more than 120°C , and it burns itself when the temperature is more than 180°C at time $t = 14\text{s}$.

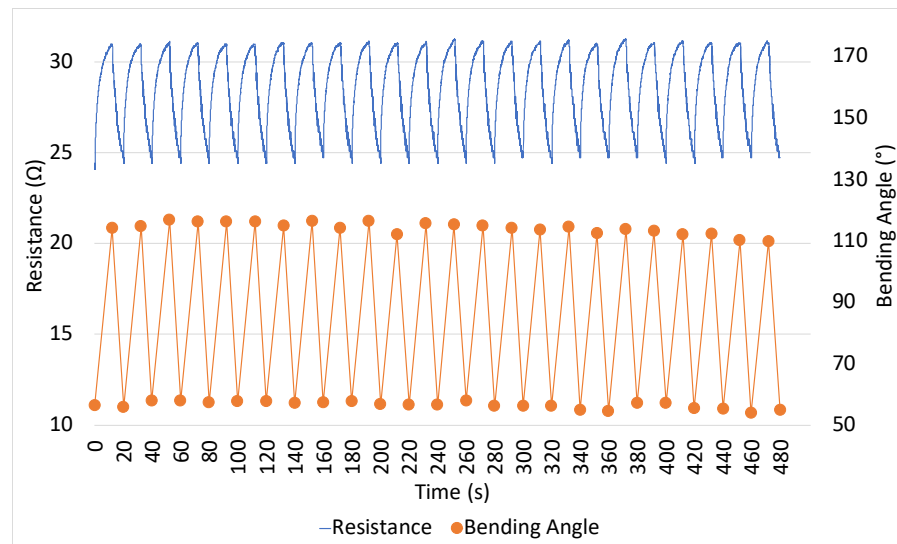
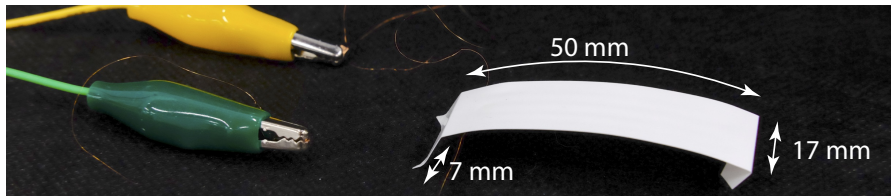
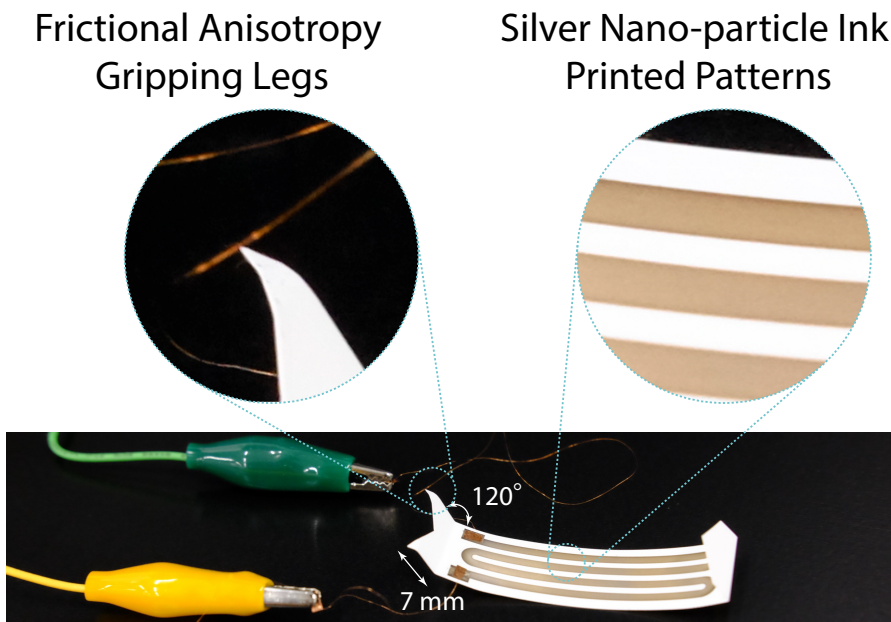


Figure 58: The instant inkjet actuator and sensor performs stably through multiple times of bending and releasing.



(a) Paper caterpillar from dorsal side



(b) Paper caterpillar from ventral side

Figure 59: The printable paper caterpillar with actuator and sensor is printed with silver nano-particle ink on white PET photo plastic film substrate.

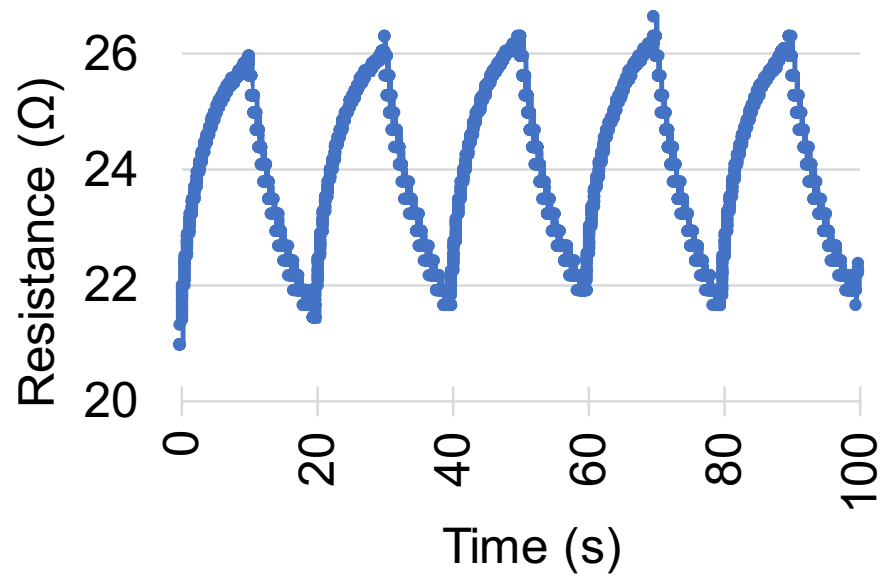


Figure 60: The bending of the robot is represented by the resistance change of silver nano-particle ink printed actuator on the body of the robot.

4.5 DISCUSSION AND FUTURE WORKS

The instant inkjet actuator and sensor have shown the possibility of rapidly printing a bending actuator that can be easily embedded into soft-bodied robots. Besides, this same pattern of the actuator can serve as a sensor for the bending angle of the body of the robot. However, there is still room for improvement in the future:

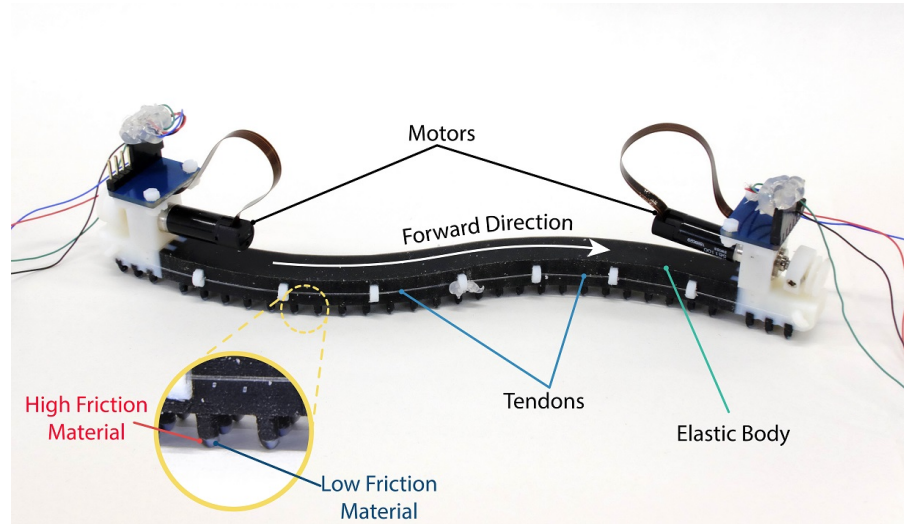
- *Power Consumption:* An instant inkjet actuator currently consumes about 3 W to 5 W which is quite large compared to other types of the actuator (for example, Shape Memory Alloys). This can be improved by overprinting to reduce the resistance of the heater.
- *Durability:* Our actuator and sensor show stable performance through multiple times of the experiment. However, it is easy to over-current the heater resulting in peeling off of the silver ink or melting of the substrate. Therefore, each actuator should be connected to a regulated circuit to assure that the heater will not be over-heated.
- *Sensitivity:* Though the bending sensor can help to detect the bending of the body, the amplitude of the of the resistance change is small thus reduces the resolution of the sensor. Computational designing of the printing pattern might help to improve the sensitivity of the sensor.
- *Bending Force:* the bending force of the actuator is weak, but it can be increased by using different types of substrate materials.
- *Bending Line:* Currently, we have not controlled the bending line of the actuator yet. However, in the future, this can be done by printing the heater pattern so that the actuator will bend at desired bending lines.
- *Bi-directional actuation:* The instant inkjet actuator is only bending to the printing side of the substrate. A bi-directional bending actuator is desirable in order to make more complex actuation and movements.
- *Self-compact:* The controlling and powering of the actuator is now tethered from an external board. In the future, it is possible to cut these wires by using an on-board thin battery or wireless power transfer.

4.6 CONCLUSIONS

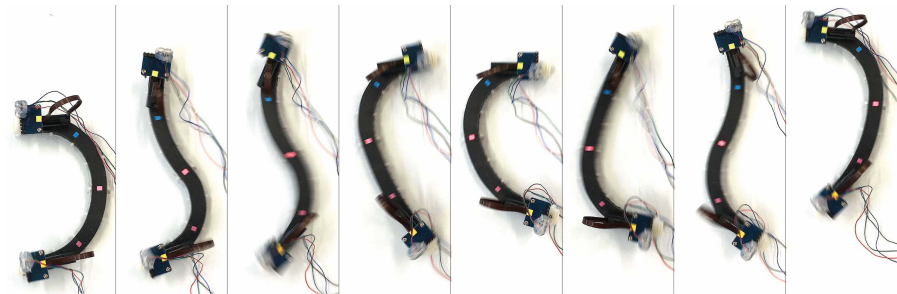
In this chapter, we proposed the instant inkjet actuator and sensor to shorten the design and fabrication time of making soft-bodied robots. With the availability of the printing materials and the precision of home-commodity inkjet printers, one can print an inching worm in just a few seconds and can start to actuate it in a few minutes. The merging of actuator and sensor into a single pattern makes the wiring much less bulky and free of frustration, thus, improves the compactness of the robots.

PRINTABLE MECHANICAL FUNCTIONALITY FOR DESIGNING SOFT-BODIED ROBOTS

Soft-bodied and continuum robots have shown great adaptability to the environment thanks to its flexibility of the body. They have great potential in environment exploring or rescuing mission. One of those robots is snake-like soft-bodied robots. A snake robot is often made by attaching passive wheels along a long body to achieve frictional anisotropy. This anisotropic structure helps to propel the body with serpentine locomotion and prevents it from sliding laterally. However, with a snake-like soft-bodied robot, attaching wheels is not only clumsy but also adding weight to the robot. In this chapter, being inspired by the scales on the skin of a snake, we propose a designing scheme to achieve an all-printed wriggle soft-bodied robot by patterning high and low friction material to the ventral side of the robot. Compared to a totally flat ventral, we are able to speed-up the serpentine locomotion 2.8 times. Besides, by changing the configuration of high/low friction material, our wriggle soft-bodied robot can easily move forward or backward just by switching the controlling signal. The fabrication time is just less than 1 hour and the robot can achieve the speed of 26 ms (equivalent of 17% body length per second).



(a) Specially designed directional friction of ventral surface to improve locomotion speed



(b) Locomotion of a robot (F_2 , period $T = 1$ s, on time $t = 0.5$ s)

Figure 61: 2-segment soft-bodied wriggle robot is fabricated from elastic material. It travels based on the undulation generated by two motors which keep winding/unwinding four tendons. The ventral of the robot is patterned with the directional friction surface to support the lateral undulation locomotion.

5.1 INTRODUCTION: SNAKE-LIKE SOFT-BODIED ROBOT

In contrast to traditional rigid robots, soft-bodied robots are constructed from highly deformable materials which allow them to adapt effectively to the environment. Soft-bodied robots are usually inspired by soft and flexible structured body of animals such as worm [119], snake [82], octopus [126], fish [65] and elephant trunk [12]. In order to adapt to different habitual environments, many animals have developed special structures of the body which assist them in hunting, hiding, and especially navigating through the environment. Mimicking those structures could be the hints to develop high adaptive soft-bodied robots. One of those structures that we want to address in this chapter is the scale of snake which is suggested to be crucial in assisting locomotion of the snake [46].

Inspired by the agility of a snake body, many research have tried to investigate and mimic its locomotion gaits such as [40, 41, 60, 98]. However, all of these research focus on multi-link rigid robots which not only require complicated controlling system but also have a low degree of adaptability. There are several other research that has tried to imitate snake locomotion in the soft-bodied robot. Zhu *et al.* [132] have intensively investigated the behavior of a continuum soft-bodied snake-like robot. However, this research assumes that the friction between ventral of the robot with the ground is uniform in every direction, which does not fit to the snake in real life. Onal *et al.* [82] and Luo *et al.* [62] solve the concerning of non-uniform friction beneath the snake-like robot by attaching passive wheel along its body. This helped to achieve smooth serpentine locomotion but also make the robot bulky and lengthen the fabrication process.

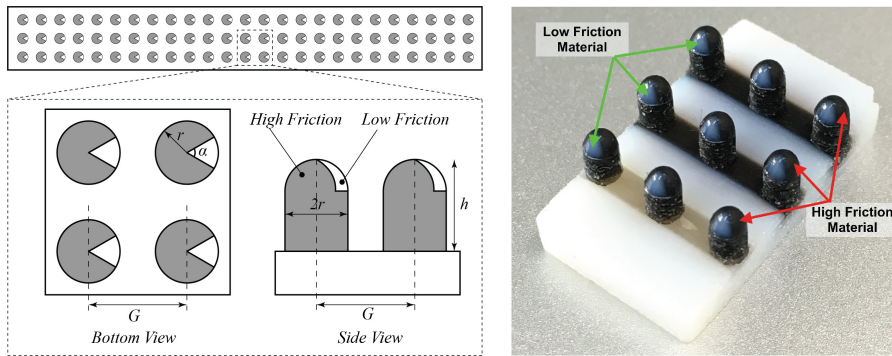
As mentioned above, scales play an important role in the locomotion of snakes. These scales are arranged to form frictional anisotropy along the body of the snake. By actively aligning the direction of each scale, the snake can easily navigate through a variety of surfaces [46]. Directional friction (anisotropic friction) surface is a surface which has high friction in several directions and low friction in the other directions. This frictional anisotropy can be realized by mimicking the tilted structure of hairs in butterfly [63] or by adding a tilted nail to contacting surface [54]. However, these approaches are neither strong enough to support locomotion of a wriggle soft-bodied robot nor robust enough to be scalable.

In designing of a soft-bodied caterpillar-like robot [118], variable friction legs have been used to push the body of the caterpillar-like robot forward. Although this is an elegant technique for off-plane locomotion, it is not applicable in in-plane locomotion as of serpentine

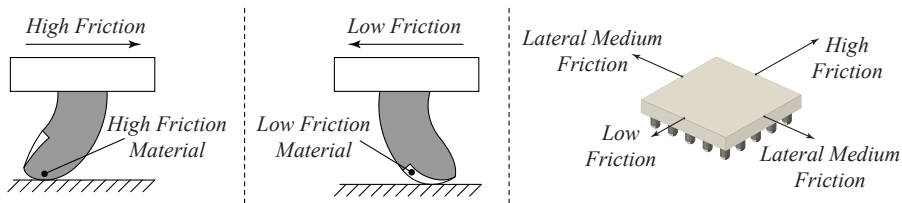
locomotion.

In our research, we propose a printable directional friction layer which supports the locomotion of a wriggle soft-bodied robot. We are able to control the soft-bodied robot with only two motors to generate the undulation movement along its body. The frictional anisotropy is not only beneficial to wriggle robots but also to any soft-bodied relatively-small robots. Our contributions include:

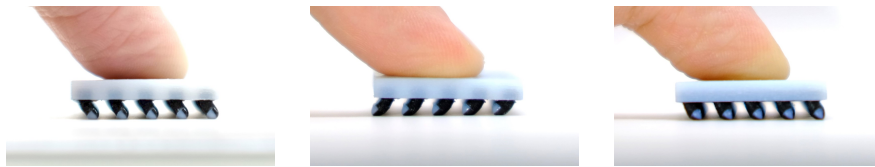
- Scheme to design directional friction surface to increase speed of serpentine locomotion
- Fabrication and evaluation performance of a 2-segment wriggle soft-bodied robot with above frictional designed properties



- (a) Ventral surface of the robot is divided into circular regions of radius r , the gap between two consecutive circular regions is G . Shaded part is high friction material, low friction material (white part) occupies a part of each region at angle α . From side view, each circular region is a rounded cylinder of height h .



- (b) Bending of the rounded cylinder will make the whole surface frictional anisotropy



- (c) Low friction forward (d) High friction backward (e) High friction laterally

Figure 62: Patterning of high and low friction material to achieve frictional anisotropy

5.2 SOFT-BODIED ROBOTS DESIGN WITH 3D PRINTER

Our robot is made from elastic material in the shape of a slender beam which acts as the body of the robot. Two DC motors at two ends of the beam will keep winding/unwinding the four tendons which are attached to the center of the beam. Suitable timing between two motors generates undulation movement which pushes the body moving forward. Ventral side of the robot is specially designed to achieve frictional anisotropy as described in the following part.

5.2.1 Directional Friction

In order to print a frictional anisotropy layer, we first divide the ventral surface into equivalent circle circular regions of radius r with a gap of G . Each region is then divided into two parts of two different friction materials as in Figure 62a. Low friction material occupies a

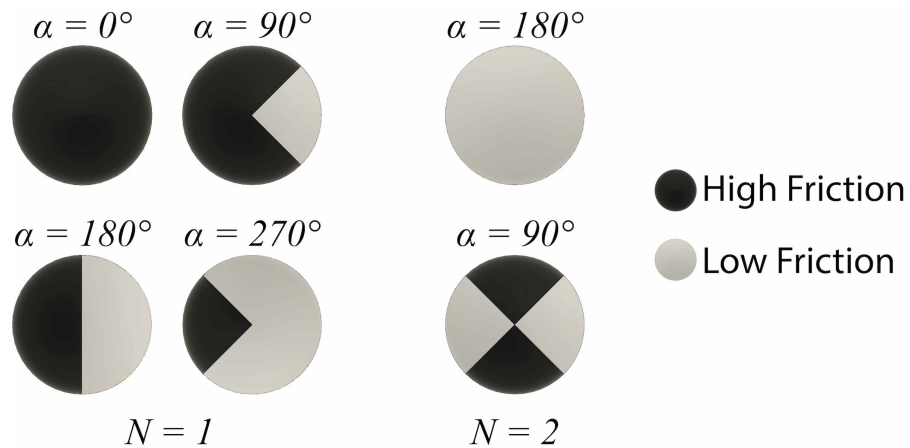


Figure 63: Configuration of the directional friction patterns with different α and N . Dark areas have high friction whilst light color areas have low friction to the ground surface.

part of each region at angle α . From the side view, each region is raised up to become a rounded cylinder of height h . This structure, when slides on a rigid surface, will bend inversely to the moving direction of the beam, thus one direction will have low friction whilst the other direction will have high friction (Figure 62b).

For printing the robot in this research, we use the Objet 260 Connex3™ multi-material 3D printer with rigid VeroWhite™- polypropylene plastic-like material - as low friction material, and soft TangoBlackPlus™- rubber-like material - as high friction material¹. TangoBlackPlus is also used to print the elastic beam of our wriggle soft-bodied robot. Figure 62a shows a 3D printed sample of a small beam with 9 circular regions ($\alpha = 90^\circ$, $r = 1$ mm, $h = 3.5$ mm, $G = 5$ mm). Its frictional anisotropy behaviors are shown in Figure 62c, 62d, and 62e.

5.2.2 Parameters of Directional Friction

In terms of morphology, the frictional anisotropy of a surface as described above can be tuned by parameters α , r , h , and G . Besides, the weight of the beam, friction coefficient, and elasticity of 3D printed materials also affect the behavior of the beam. For the simplicity of analysis, we keep all parameters fixed, except angle α which we can design to meet our frictional requirements. Another parameter we want to introduce into this analysis is the number N of separated low friction parts in each circular region. In another word, in one circular region there can be several separated pie regions of low friction material as in Figure 63 in case $N = 2$ and $\alpha = 90^\circ$. Changing value N enables us to achieve multi-directional friction.

¹ <http://www.stratasys.com>

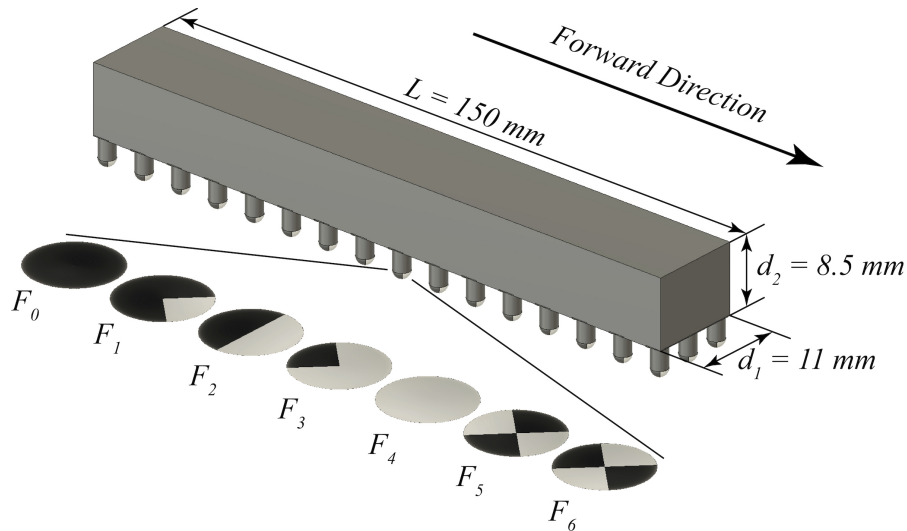


Figure 64: The wriggle soft-bodied robot is assembled from a $150 \text{ mm} \times 11 \text{ mm} \times 8.5 \text{ mm}$ beam and a directional friction surface at ventral side. Locomotive behavior of the robot will change according to the patterning of high/low friction material in the directional friction surface. Here we have 7 types of combination: $F_0, F_1, F_2, F_3, F_4, F_5, F_6$. In the Experiment part, we will add one more type, F_7 , which has flat ventral for comparison.

Theoretically, these two parameters α and N can be infinitely combined to achieve different directional surface. However, due to the limitation of the fabrication process such as the resolution of the printer and the mechanical properties of the printing materials, it is more practical to print with $\alpha = \{0^\circ, 90^\circ, 180^\circ, 270^\circ\}$ and $N = \{1, 2\}$. This leaves us with configurations as shown in Figure 63. We later find that these configurations are good enough to support serpentine locomotion of a slender elastic wriggle soft-bodied robot.

5.2.3 Soft-bodied Robot Assembly

Our wriggle soft-bodied robot consists of a slender beam with length $L = 150 \text{ mm}$ and rectangular cross-section $d_1 \times d_2 = 11 \text{ mm} \times 8.5 \text{ mm}$. Ventral side of the beam is patterned with directional friction surface as described above ($r = 1 \text{ mm}$, $h = 3.5 \text{ mm}$, $G = 5 \text{ mm}$). Based on this design, we change values of parameter α and N to get robots with different locomotive behaviors (Figure 64).

5.2.4 Undulation Generation

The serpentine locomotion of our wriggle soft-bodied robot is supported by the undulation movement of its beam. We use two bidi-

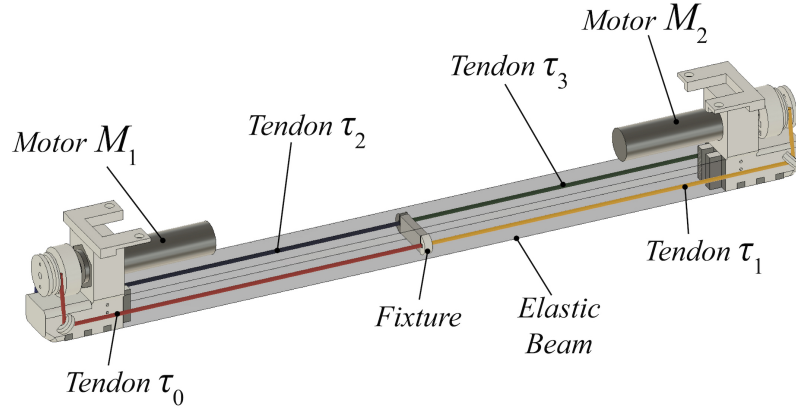


Figure 65: The wriggle soft-bodied robot is actuated by two motors put at two ends of the beam. Four tendons are attached to the motor and the center of the beam so that when motor M_1 winds tendon τ_0 , it will unwind tendon τ_2 . Same principle is applied for M_2 , τ_1 , τ_3 .

rectional motor to generate this undulation movement. These two motors are attached to two ends of the beam. Four nylon tendons (diameter $\phi = 0.3$ mm), which are attached to the two motors (two tendons for each motor) by a pulley, run along the beam and are fixed at the center of the beam as in Figure 65. When the motor rotates, one tendon will be wound whilst the another will be unwound. This enable us to freely bend the whole beam or just half length of it. By timely control the winding/unwinding of the motors as well as its winding/unwinding speed, we can generate an undulation as shown in Figure 66.

Let T be the period of the undulation movement, on time t be the time that a tendon is being wound, overlapping time Δt , where $-\infty \leq \Delta t \leq t$, be the time that two consecutive tendons are being wound. $\Delta t < 0$ means there is no overlapping on time between two tendons and time span between ending of on state of a tendon and beginning of on state of the next tendon is $|\Delta t|$. By controlling these t and Δt , we are able to bend the beam into 8 different states. Each state is instantiated in a time slot as in Figure 66. It is worth to note that the undulation generated by two motors in a 2-segment beam like this is not sinusoidal wave as its wavelength is changing periodically. For example, wavelength in time slot T_2 is longer than wavelength in time slot T_4 or T_8 .

In this configuration, the ratio between overlapping time and on time $\xi = \Delta t/t$ will affect the speed of the undulation.

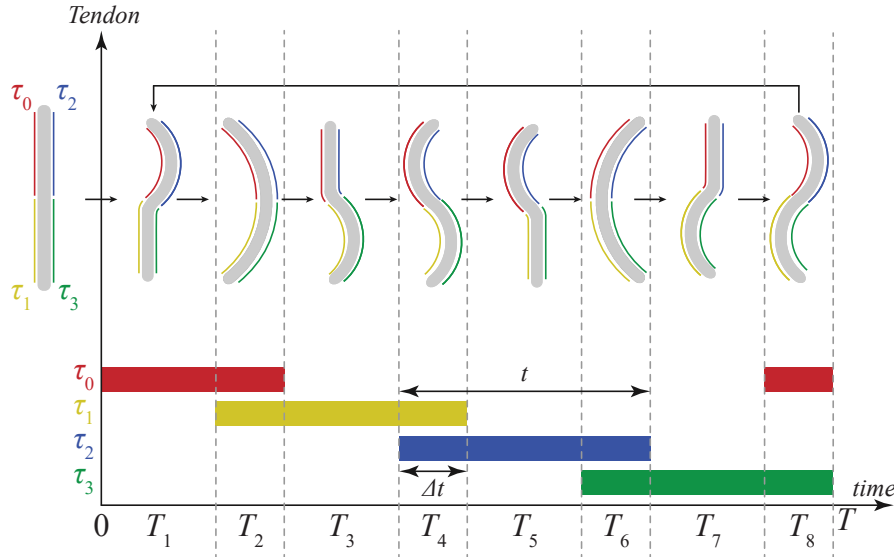


Figure 66: By timely winding and unwinding two motors, we are able to sequentially bend parts of the beam to form an undulation movement. T is period of the undulation, t is the time that a tendon is being wound, Δt is the time that two consecutive tendons are being wound.

- $\xi \leq 0$: there is not any overlapping time between on time of each pair of tendons. This leads to a discrete undulation movement which slows down the speed of the wriggle soft-bodied robot.
- $0 < \xi \leq 0.5$: the undulation wave will travel faster with larger value of ξ , which means faster locomotion of the wriggle soft-bodied robot.
- $0.5 < \xi \leq 1$: Due to the symmetry in arrangement of tendons, there will be overlapping between on state of tendons τ_0 and τ_2 , τ_1 and τ_3 . This is not acceptable as each pairs of these tendons is controlled by only one motor.
- ξ cannot be greater than 1 as $\Delta t \leq t$

Therefore, we choose $\xi = 0.5$ to maximize the traveling speed of the undulation without overlapping on time of tendons.

In order to implement this control system, we built a open loop control for the robot with an Arduino Nano board and a dual bidirectional motor driver chip (TB6612FNG, Toshiba) to control two bidirectional motors (Maxon 3477264 DC Motor 8 mm 0.5 W). The two motors as well as Arduino Nano board are driven by an external 9 V DC power source. Rotating speed of the two motors are set to maximum speed by setting the Pulse Width Modulation (PWM) signal to 255.

5.3 LOCOMOTION MODEL

The lateral undulation locomotion of a natural snake or a snake-like robot is usually modeled as the propagation of a sinusoidal wave in a curvature $\kappa(s, \eta) = A \cos(k\pi(s + \eta))$ [46], where s and η , in dimensionless unit, are position on the beam (normalized to body length) and time (normalized to period T). A is the amplitude of the wave.

In our research, we employ the same wave-propagation model for soft-bodied robots as in [82]. Different to the multi-link model of rigid snake-like robots, our wriggle soft-bodied robot takes advantage of the deformable and continuum body to achieve the lateral undulation locomotion. For traditional rigid robots which move forward by generating traveling wave, it is necessary to make the robot in at least four segments with three joints so that a full single period of the wave can trace along the body shape. However, in our approach, in order to reduce the number of actuators, we make our robot in two segments with two actuators at two end of the body. Along with the continuum characteristic of the elastic beam, our controlling mechanism (Figure 66) enables the wriggle soft-bodied robot to generate an approximate sine wave along its body. Our directional friction design, together with the wave-propagation, creates the propulsion force for the robot.

Due to Poisson ratio of the elastic rubber-like material which our soft-bodied robot is made of, the deformation of the body is not only in 2D but there are deformations in the z axis also. In case of a uniform friction ventral, this effect of Poisson ratio creates a temporary frictional anisotropy (subtle effect, though) at the length-wise edges of the robot to push it moving forward [14]. In our soft-bodied robot, we observed the same effect of Poisson ratio deformation on the body of the robot, thus the rounded cylinder shaped directional friction regions along two sides of the robot alternatively lift up and touch down the ground surface (Figure 67). The directional friction ventral, along with the Poisson ratio deformation, is the factor that assists the locomotion of our wriggle soft-bodied robot.

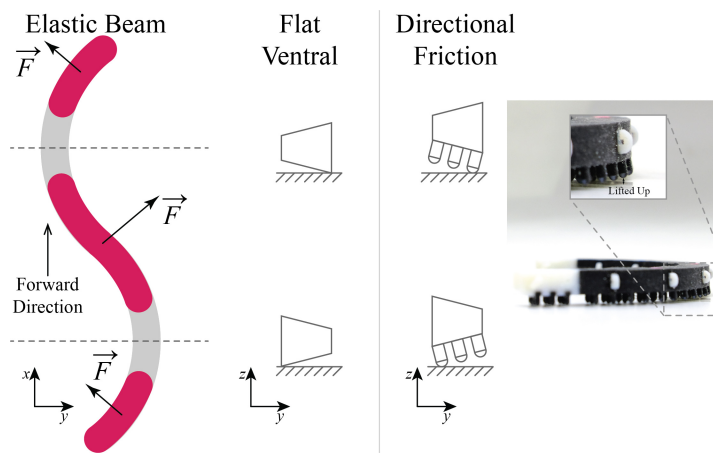


Figure 67: The robot moves forward based on the traveling wave along its body. The traveling wave alternatively kicks the ground to push the robot forward. Poisson ratio of the elastic beam makes edges of the flat ventral beam lift up when bent. When the ventral side is patterned with directional friction regions, these regions will lift up and touch down the ground accordingly to the bending and relaxing of the beam.

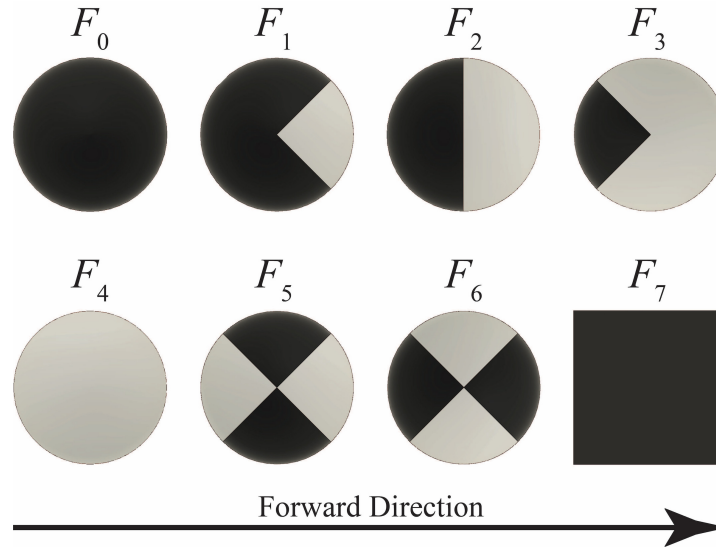


Figure 68: 8 robots with 8 different ventral surfaces named from F_0 to F_7 . $F_{0..4}$ have α and N as mentioned in Figure 63. F_5 and F_6 have same value of $\alpha = 90^\circ$ and $N = 2$ but are different in alignment to the orientation of the beam. F_7 is a flat ventral robot without directional friction surface.

5.4 EXPERIMENT ON LOCOMOTION

To evaluate the influence of our designed directional friction, we measure the locomotion speed of the wriggle soft-bodied robot with different patterns of directional friction surface. Footage of the real locomotion of the wriggle soft-bodied robots is included in the accompanying video.

5.4.1 Experiment Setup

5.4.1.1 Directional Friction

We have 6 combinations of the high/low friction material to realize directional friction surface (Figure 63). From these combinations, we make 8 samples of robots with different ventral surfaces as shown in Figure 68. Figure 69 shows a really printed and actuated robot.

5.4.1.2 Controlling Parameter

As for controlling parameters, from empirical experiments with the mechanical properties of the printing material as well as morphology of the robot, we set controlling parameters as Table 6

5.4.1.3 Experiment Environment

We test the locomotion of our robot on three different surfaces including a rigid glossy white board surface, a wrapping paper surface, and

Table 6: Setup value of controlling parameters

Parameter	Value
Tendon on time t	500 ms
Tendon overlapping time Δt	$0.5t = 250$ ms
Motor Speed	Maximum (PWM= 255)
Tendon length at rest	75 mm

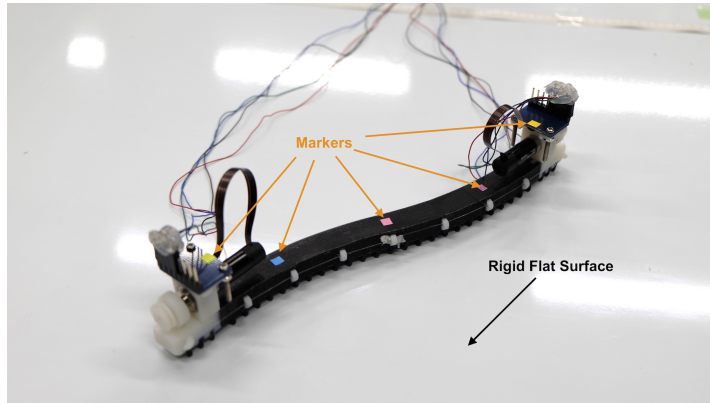


Figure 69: Each robot is put onto a horizontal flat rigid glassy surface. We run the robot for 20s then measure its traveled distance. Each robot has markers so that we can analyze its locomotion using Kinovea.

a non-woven fabric surface. All three surfaces are put horizontally flat. The friction coefficient for each ventral pattern with each surface are listed in Figure 70. Each robot will run for 20s then we measure its traveled distance. The average speed of each robot is calculated based on these time and distance values. Each test is recorded by a camera (Sony Handycam FDR – AX55²). We add markers to the robot as Figure 69 and analyzed trajectory as well as the speed of the robots using Kinovea³.

5.4.2 Experiment Result

5.4.2.1 Lateral Undulation

For all 8 types of robots, we are able to generate stable undulation movement. A capture of the locomotion of robot F_1 is shown in Figure 61b. Because all 8 types of the robots share the same beam design as well as a controlling mechanism, they have same beam elasticity. However, due to the difference in ventral friction, the degree of the

² <http://sony.jp>

³ <https://www.kinovea.org/>

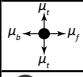
	Fabric			Paper			White Board		
	μ_f	μ_b	μ_t	μ_f	μ_b	μ_t	μ_f	μ_b	μ_t
F0	1.43	1.43	1.43	1.73	1.73	1.73	2.25	2.25	2.25
F1	0.93	1.19	1.19	1.48	1.80	1.80	0.70	1.28	1.28
F2	0.58	1.19	0.88	0.78	1.60	1.19	0.90	1.88	1.39
F3	0.31	0.53	0.31	0.45	0.67	0.45	0.42	0.58	0.42
F4	0.31	0.31	0.31	0.45	0.45	0.45	0.42	0.42	0.42
F5	0.60	0.60	0.67	0.67	0.67	0.93	0.70	0.70	0.75
F6	0.67	0.67	0.60	0.93	0.93	0.67	0.75	0.75	0.70
F7	1.28	1.28	1.28	1.54	1.54	1.54	2.75	2.75	2.75

Figure 70: Friction coefficient of ventral pattern on the experimental surfaces in forward direction μ_f , backward direction μ_b , and transverse direction μ_t . Reddish cells indicate high friction coefficient. Greenish cells indicate low friction coefficient.

curvature in undulation formed in each robot is different. We analyze this difference based on chord length (the distance between two ends of an arc) of the curvature formed by a tendon in its maximum wound state. Figure 71 shows the chord length of the curvature in case of locomotion on *White Board*. Robots F_2 and F_5 have the shortest chord length. The ventral directional friction enables F_2 and F_5 to bend more, thus increase the locomotive propulsion force. F_1 ventral pattern, although is close to that of F_2 and F_5 , have large transverse friction coefficient which make it more difficult to bend. We later find in the next part that the speed of F_2 and F_5 is at the top among 8 experimental robots.

5.4.2.2 Locomotion Speed

We use Kinovea to analyze the trajectory and speed of each robot. Figure 73 shows the trajectory of each robot when run for 20s on the experimental surfaces. Although all of robots manage to move forward, the speed and trajectories vary.

Locomotion on White Board: Only F_2 and F_5 have stable locomotive direction (Figure 73a). The others are steering away from the designed route. One explanation is that the difference between directional friction coefficient (μ_f , μ_b , μ_t) in case of F_2 is large compared to others. F_1 also have large difference in terms of directional friction coefficient. However, its high transverse friction coefficient μ_t makes it more difficult to bend. This is clearly shown in Figure 71. F_1 has long chord length compare to that of F_2 and F_5 , hence inferior in locomotion. Regarding locomotion speed, as evidently shown in Figure 72 and Figure 73a, in 20s, robot F_2 has the longest travel distance thus it is the fastest design ($\alpha = 180^\circ$, $N = 1$). F_2 is 2.8 times faster than F_7 - the flat ventral robot without directional friction design and 8 times faster than the slowest design F_0 . F_0 is slowest as its ventral is printed

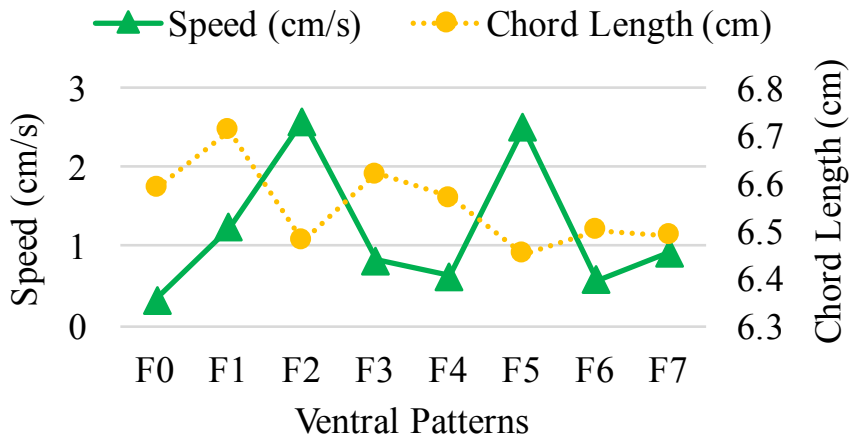


Figure 71: Chord length of the curvature formed by a tendon in its maximum wound state and locomotion speed of robots on *White Board* surface. All 8 robots have the same beam structure and controlling mechanism so the chord length depend on the friction between ventral of the robot and the experimental surfaces.

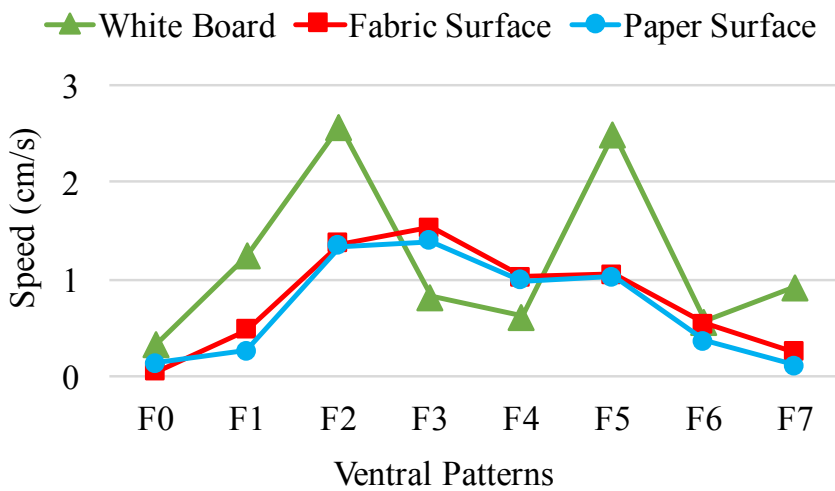


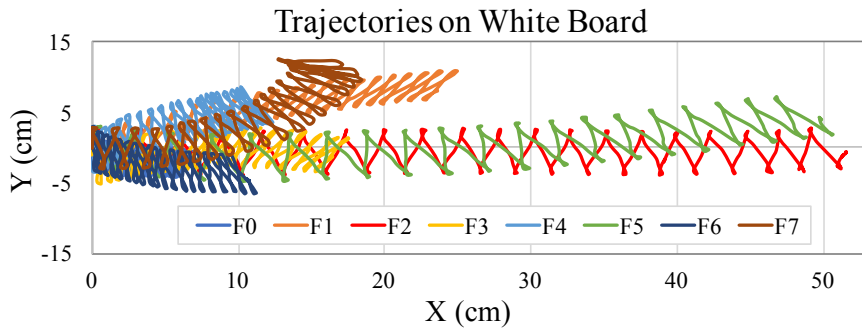
Figure 72: Speed of each robots on different experimental surfaces. In case of *White Board* surface, F₂ and F₅ showed the best locomotion speed. In case of *Fabric* and *Paper* surface, F₂, F₃, and F₅ have the highest locomotion speed.

with high friction material. Undulation has little effect in case of F_0 . It is worth to mention that although trajectory of F_5 is less stable than that of F_2 , they have approximately the same locomotion speed. This suggests that in terms of locomotion speed, the transverse high friction is more important than the backward high friction.

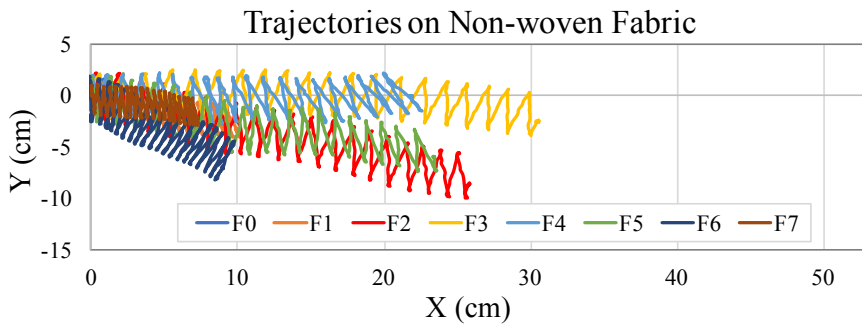
Locomotion on Fabric and Paper: Although still moving forward stably, F_2 and F_5 are out-performed by F_3 (Figure 73b, 73c). As shown in Figure 70, forward and transverse friction coefficient of F_3 are the same ($\mu_f = \mu_t$) regardless of the locomotion surfaces. However, the difference in forward and backward friction coefficient (μ_f, μ_b) in case of *Fabric* and *Paper* are larger than that of *White Board* case. This makes F_3 move better on *Fabric* and *Paper*.

5.4.2.3 Backward locomotion

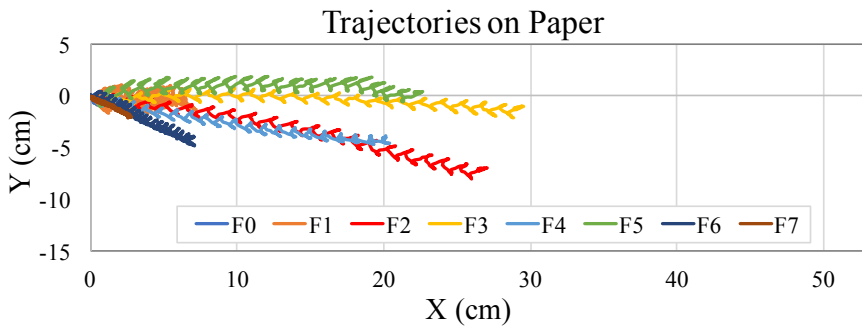
Backward locomotion is not a common locomotive behavior in snakes but can be found in other creatures which travel by lateral undulation (such as *C. Elegans* [131]). In our experiment, we notice that robot F_5 , although does not have the highest locomotion speed, has this backward locomotion mode thanks to its symmetry in directional friction surface. F_5 has bi-directionally low friction along the beam and high friction transversely. Therefore, just by switching the direction of the undulation wave propagation, we are able to make F_5 moving forward or backward.



(a) Trajectories on white board surface. Tracking point is center point of the beam.



(b) Trajectories on non-woven fabric surface. Tracking point is center point of the beam.



(c) Trajectories on paper surface. Tracking point is hind end point of the beam.

Figure 73: Trajectory of the robots when run for 20s on the experimental surface. On the XY plane of the experimental surfaces, each robot is placed along the X-axis so that one end of the robot is positioned at point (0,0). The robots are controlled to move on the same direction as the positive X-axis.

5.5 DISCUSSION

Directional friction surface as designed in our approach can support the locomotion of a wriggle soft-bodied robot. In compare to other wriggle rigid/soft robot, our wriggle soft-bodied robot stay in the range of small size crawling robot as shown in Table 7. Nevertheless,

Table 7: Comparison to other wriggle robots

Robot	Max Speed (mm/s)	Weight (kg)	Length (mm)	Rigid or Soft
ACM III [44]	400	28		Rigid
AmphiBot II [44]	400		772	Rigid
Koryu II [44]	500	370	3300	Rigid
OmniTread OT-8 [44]	100	13.6	1270	Rigid
CMU's Modular Snake Robot [44]	101.6	1.26	838	Rigid
Onal's FEA Snake Robot [82]	19		307	Soft
Our Wriggle Robot	26	0.238	19.6	Soft

there are several challenges and questions we want to explore further:

- Theoretical model: in order to optimize the design of our frictional anisotropy, we need to develop a thorough model which find the relationship between high/low friction material as well as the control mechanism with locomotion speed and gait.
- Miniaturization: the friction force between ventral of the robot and the ground depends on the weight of the robot as well as the contacting area. Exploring effects of directional friction in miniaturized crawling soft-bodied robots will give better insight in how to design with frictional anisotropy.
- Beam elasticity: elasticity of the beam has a large impact on the curvature of the undulation. This raises a question about how can we design and control the undulation to get the optimal performance of the wriggle soft-bodied robot.
- Other parameters: in this research, we deliberately fix all parameter except α and N . A thorough investigation on how other factors affect the locomotion of the wriggle soft-bodied robot is necessary to design a highly adaptive robot.

5.6 CONCLUSIONS

We have proposed a wriggle soft-bodied robot with the adoption of frictional anisotropy to support serpentine locomotion. By combining the high and low friction material to print ventral of the robot, we increased the forward serpentine locomotion. Besides, we can also introduce switch back mode (backward serpentine locomotion) into the robot behavioral set by making its ventral low friction length-wisely and high friction transversely. Our model of the 2-segment wriggle soft-bodied robot is effective yet simple enough to be fabricated using rapid prototyping tool in very short time (less than one hour where a large portion of the fabricating process is waiting for the 3D printer to finish the printing job).

FUTURE WORKS

Future works of each project in this dissertation are discussed at the end of each Chapter. In this Chapter 6, we consider the future of digital fabrication in the context of a streamlined fabrication process for printable electronic and mechanical devices.

Dynamic electronics for dynamic soft-material: Digital fabrication is shifting from traditional rigid materials to soft and flexible materials. The printed structure can be stretched, twisted, or pressed. In order to add functionality to a soft structure, the electronics need to be made flexible enough not to be broken under the dynamic transformation of compliant materials. Exploration at the combination of deformable conductive materials and deformable mechanical materials will shed light to question of how to design soft devices which both flexible and resilient.

Programmable stiffness: Selectively programmable stiffness is a desirable property for designing smart matter. The capability of changing the stiffness of a region dynamically makes it easier for a structure to adapt to the change of the environment. One of the approaches to programmable stiffness is to use the computational and generative design for iterating through a large number of different designs in searching for the best pattern(s).

Fabrication of Bio-powered Robots: Beside printable electronics, printable bio-structures are quickly developing and drastically transforming the way biology-related researches are conducted. How will this change the way we make things in the future? How can this help to make more agile, more durable, and lighter robots? Several types of bacteria have been used to make environment responsive actuators[128]. How will these biology organisms cooperate to be an actuator, then be a sensor for robots?

CONCLUSIONS

In this dissertation, we have discussed the role of functional design in digital fabrication of printable electronic circuits and mechanical devices. For the printable electronic circuits fabrication, we focused on the application of sintering-free silver nano-particle ink to rapidly print conductive patterns on flexible substrates such as photopapers, transparent PET films, and white PET films.

The competence of instantly printing electronic circuits has opened a whole new designing space for users such as researchers, makers, designers to blend electronic components to almost anything. However, working with the complicated behaviors of electronic circuits is not always easy, even for expert users. We noticed that one of the most common applications, when a user tries to play with silver nano-particle ink, is to light up a bunch of LEDs and fail when the number of LEDs increases. The wiring is difficult to imagine, and the brightness of all the LEDs is not uniform due to the intrinsic resistance of silver nano-particle ink printed traces. We have proposed in Chapter 2 an autorouter to generate the wiring pattern of multiple different color LEDs so that all the LEDs are lit up with averagely the same brightness. Our tool and algorithm enable novice users to design complicated LEDs based applications with a large number of LEDs. Instead of having to deal with the tricky electrical behaviors of the electronic circuits, a user can direct their focus to the creative aesthetic designing of the application. This proposal improved the performance and usability of the silver nano-particle in printed patterns and adds more freedom to the design of such electronic circuits.

Maneuvering on the 2D planar printing, we found that the integration of electronic circuits into 3D printing process will bring huge benefits to users who want to 3D print fully functional objects at once. In Chapter 3, we proposed PEP (3D Printed Electronic Papercrafts), a fabrication method to streamline morphology and functional fabrication of 3D objects. Taking advantages from the thin-film technology, our approach is to stack functional thin-films into the paper laminate object manufacturing process to blend the active functionality into 3D printed objects. In laminate object manufacturing, thin sheet materials are cut and stacked, layer-by-layer, to form a physical 3D object. In

our proposal, the material for forming the shape of the 3D objects is cut-out normal office paper. The functional thin-film can be pre-fabricated with silver nano-particle ink printing, silk-screening, or using any commercially available thin-film electronic components. We are able to embed functional primitives such as sensors, actuators, displays, and communications into 3D printed papercraft objects. The interconnections between functional layers are established using via-hole techniques introduced in Section 3.2. We also developed an editor based on Autodesk Fusion 360 to let users drag and drop functionality into the designed 3D model and print it in a unified process.

Chapter 4 is built on top of the idea that using silver nano-particle ink to print robots will start a new paradigm shift in how soft-bodied robots are prototyped and fabricated. For a long time, designing of soft-bodied robots is heavily constrained by available sensors, actuators, and other electronic parts. We argued here that it is possible to fuse the processes of fabricating body and attaching active components into a single process using silver nano-particle ink printing. We exemplified the idea with an all printed paper caterpillar robot which consists of a bending sensor and a bi-layer thermal based actuator printed with silver nano-particle ink. The paper caterpillar robot is flat at resting state. When an electrical current flows through the silver nano-particle ink printed actuators, the whole body of the robot will bend which push the robot to crawl. The bending and heating up of the body make the resistance of the actuators change. And thus, we have a measure to detect the bending angle of the robot and close the loop of controlling the paper caterpillar robot.

Beside exploring functional design for electronic circuits, we set foot to the territory of functional design for mechanical devices. Multi-material 3D printers enable users to print with different material simultaneously to form different mechanical characteristic in different parts of the printed body. We used a combination of soft and rigid materials for the structuring of a snake-like wriggle robot. The robot is inspired from the scales on the skin of a snake. These scales generate a frictional anisotropy surface along the body of the snake which makes it much more difficult to slide backward or sideways. In Chapter 5, we designed and tested a set of 8 types of the robot body skin to search for the best pattern which helps the wriggle robot to move fastest.

In short, we have moved from a 2D printing world of electronic circuits to the integration of electronic circuits and components into a 3D printing process. We have tried to push the soft-robotics toward the future of all-printed soft robots which will give designers more freedom in robots design and fabrication. The printable soft-bodied robots consist of printable sensors, printable actuators, and printable mechanical functionality of the body structure. Our research as a whole tried to answer the question of how to equip an average user with tools, algorithms, and mindsets so that he/she can arbitrarily breathe life into the surrounded digitally fabricated objects.

APPENDIX: GRADUATE PROGRAM FOR SOCIAL ICT GLOBAL CREATIVE LEADERS

Graduate Program for Social ICT Global Creative Leaders (GCL) is The University of Tokyo program for leading graduate schools which aims at enabling graduate school students to engage in socially interdisciplinary high impact research. I was a GCL student since my first year of graduate school. Besides taking classes in different disciplines such as law, management, and entrepreneurship, I also fulfilled internships and workshops under support from GCL.

A.1 INTERDISCIPLINARY CLASSES

The interdisciplinary classes aimed at providing students with different perspectives on social problems and how to work with different background researchers. These classes were also great places to meet other people from other fields. We talked about our major, about our point of view on how to create a better society. From these discussions, time to time, a problem on one research field can be solved by proposals from another field. I have collaborated with a student from the Department of Social Psychology on a project of remotely mental health counseling. I was also benefited from the advice of other professors from other fields to brush-up my research.

A.2 INTERNSHIPS

I took a 3-month internship in Microsoft Research Asia (MSRA) to conduct my research on double-sided circuits with Instant Inkjet Circuits. The result of this research was published in the proceedings of ACM UbiComp 2015. I also had another two internships in AgIC Inc. (Elephantech Inc.) to work on an autorouter for circuits made by silver ink, and a project on electrode-less plating for fabricating flexible electronic circuit boards. These two internships were also fruitful as we published a conference paper and a journal paper on the autorouter, which are included in Chapter 2.

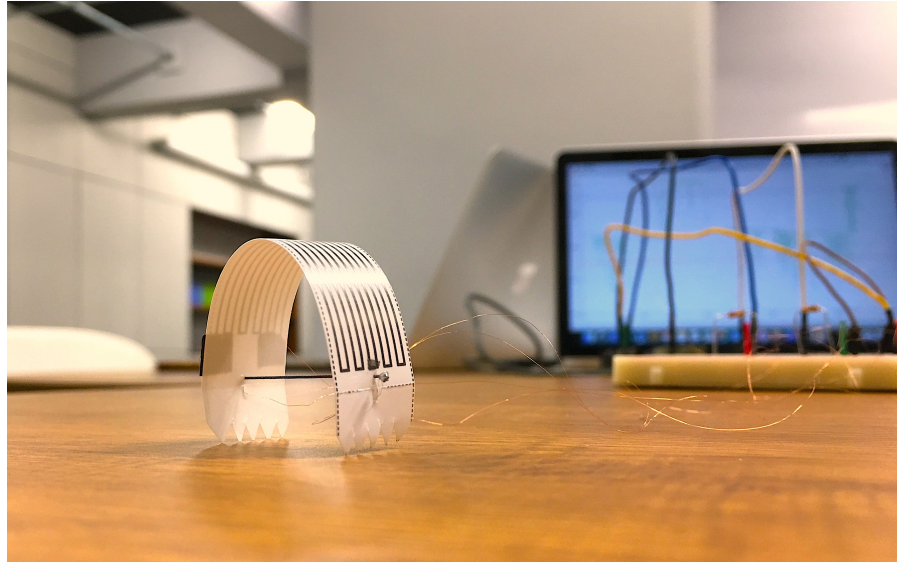


Figure 74: A Paper Caterpillar robot with its gripping legs

A.3 WORKSHOPS

A workshop is a great way for us to learn how to communicate with general audiences about our research. I have attended Global Design Workshop (GDWS) A (small, medium, large), Workshop B, and organized my own Workshop C on making paper caterpillar with silver ink.

In order to study how a non-expert user benefits from all-printable soft-bodied robots, we organized a workshop where attendees are divided into groups of 3 to 4 members. Each group would try to make a Paper Caterpillar with bending sensor built-in. For simplicity, we asked each group to use Shape Memory Alloys (SMA) as an actuator for actuating the Paper Caterpillar. After making Paper Caterpillar robots, we would let them race to see which group has the fastest robot. Figure 74 shows a Paper caterpillar robot with its gripping legs. Figure 75 shows a race between three Paper Caterpillar robots. By the end of the workshop, all the attendees can make a simple Paper Caterpillar robot with a bending sensor. With a well-designed sensor, printing the robot is just one click away. On the other hands, working with SMA is messier as manipulation of a fragile element as SMA is challenging for non-experience users. In the next workshop, we will introduce the printable actuator as mentioned in Chapter 4. We believe with both sensor and actuator being printable, the fabrication

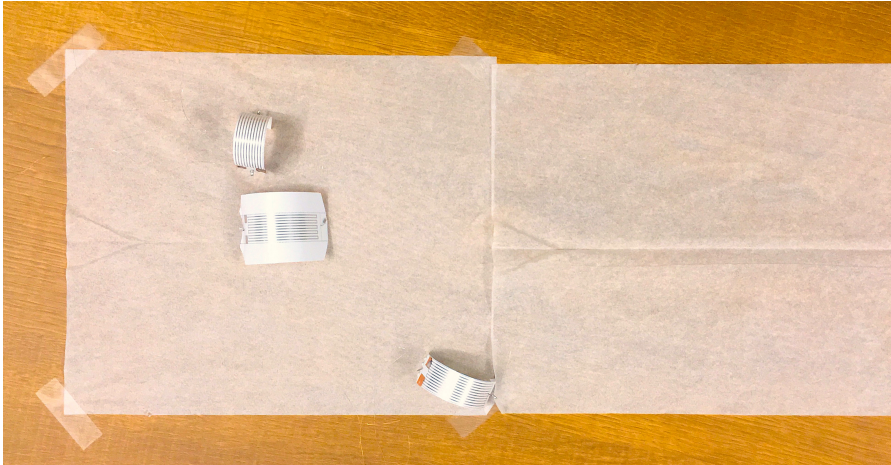


Figure 75: Three Paper Caterpillar robots in a race

of the Paper Caterpillar robot will even easier. And users can focus on the design of the gripping leg to have faster-crawling robots.

A.4 GCL SOCIAL INNOVATION PROJECT

My social innovation project is to develop human and environment-friendly technologies for learning and exploring. My research aim at lowering the entry bar to electronic circuits fabrication. We integrated electronic circuits into the 3D printing process with environment-friendly material (paper). Finally, we developed printable sensors, actuators, and mechanical functionality for designing disposable robots. In the future, these disposable robots could be used for exploring the environment, and after finishing their mission, they can be self-disposed back to the environment.

PUBLICATIONS

JOURNAL

- [1] **T. D. Ta**, F. Okuya, and Y. Kawahara. "Traveling Salesman Problem Based Auto-router for Designing LEDs Applications with Conductive Inkjet Printing." In: *The SICE Journal of Control, Measurement, and System Integration, Special Issue on Principles and Applications of Smart Sensing*. Jul. 2018. Vol. 11, No. 4, pp. 292–301, DOI: 10.9746/jcmsi.11.292.

INTERNATIONAL CONFERENCES

- [2] **T. D. Ta**, T. Umedachi, and Y. Kawahara. "Instant Inkjet Actuator and Sensor for Soft-bodied Crawling Robots." In: *Proc. of IEEE ICRA'19*. IEEE. 2019, To Appear.
- [3] **T. D. Ta**, T. Umedachi, and Y. Kawahara. "Design of Frictional 2D-Anisotropy Surface for Wriggle Locomotion of Printable Soft-bodied Robots." In: *Proc. of IEEE ICRA'18*. IEEE. 2018, pp. 6779–6785.
- [4] H. Oh, **T. D. Ta**, R. Suzuki, M. D. Gross, Y. Kawahara, and L. Yao. "PEP (3D Printed Electronic Papercrafts): An Integrated Approach for 3D Sculpting Paper-Based Electronic Devices." In: *Proc. of ACM CHI '18*. ACM. 2018, Paper No. 441. DOI: 10.1145/3173574.3174015.
- [5] **T. D. Ta**, F. Okuya, and Y. Kawahara. "LightTrace: Auto-router for Designing LED Based Applications with Conductive Inkjet Printing." In: *Proc. of ACM SCF '17*. ACM. 2017, Article No. 3. DOI: 10.1145/3083157.3083160.
- [6] **T. D. Ta**, M. Fukumoto, K. Narumi, S. Shino, Y. Kawahara, and T. Asami. "Interconnection and Double Layer for Flexible Electronic Circuit with Instant Inkjet Circuits." In: *Proc. of UbiComp '15*. ACM. 2015, pp. 181–190. DOI: 10.1145/2750858.2804276.

INTERNATIONAL POSTERS & DEMOS

- [7] Z. Chang, H. Kim, K. Kato, K. Saito, **T. D. Ta**, W. Jiang, K. Narumi, Y. Miyamoto, and Y. Kawahara. "Kirigami Keyboard: Inkjet Printable Paper Interface with Kirigami Structure Presenting Kinesthetic Feedback." In: *Proc. of ACM CHI '19*. ACM. 2019, Under Reviewing.
- [8] D. Lee, K. Saito, T. Umedachi, **T. D. Ta**, and Y. Kawahara. "Origami Robots with Flexible Circuit Sheets." In: *Proc. of UbiComp '18*. ACM. 2018, pp. 392–395. DOI: 10.1145/3267305.3267620.
- [9] **T. D. Ta**, K. Narumi, and Y. Kawahara. "Assistant Tools and Techniques for Conductive Inkjet Printing Technology." In: *UbiComp '15, GadgetShow Plus Demo*. 2015. Osaka, Japan.
- [10] **T. D. Ta**, and Y. Kawahara. "Implementation of via hole and multi-layered circuit with Instant Inkjet Circuit." In: *Microsoft Research Asia Faculty Summit, Asia Faculty Summit*. 2014. Beijing, China.

DOMESTIC WORKSHOPS

- [11] **T. D. Ta**, W. Wei, Q. M. Duong, Y. Kawahara, and T. Asami. "Tweaking Printer Driver for Improved Conductivity in Instant Inkjet Circuits." In: *IPSJ SIG Technical Report (Ubiquitous Computing System)*. 2014-UBI-42(2). 2014, pp. 1–4.

DOMESTIC GENERAL CONFERENCES

- [12] T. Umedachi, **T. D. Ta**, S. Masahiro, and Y. Kawahara. "Autonomous decentralized control on caterpillar-inspired robot developed with silver-nano ink and discrepancy function." In: *The 30th SICE Symposium of Autonomous Decentralized System*. 2019. To Appear.
- [13] M. Morita, T. Umedachi, **T. D. Ta**, K. Narumi, and Y. Kawahara. "Inchworm-inspired Robot that Locomotes on Steps and Vertical Walls." In: *IEICE Society Conference 2018*. 2018, A-1-11.

- [14] K. Narumi, T. Cheng, **T. D. Ta**, Y. Kawahara, and L. Yao. "Evaluation of Sticky Material which can Transfer Inkjet-printed Silver Nano-particle Ink." In: *IEICE Society Conference 2018*. 2018.
- [15] **T. D. Ta**, F. Okuya, and Y. Kawahara. "Traveling Salesman Problem Based Conductive Pattern Generation for Multiple Color LEDs Brightness Balance." In: *IEICE Society Conference 2017*. 2017, BS-7-24.
- [16] **T. D. Ta**, F. Okuya, and Y. Kawahara. "Traveling Salesman Problem Based Conductive Inkjet Printed Pattern Generation for Brightness Balancing of Multiple LEDs." In: *Proc. of The 79th National Convention of IPSJ*. 2017, 1E-03.
- [17] **T. D. Ta**, Y. Kawahara, and T. Asami. "Error Reduction in Capacitive Based Water Level Sensor for Paddy Field." In: *IEICE General Conference 2016*. 2016, B-18-16.
- [18] **T. D. Ta**, Y. Kawahara, and T. Asami. "Approach to Controlling of Smart Phone Based Virtual Reality Head-Mounted-Devices Through Touch Screen Indirectly." In: *IEICE General Conference 2015*. 2015, BS-3-11.
- [19] **T. D. Ta**, W. Wei, Q. M. Duong, Y. Kawahara, and T. Asami. "Modified Printer Driver to Improve Conductivity of Inkjet Printed Silver Ink Pattern by Overprinting." In: *IEICE General Conference 2014*. 2014, BS-1-46.

BIBLIOGRAPHY

- [1] Nadine Abboud, Martin Grötschel, and Thorsten Koch. “Mathematical methods for physical layout of printed circuit boards: an overview.” In: *OR Spectrum* 30.3 (June 2008), p. 453. DOI: [10.1007/s00291-007-0080-9](https://doi.org/10.1007/s00291-007-0080-9).
- [2] *Adafruit PN532 NFC/RFID Controller Shield*. 2017. URL: <https://www.adafruit.com/product/789>.
- [3] Sung-Hoon Ahn, Kyung-Tae Lee, Hyung-Jung Kim, Renzhe Wu, Ji-Soo Kim, and Sung-Hyuk Song. “Smart soft composite: An integrated 3D soft morphing structure using bend-twist coupling of anisotropic materials.” In: *International Journal of Precision Engineering and Manufacturing* 13.4 (Apr. 2012), pp. 631–634. DOI: [10.1007/s12541-012-0081-8](https://doi.org/10.1007/s12541-012-0081-8).
- [4] Morteza Amjadi and Metin Sitti. “High-Performance Multiresponsive Paper Actuators.” In: *ACS Nano* 10.11 (Nov. 2016), pp. 10202–10210. DOI: [10.1021/acs.nano.6b05545](https://doi.org/10.1021/acs.nano.6b05545).
- [5] Henrik A. Andersson, Anatoliy Manuilskiy, Stefan Haller, Magnus Hummelgård, Johan Sidén, Christine Hummelgård, Håkan Olin, and Hans-Erik Nilsson. “Assembling surface mounted components on ink-jet printed double sided paper circuit board.” In: *Nanotechnology* 25.9 (Mar. 2014), p. 094002. DOI: [10.1088/0957-4484/25/9/094002](https://doi.org/10.1088/0957-4484/25/9/094002).
- [6] David Applegate, Robert E. Bixby, Vašek Chvátal, and William J. Cook. *Concorded TSP Solver*. 2017. URL: <http://www.math.uwaterloo.ca/tsp/concorde/index.html>.
- [7] Hiroki Arazoe, Daigo Miyajima, Kouki Akaike, Fumito Araoka, Emiko Sato, Takaaki Hikima, Masuki Kawamoto, and Takuzo Aida. “An autonomous actuator driven by fluctuations in ambient humidity.” In: *Nature Materials* 15.10 (Oct. 2016), pp. 1084–1089. DOI: [10.1038/nmat4693](https://doi.org/10.1038/nmat4693).
- [8] *Arduino Capacitive Sensing Library*. 2017. URL: <https://playground.arduino.cc/Main/CapacitiveSensor>.
- [9] *Autodesk Fusion 360*. 2017. URL: <https://www.autodesk.com/products/fusion-360/>.

- [10] Moritz Bacher, Benjamin Hepp, Fabrizio Pece, Paul G. Kry, Bernd Bickel, Bernhard Thomaszewski, and Otmar Hilliges. "Dense: Computational design of customized deformable input devices." In: *Proceedings of the 2016 CHI Conference on Human Factors in Computing Systems (CHI '16)*. ACM, May 2016, pp. 3806–3816. DOI: [10.1145/2858036.2858354](https://doi.org/10.1145/2858036.2858354).
- [11] BareConductive. *BarePaint*. 2017. URL: www.bareconductive.com.
- [12] Salar Bayani, Rambod Rastegari, and Farzad Cheraghpour Samavati. "Design of hyper redundant robot using ball screw mechanism approach." In: *2015 IEEE International Conference on Advanced Intelligent Mechatronics (AIM)*. July 2015, pp. 1271–1276. DOI: [10.1109/AIM.2015.7222713](https://doi.org/10.1109/AIM.2015.7222713).
- [13] Marshall W. Bern and Ronald L. Graham. "The Shortest-Path Problem." In: *Scientific American* 260.1 (1989), pp. 84–89. DOI: [10.1038/scientificamerican0189-84](https://doi.org/10.1038/scientificamerican0189-84).
- [14] Yunteng Cao, Yilun Liu, Youlong Chen, Liangliang Zhu, Yuan Yan, and Xi Chen. "A novel slithering locomotion mechanism for a snake-like soft robot." In: *Journal of the Mechanics and Physics of Solids* 99.C (Feb. 2017), pp. 304–320. DOI: [10.1016/j.jmps.2016.11.019](https://doi.org/10.1016/j.jmps.2016.11.019).
- [15] Ting-Hai Chao, Yu-Chin Hsu, Jan-Ming Ho, and A. B. Kahng. "Zero skew clock routing with minimum wirelength." In: *IEEE Transactions on Circuits and Systems II: Analog and Digital Signal Processing* 39.11 (Nov. 1992), pp. 799–814. DOI: [10.1109/82.204128](https://doi.org/10.1109/82.204128).
- [16] ChemCubed. 2017. URL: <http://www.chemcubed.com/>.
- [17] Chibitronics. 2017. URL: <https://chibitronics.com/>.
- [18] Nicos Christofides. *Worst-case analysis of a new heuristic for the travelling salesman problem*. Tech. rep. Carnegie-Mellon University, Feb. 1976.
- [19] Circuit Marker. 2017. URL: <https://www.mpm.co.jp/electronic/eng/silver-nano/index.html>.
- [20] CircuitScribe. 2017. URL: <https://www.circuitscribe.com/>.
- [21] Edsger W. Dijkstra. "A note on two problems in connexion with graphs." In: *Numerische Mathematik* 1.1 (Dec. 1959), pp. 269–271.
- [22] EAGLE PCB design software. 2017. URL: <http://www.autodesk.com/products/eagle/overview>.

- [23] ENSON silver conductive glue HE-HE-6106B8. 2017. URL: <https://www.aliexpress.com/item/Silver-Conductive-0-2ML-Glue-Wire-Electrically-Paste-Adhesive-Paint-PCB-Repair-U/32767831630.html>.
- [24] Electroluminescent Kits. 2017. URL: http://www.gwent.org/gem_electroluminescent_kit.html.
- [25] Elephantech. 2017. URL: <https://www.elephantech.co.jp/en/>.
- [26] Tomasz Falat, Jan Felba, Andrzej Moscicki, and Janusz Borecki. "Nano-silver Inkjet Printed Interconnections through the Microvias for Flexible Electronics." In: *Proceedings of the 11th IEEE International Conference on Nanotechnology*. IEEE, Aug. 2011, pp. 473–477. DOI: [10.1109/NANO.2011.6144291](https://doi.org/10.1109/NANO.2011.6144291).
- [27] A. C. Finch, K. J. Mackenzie, G. J. Balsdon, and G. Symonds. "A method for gridless routing of printed circuit boards." In: *Proceedings of the 22nd ACM/IEEE Design Automation Conference (DAC '85)*. IEEE, June 1985, pp. 509–515. DOI: [10.1145/317825.317937](https://doi.org/10.1145/317825.317937).
- [28] Eric K. W. Gan, H. Y. Zheng, and G. C. Lim. "Laser Drilling of Micro-Vias in PCB Substrates." In: *Proceedings of 3rd Electronics Packaging Technology Conference (EPTC 2000)*. IEEE, Dec. 2000, pp. 321–326. DOI: [10.1109/EPTC.2000.906394](https://doi.org/10.1109/EPTC.2000.906394).
- [29] Xiutang Geng, Zhihua Chen, Wei Yang, Deqian Shi, and Kai Zhao. "Solving the traveling salesman problem based on an adaptive simulated annealing algorithm with greedy search." In: *Applied Soft Computing Journal* 11.4 (June 2011), pp. 3680–3689. DOI: [10.1016/j.asoc.2011.01.039](https://doi.org/10.1016/j.asoc.2011.01.039).
- [30] David E. Goldberg and Kalyanmoy Deb. "A Comparative Analysis of Selection Schemes Used in Genetic Algorithms." In: *Foundations of Genetic Algorithms*. Ed. by Gregory J. E. Rawlins. Vol. 1. Elsevier, Jan. 1991, pp. 69–93. DOI: [10.1016/B978-0-08-050684-5.50008-2](https://doi.org/10.1016/B978-0-08-050684-5.50008-2).
- [31] Nan-Wei Gong, Amit Zoran, and Joseph A. Paradiso. "Inkjet-printed conductive patterns for physical manipulation of audio signals." In: *Proceedings of the Adjunct Publication of the 26th Annual ACM Symposium on User Interface Software and Technology (UIST '13 Adjunct)*. ACM, Oct. 2013, pp. 13–14. DOI: [10.1145/2508468.2514932](https://doi.org/10.1145/2508468.2514932).

- [32] Nan-Wei Gong, Jürgen Steimle, Simon Olberding, Steve Hodges, Nicholas Edward Gillian, Yoshihiro Kawahara, and Joseph A. Paradiso. "PrintSense: a versatile sensing technique to support multimodal flexible surface interaction." In: *Proceedings of the 2014 CHI Conference on Human Factors in Computing Systems (CHI '14)*. ACM, Apr. 2014, pp. 1407–1410. DOI: [10.1145/2556288.2557173](https://doi.org/10.1145/2556288.2557173).
- [33] John J. Grefenstette, Rajeev Gopal, Brian J. Rosmaita, and Dirk Van Gucht. "Genetic algorithms for the traveling salesman problem." In: *Proceedings of the first International Conference on Genetic Algorithms and their Applications*. 1985, pp. 160–168.
- [34] Christian Greiner and Michael Schäfer. "Bio-inspired scale-like surface textures and their tribological properties." In: *Bioinspir. Biomim.* 10.4 (June 2015), p. 044001. DOI: [10.1088/1748-3190/10/4/044001](https://doi.org/10.1088/1748-3190/10/4/044001).
- [35] F. O. Hadlock. "A shortest path algorithm for grid graphs." In: *Networks* 7.4 (1977), pp. 323–334. DOI: [10.1002/net.3230070404](https://doi.org/10.1002/net.3230070404).
- [36] Mahiar M. Hamed, Victoria E. Campbell, Philipp Rothmund, Firat Güder, Dionysios C. Christodouleas, Jean-Francis Bloch, and George M. Whitesides. "Electrically Activated Paper Actuators." In: *Advanced Functional Materials* 26.15 (Apr. 2016), pp. 2446–2453. DOI: [10.1002/adfm.201505123](https://doi.org/10.1002/adfm.201505123).
- [37] *Harinacs Press*. Oct. 2014.
- [38] Felix Heibeck, Basheer Tome, Clark Della Silva, and Hiroshi Ishii. "uniMorph: Fabricating Thin Film Composites for Shape-Changing Interfaces." In: *Proceedings of the 28th Annual ACM Symposium on User Interface Software and Technology (UIST '15)*. ACM, Nov. 2015, pp. 233–242. DOI: [10.1145/2807442.2807472](https://doi.org/10.1145/2807442.2807472).
- [39] David W. Hightower. "A solution to line-routing problems on the continuous plane." In: *Proceedings of the 6th annual Design Automation Conference*. ACM, Jan. 1969, pp. 1–24. DOI: [10.1145/800260.809014](https://doi.org/10.1145/800260.809014).
- [40] Shigeo Hirose. *Biologically inspired robots: snake-like locomotors and manipulators*. Oxford University Press Oxford, 1993. DOI: [10.1017/S0263574700017264](https://doi.org/10.1017/S0263574700017264).
- [41] Shigeo Hirose and Makoto Mori. "Biologically Inspired Snake-like Robots." In: *2004 IEEE International Conference on Robotics and Biomimetics (ROBIO)*. IEEE, Aug. 2004, pp. 1–7. DOI: [10.1109/ROBIO.2004.1521742](https://doi.org/10.1109/ROBIO.2004.1521742).

- [42] Steve Hodges, Nicolas Villar, Nicholas Chen, Tushar Chugh, Jie Qi, Diana Nowacka, and Yoshihiro Kawahara. "Circuit stickers: peel-and-stick construction of interactive electronic prototypes." In: *Proceedings of the 2014 CHI Conference on Human Factors in Computing Systems (CHI '14)*. ACM, Apr. 2014, pp. 1743–1746. DOI: [10.1145/2556288.2557150](https://doi.org/10.1145/2556288.2557150).
- [43] Y Holovenko, M Antonov, L Kollo, and I Hussainova. "Friction studies of metal surfaces with various 3D printed patterns tested in dry sliding conditions." In: *Proc. Inst. Mech. Eng. Pt. J: J. Eng. Tribol.* 232.1 (Jan. 2018), pp. 43–53. DOI: [10.1177/1350650117738920](https://doi.org/10.1177/1350650117738920).
- [44] James K. Hopkins, Brent W. Spranklin, and Satyandra K. Gupta. "A survey of snake-inspired robot designs." In: *Bioinspiration & Biomimetics* 4.2 (June 2009), p. 021001. DOI: [10.1088/1748-3182/4/2/021001](https://doi.org/10.1088/1748-3182/4/2/021001).
- [45] Hozan. *Hozan DT-124*. 2017. URL: <http://www.hozan.co.jp/E/catalog/Measuring/DT124.html>.
- [46] David L. Hu, Jasmine Nirody, Terri Scott, and Michael J. Shelley. "The mechanics of slithering locomotion." In: *Proceedings of the National Academy of Science of the United States of America (PNAS)* 106.25 (June 2009), pp. 10081–10085. DOI: [10.1073/pnas.0812533106](https://doi.org/10.1073/pnas.0812533106).
- [47] Wenqi Hu, Guo Zhan Lum, Massimo Mastrangeli, and Metin Sitti. "Small-scale soft-bodied robot with multimodal locomotion." In: *Nature* 554.7690 (Feb. 2018), pp. 81–85. DOI: [10.1038/nature25443](https://doi.org/10.1038/nature25443).
- [48] Scott E. Hudson. "Printing Teddy Bears: A Technique for 3D Printing of Soft Interactive Objects." In: *Proceedings of the 2014 CHI Conference on Human Factors in Computing Systems (CHI '14)*. Toronto, Ontario, Canada: ACM, Apr. 2014, pp. 459–468. DOI: [10.1145/2556288.2557338](https://doi.org/10.1145/2556288.2557338).
- [49] Alexandra Ion, Johannes Frohnhofen, Ludwig Wall, Robert Kovacs, Mirela Alistar, Jack Lindsay, Pedro Lopes, Hsiang-Ting Chen, and Patrick Baudisch. "Metamaterial Mechanisms." In: *Proceedings of the 29th Annual Symposium on User Interface Software and Technology (UIST '16)*. ACM, Oct. 2016, pp. 529–539. DOI: [10.1145/2984511.2984540](https://doi.org/10.1145/2984511.2984540).
- [50] Norihiro Kamamichi, Masaki Yamakita, Kinji Asaka, and Zhi-Wei Luo. "A snake-like swimming robot using IPMC actuator/sensor." In: *2006 IEEE International Conference on*

- Robotics and Automation (ICRA)*. IEEE, pp. 1812–1817. DOI: [10 . 1109/ROBOT.2006.1641969](https://doi.org/10.1109/ROBOT.2006.1641969).
- [51] Çağdaş Karataş and Marco Gruteser. “Printing multi-key touch interfaces.” In: *Proceedings of the 2015 ACM International Joint Conference on Pervasive and Ubiquitous Computing (UbiComp '15)*. ACM, Sept. 2015, pp. 169–179. DOI: [10 . 1145 / 2750858.2804285](https://doi.org/10.1145/2750858.2804285).
- [52] Kunihiro Kato and Homei Miyashita. “Extension sticker: a method for transferring external touch input using a striped pattern sticker.” In: *Proceedings of the Adjunct Publication of the 27th Annual ACM Symposium on User Interface Software and Technology (UIST '14)*. ACM, Oct. 2014, pp. 59–60. DOI: [10 . 1145/2658779.2668032](https://doi.org/10.1145/2658779.2668032).
- [53] Yoshihiro Kawahara, Steve Hodges, Benjamin S. Cook, Cheng Zhang, and Gregory D. Abowd. “Instant inkjet circuits: lab-based inkjet printing to support rapid prototyping of UbiComp devices.” In: *Proceedings of the 2013 ACM International Joint Conference on Pervasive and Ubiquitous Computing (UbiComp '13)*. ACM, Sept. 2013, pp. 363–372. DOI: [10 . 1145 / 2493432.2493486](https://doi.org/10.1145/2493432.2493486).
- [54] Raisuddin Khan, M. Watanabe, and A. A. Shafie. “Kinematics Model of Snake Robot Considering Snake Scale.” In: *American Journal of Applied Sciences* 7.5 (May 2010), pp. 669–674. DOI: [10 . 3844/ajassp.2010.669.674](https://doi.org/10.3844/ajassp.2010.669.674).
- [55] Ryszard Kisiel, Artur Markowski, and Marcin Lubiak. “Conductive Adhesive Fillets for Double Sided PCBs.” In: *Proceedings of the 2nd International IEEE Conference on Polymers and Adhesives in Microelectronics and Photonics (POLYTRONIC 2002)*. IEEE, June 2002, pp. 13–16. DOI: [10 . 1109 / POLYTR . 2002 . 1020176](https://doi.org/10.1109/POLYTR.2002.1020176).
- [56] *LPKF ProConduct – Chemical Free Through Hole Plating*. 2015.
- [57] Ulrich Lauther. “A data structure for gridless routing.” In: *Proceedings of the 17th Design Automation Conference (DAC '80)*. ACM, June 1980, pp. 603–609. DOI: [10 . 1145/800139.804593](https://doi.org/10.1145/800139.804593).
- [58] David Ledo, Fraser Anderson, Ryan Schmidt, Lora Oehlberg, Saul Greenberg, and Tovi Grossman. “Pineal: Bringing Passive Objects to Life with Embedded Mobile Devices.” In: *Proceedings of the 2017 CHI Conference on Human Factors in Computing Systems (CHI '17)*. ACM, May 2017, pp. 2583–2593. DOI: [10 . 1145/3025453.3025652](https://doi.org/10.1145/3025453.3025652).

- [59] C. Y. Lee. "An Algorithm for Path Connections and Its Applications." In: *IRE Transactions on Electronic Computers* EC-10.3 (1961), pp. 346–365. DOI: [10.1109/TEC.1961.5219222](https://doi.org/10.1109/TEC.1961.5219222).
- [60] C. Y. Liu and W. H. Liao. "A Snake Robot Using Shape Memory Alloys." In: *2004 IEEE International Conference on Robotics and Biomimetics (ROBIO)*. Aug. 2004, pp. 601–605. DOI: [10.1109/ROBIO.2004.1521848](https://doi.org/10.1109/ROBIO.2004.1521848).
- [61] Joanne Lo, Cesar Torres, Isabel Yang, Jasper O’Leary, Danny Kaufman, Wilmot Li, Mira Dontcheva, and Eric Paulos. "Aesthetic Electronics: Designing, Sketching, and Fabricating Circuits Through Digital Exploration." In: *Proceedings of the 29th Annual Symposium on User Interface Software and Technology (UIST '16)*. Tokyo, Japan: ACM, Oct. 2016, pp. 665–676. DOI: [10.1145/2984511.2984579](https://doi.org/10.1145/2984511.2984579).
- [62] Ming Luo, Yixiao Pan, Erik H. Skorina, Weijia Tao, Fuchen Chen, Selim Ozel, and Cagdas D. Onal. "Slithering towards autonomy: a self-contained soft robotic snake platform with integrated curvature sensing." In: *Bioinspiration & Biomimetics* 10.5 (Sept. 2015), p. 055001. DOI: [10.1088/1748-3190/10/5/055001](https://doi.org/10.1088/1748-3190/10/5/055001).
- [63] Niranjana A. Malvadkar, Matthew J. Hancock, Koray Sekeroglu, Walter J. Dressick, and Melik C. Demirel. "An engineered anisotropic nanofilm with unidirectional wetting properties." In: *Nature Materials* 9.12 (Dec. 2010), pp. 1023–1028. DOI: [10.1038/nmat2864](https://doi.org/10.1038/nmat2864).
- [64] Andrew D Marchese, Robert K Katzschmann, and Daniela Rus. "A Recipe for Soft Fluidic Elastomer Robots." In: *Soft Robot* 2.1 (Mar. 2015), pp. 7–25. DOI: [10.1089/soro.2014.0022](https://doi.org/10.1089/soro.2014.0022).
- [65] Andrew D. Marchese, Cagdas D. Onal, and Daniela Rus. "Autonomous Soft Robotic Fish Capable of Escape Maneuvers Using Fluidic Elastomer Actuators." In: *Soft Robotics* 1.1 (Mar. 2014), pp. 75–87. DOI: [10.1089/soro.2013.0009](https://doi.org/10.1089/soro.2013.0009).
- [66] Ramses V. Martinez, Carina R. Fish, Xin Chen, and George M. Whitesides. "Elastomeric Origami: Programmable Paper-Elastomer Composites as Pneumatic Actuators." In: *Advanced Functional Materials* 22.7 (Apr. 2012), pp. 1376–1384. DOI: [10.1002/adfm.201102978](https://doi.org/10.1002/adfm.201102978).
- [67] Malcolm McCollough. *Abstracting Craft: The Practiced Digital Hand*. The MIT Press, 1996.

- [68] Mcor IRIS Printer. 2017. URL: <http://www.mcor technologies.com/3d-printers/iris/>.
- [69] Noel Menezes, Ashok Balivada, Satyamurthy Pullela, and Lawrence T. Pillage. "Skew reduction in clock trees using wire width optimization." In: *Proceedings of 1993 IEEE Custom Integrated Circuits Conference (CICC '93)*. IEEE, May 1993, pp. 961–964. DOI: [10.1109/CICC.1993.590684](https://doi.org/10.1109/CICC.1993.590684).
- [70] Koichi Mikami and Kinya Tabuchi. "A Computer Program for Optimal Routing of Printed Circuit Connectors." In: *Proceedings of IFIP Congress 1968*. 1968, pp. 1475–1478.
- [71] Mitsubishi Paper Mills Inc. *Silver Nano Particle Inks Special Media*. 2013. URL: http://www.k-mpm.com/agnanoen/agnano_media.html.
- [72] Mitsubishi Paper Mills Inc. *Silver Nano Particle Inks*. 2013. URL: http://www.k-mpm.com/agnanoen/agnano_ink.html.
- [73] Mod Podge. 2017. URL: <https://plaidonline.com/brands/mod-podge>.
- [74] Kenichi Nakahara, Koya Narumi, Ryuma Niiyama, and Yoshihiro Kawahara. "Electric phase-change actuator with inkjet printed flexible circuit for printable and integrated robot prototyping." In: *Proceedings of the 2017 IEEE International Conference on Robotics and Automation (ICRA)*. May 2017, pp. 1856–1863. DOI: [10.1109/ICRA.2017.7989217](https://doi.org/10.1109/ICRA.2017.7989217).
- [75] Koya Narumi, Steve Hodges, and Yoshihiro Kawahara. "ConductAR: an augmented reality based tool for iterative design of conductive ink circuits." In: *Proceedings of the 2015 ACM International Joint Conference on Pervasive and Ubiquitous Computing (UbiComp '15)*. ACM, Sept. 2015, pp. 791–800. DOI: [10.1145/2750858.2804267](https://doi.org/10.1145/2750858.2804267).
- [76] Ryuma Niiyama, Daniela Rus, and Sangbae Kim. "Pouch Motors: Printable/inflatable soft actuators for robotics." In: *2014 IEEE International Conference on Robotics and Automation (ICRA)*. IEEE, May 2014, pp. 6332–6337. DOI: [10.1109/ICRA.2014.6907793](https://doi.org/10.1109/ICRA.2014.6907793).
- [77] Marek Obitko. *Introduction to Genetic Algorithms*. 1998. URL: <http://www.obitko.com/tutorials/genetic-algorithms/crossover-mutation.php>.

- [78] Hyunjoon Oh, Tung D. Ta, Ryo Suzuki, Mark D Gross, Yoshihiro Kawahara, and Lining Yao. "PEP (3D Printed Electronic Papercrafts): An Integrated Approach for 3D Sculpting Paper-Based Electronic Devices." In: *Proceedings of the 2018 CHI Conference on Human Factors in Computing Systems*. ACM, Apr. 2018, Paper No. 441. DOI: [10.1145/3173574.3174015](https://doi.org/10.1145/3173574.3174015).
- [79] Simon Olberding, Michael Wessely, and Jürgen Steimle. "PrintScreen: Fabricating Highly Customizable Thin-film Touch-Displays." In: *Proceedings of the 27th Annual ACM Symposium on User Interface Software and Technology (UIST '14)*. ACM, Oct. 2014, pp. 281–290. DOI: [10.1145/2642918.2647413](https://doi.org/10.1145/2642918.2647413).
- [80] Simon Olberding, Sergio Soto Ortega, Klaus Hildebrandt, and Jürgen Steimle. "Foldio: Digital Fabrication of Interactive and Shape-Changing Objects With Foldable Printed Electronics." In: *Proceedings of the 28th Annual ACM Symposium on User Interface Software and Technology (UIST '15)*. Charlotte, NC, USA: ACM, Nov. 2015, pp. 223–232. DOI: [10.1145/2807442.2807494](https://doi.org/10.1145/2807442.2807494).
- [81] Cagdas D. Onal and Daniela Rus. "A modular approach to soft robots." In: *2012 4th IEEE RAS EMBS International Conference on Biomedical Robotics and Biomechatronics (BioRob)*. June 2012, pp. 1038–1045. DOI: [10.1109/BioRob.2012.6290290](https://doi.org/10.1109/BioRob.2012.6290290).
- [82] Cagdas D. Onal and Daniela Rus. "Autonomous undulatory serpentine locomotion utilizing body dynamics of a fluidic soft robot." In: *Bioinspiration & Biomimetics* 8.2 (June 2013), pp. 026003–026010. DOI: [10.1088/1748-3182/8/2/026003](https://doi.org/10.1088/1748-3182/8/2/026003).
- [83] Christos H. Papadimitriou. "The Euclidean travelling salesman problem is NP-complete." In: *Theoretical Computer Science* 4.3 (June 1977), pp. 237–244. DOI: [10.1016/0304-3975\(77\)90012-3](https://doi.org/10.1016/0304-3975(77)90012-3).
- [84] *Paper Speakers*. 2017. URL: <http://highlowtech.org/?p=1372>.
- [85] Topon Kumar Paul. *Traveling Salesman Problem by Genetic Algorithm*. 2005. URL: <http://www.iba.t.u-tokyo.ac.jp/english/Online/TSP/Method.html>.
- [86] Huaishu Peng, Jennifer Mankoff, Scott E Hudson, and James McCann. "A Layered Fabric 3D Printer for Soft Interactive Objects." In: *Proceedings of the 2015 CHI Conference on Human Factors in Computing Systems (CHI '15)*. ACM, Apr. 2015, pp. 1789–1798. DOI: [10.1145/2702123.2702327](https://doi.org/10.1145/2702123.2702327).

- [87] Varun Perumal and Daniel Wigdor. "Foldem: Heterogeneous object fabrication via selective ablation of multi-material sheets." In: *Proceedings of the 2016 CHI Conference on Human Factors in Computing Systems (CHI '16)*. ACM, May 2016, pp. 5765–5775. DOI: [10.1145/2858036.2858135](https://doi.org/10.1145/2858036.2858135).
- [88] Jean-Yves Potvin. "Genetic algorithms for the traveling salesman problem." In: *Annals of Operations Research* 63.3 (June 1996), pp. 337–370. DOI: [10.1007/BF02125403](https://doi.org/10.1007/BF02125403).
- [89] Jie Qi. *Pu Gong Ying Tu (Dandelion Painting)*. 2012. URL: <http://technologjie.com/pu-gong-ying-tu-dandelion-painting/>.
- [90] Jie Qi and Leah Buechley. "Electronic Popables: Exploring Paper-Based Computing through an Interactive Pop-Up Book." In: *Proceedings of the fourth international conference on Tangible, embedded, and embodied interaction (TEI '10)*. ACM, Jan. 2010, pp. 121–128. DOI: [10.1145/1709886.1709909](https://doi.org/10.1145/1709886.1709909).
- [91] Raf Ramakers, Kashyap Todi, and Kris Luyten. "PaperPulse: An Integrated Approach for Embedding Electronics in Paper Designs." In: *Proceedings of the 2015 CHI Conference on Human Factors in Computing Systems (CHI '15)*. ACM, Apr. 2015, pp. 2457–2466. DOI: [10.1145/2702123.2702487](https://doi.org/10.1145/2702123.2702487).
- [92] P. Ramanathan and K. G. Shin. "A clock distribution scheme for nonsymmetric VLSI circuits." In: *1989 IEEE International Conference on Computer-Aided Design. Digest of Technical Papers*. Nov. 1989, pp. 398–401. DOI: [10.1109/ICCAD.1989.76978](https://doi.org/10.1109/ICCAD.1989.76978).
- [93] Michael L. Rivera, Melissa Moukperian, Daniel Ashbrook, Jennifer Mankoff, and Scott E. Hudson. "Stretching the Bounds of 3D Printing with Embedded Textiles." In: *Proceedings of the 2017 CHI Conference on Human Factors in Computing Systems (CHI '17)*. ACM, May 2017, pp. 497–508. DOI: [10.1145/3025453.3025460](https://doi.org/10.1145/3025453.3025460).
- [94] Daniela Rus and Michael T Tolley. "Design, fabrication and control of soft robots." In: *Nature* 521.7553 (May 2015), pp. 467–475.
- [95] *SMD LED Product Datasheet LTST-C150CKT*. DS-22-98-002. LITE-ON Optoelectronics. Jan. 2006. URL: http://optoelectronics.liteon.com/upload/download/DS-22-98-0002/S_110_LTST-C150CKT.pdf.

- [96] *SMD LED Product Datasheet LTST-C150TBKT*. DS22-2000-026. LITE-ON Optoelectronics. Jan. 2010. URL: [http://optoelectronics.liteon.com/upload/download/DS22-2000-026/LTST-C150TBKT\(0630\).pdf](http://optoelectronics.liteon.com/upload/download/DS22-2000-026/LTST-C150TBKT(0630).pdf).
- [97] Erol Sancaktar and Lan Bai. "Electrically Conductive Epoxy Adhesives." In: *Polymers* 3.1 (Feb. 2011), pp. 427–466. DOI: [10.3390/polym3010427](https://doi.org/10.3390/polym3010427).
- [98] Masashi Sato, Masakazu Fukaya, and Tetsuya Iwasaki. "Serpentine locomotion with robotic snakes." In: *IEEE Control Systems* 22.1 (Feb. 2002), pp. 64–81. DOI: [10.1109/37.980248](https://doi.org/10.1109/37.980248).
- [99] Greg Saul, Cheng Xu, and Mark D. Gross. "Interactive Paper Devices: End-user Design & Fabrication." In: *Proceedings of the Fourth International Conference on Tangible, Embedded, and Embodied Interaction (TEI '10)*. Cambridge, Massachusetts, USA: ACM, 2010, pp. 205–212. DOI: [10.1145/1709886.1709924](https://doi.org/10.1145/1709886.1709924).
- [100] Valkyrie Savage, Xiaohan Zhang, and Björn Hartmann. "Midas: Fabricating Custom Capacitive Touch Sensors to Prototype Interactive Objects." In: *Proceedings of the 25th Annual ACM Symposium on User Interface Software and Technology (UIST '12)*. Cambridge, Massachusetts, USA: ACM, Oct. 2012, pp. 579–588. DOI: [10.1145/2380116.2380189](https://doi.org/10.1145/2380116.2380189).
- [101] W. L. Schiele, T. Krüger, K. M. Just, and F. H. Kirsch. "A Gridless Router for Industrial Design Rules." In: *Proceedings of the 27th ACM/IEEE Design Automation Conference (DAC '90)*. Orlando, Florida, USA: ACM, 1990, pp. 626–631. DOI: [10.1145/123186.123422](https://doi.org/10.1145/123186.123422).
- [102] Martin Schmitz, Mohammadreza Khalilbeigi, Matthias Balwierz, Roman Lissermann, Max Mühlhäuser, and Jürgen Steimle. "Capricate: A Fabrication Pipeline to Design and 3D Print Capacitive Touch Sensors for Interactive Objects." In: *Proceedings of the 28th Annual ACM Symposium on User Interface Software and Technology (UIST '15)*. Charlotte, NC, USA: ACM, Nov. 2015, pp. 253–258. DOI: [10.1145/2807442.2807503](https://doi.org/10.1145/2807442.2807503).
- [103] Martin Schmitz, Jürgen Steimle, Jochen Huber, Niloofar Dezfouli, and Max Mühlhäuser. "Flexibles: Deformation-Aware 3D-Printed Tangibles for Capacitive Touchscreens." In: *Proceedings of the 2017 CHI Conference on Human Factors in Computing Systems (CHI '17)*. Denver, Colorado, USA: ACM, May 2017, pp. 1001–1014. DOI: [10.1145/3025453.3025663](https://doi.org/10.1145/3025453.3025663).

- [104] Seiko Epson Corp. *Epson PX-S160T*. 2018. URL: <https://www.epson.jp/support/portal/used/px-s160t.htm>.
- [105] Hiroki Shigemune, Shingo Maeda, Yusuke Hara, Uori Koike, and Shuji Hashimoto. "Kirigami robot: Making paper robot using desktop cutting plotter and inkjet printer." In: *2015 IEEE/RSJ International Conference on Intelligent Robots and Systems (IROS)*. Sept. 2015, pp. 1091–1096. DOI: [10.1109/IROS.2015.7353506](https://doi.org/10.1109/IROS.2015.7353506).
- [106] Beomjune Shin, Jonghyun Ha, Minhee Lee, Keunhwan Park, Gee Ho Park, Tae Hyun Choi, Kyu-Jin Cho, and Ho-Young Kim. "Hygrobot: A self-locomotive ratcheted actuator powered by environmental humidity." In: *Science Robotics* 3.14 (Jan. 2018), eaar2629. DOI: [10.1126/scirobotics.aar2629](https://doi.org/10.1126/scirobotics.aar2629).
- [107] Michael Shorter, Jon Rogers, and John McGhee. "Enhancing everyday paper interactions with paper circuits." In: *Proceedings of the 2014 Conference on Designing Interactive Systems (DIS '14)*. ACM, June 2014, pp. 39–42. DOI: [10.1145/2598510.2598584](https://doi.org/10.1145/2598510.2598584).
- [108] Sankaran Sivaramakrishnan, Perq-Jon Chia, Yee-Chia Yeo, Lay-Lay Chua, and Peter K-H Ho. "Controlled insulator-to-metal transformation in printable polymer composites with nanometal clusters." In: *Nature Materials* 6.2 (Feb. 2007), pp. 149–155. DOI: [10.1038/nmat1806](https://doi.org/10.1038/nmat1806).
- [109] *Slice of Light*. 2015. URL: <https://agic.cc/projects/1?locale=en>.
- [110] TEXIO. *TEXIO Regulated DC Power Supply PA36-3B*. 2017. URL: <http://www.texio.co.jp/en/product/detail/5>.
- [111] Tung D. Ta, Fuminori Okuya, and Yoshihiro Kawahara. "Light-Trace: auto-router for designing LED based applications with conductive inkjet printing." In: *Proceedings of the 1st Annual ACM Symposium on Computational Fabrication*. ACM, June 2017, Article No. 3. DOI: [10.1145/3083157.3083160](https://doi.org/10.1145/3083157.3083160).
- [112] Tung D. Ta, Fuminori Okuya, and Yoshihiro Kawahara. "Traveling Salesman Problem Based Auto-Router for Designing LEDs Applications with Conductive Inkjet Printing." In: *SICE Journal of Control, Measurement, and System Integration* 11.4 (2018), pp. 292–301. DOI: [10.9746/jcmsi.11.292](https://doi.org/10.9746/jcmsi.11.292).

- [113] Tung D. Ta, Takuya Umedachi, and Yoshihiro Kawahara. "Design of Frictional 2D-Anisotropy Surface for Wriggle Locomotion of Printable Soft-bodied Robots." In: *2018 IEEE International Conference on Robotics and Automation (IEEE ICRA'18)*. Brisbane, Australia: IEEE, May 2018, pp. 6779–6785. DOI: [10.1109/ICRA.2018.8463177](https://doi.org/10.1109/ICRA.2018.8463177).
- [114] Tung D. Ta, Takuya Umedachi, and Yoshihiro Kawahara. "Instant Inkjet Actuators and Sensors for Soft-bodied Crawling Robots." In: *2019 IEEE International Conference on Robotics and Automation (IEEE ICRA'19)*. IEEE, May 2019, To Appear.
- [115] Tung Ta, Masaaki Fukumoto, Koya Narumi, Shigeki Shino, Yoshihiro Kawahara, and Tohru Asami. "Interconnection and double layer for flexible electronic circuit with instant inkjet circuits." In: *Proceedings of the 2015 ACM International Joint Conference on Pervasive and Ubiquitous Computing (UbiComp '15)*. ACM, Sept. 2015, pp. 181–190. DOI: [10.1145/2750858.2804276](https://doi.org/10.1145/2750858.2804276).
- [116] Ren-Song Tsay. "An exact zero-skew clock routing algorithm." In: *IEEE Transaction of Computer-Aided Design of Integrated Circuits and Systems* 12.2 (Feb. 1993), pp. 242–249. DOI: [10.1109/43.205004](https://doi.org/10.1109/43.205004).
- [117] Takahiro Tsujii, Naoya Koizumi, and Takeshi Naemura. "Inkantatory paper: dynamically color-changing prints with multiple functional inks." In: *Proceedings of the Adjunct Publication of the 27th Annual ACM Symposium on User Interface Software and Technology (UIST '14)*. ACM, Oct. 2014, pp. 39–40. DOI: <http://dx.doi.org/10.1145/2658779.2659103>.
- [118] Takuya Umedachi and Barry A. Trimmer. "Design of a 3D-printed soft robot with posture and steering control." In: *2014 IEEE International Conference on Robotics and Automation (ICRA)*. May 2014, pp. 2874–2879. DOI: [10.1109/ICRA.2014.6907272](https://doi.org/10.1109/ICRA.2014.6907272).
- [119] Takuya Umedachi, Vishesh Vikas, and Barry A. Trimmer. "Highly deformable 3-D printed soft robot generating inching and crawling locomotions with variable friction legs." In: *2013 IEEE/RSJ International Conference on Intelligent Robots and Systems (IROS)*. IEEE, Nov. 2013, pp. 4590–4595. DOI: [10.1109/IROS.2013.6697016](https://doi.org/10.1109/IROS.2013.6697016).
- [120] Nobuyuki Umetani and Ryan Schmidt. "SurfCuit: Surface-Mounted Circuits on 3D Prints." In: *IEEE Computer Graphics and Applications* 37.3 (Apr. 2017), pp. 52–60. DOI: [10.1109/MCG.2017.40](https://doi.org/10.1109/MCG.2017.40).

- [121] Nirzaree Vadgama and Jürgen Steimle. “Flexy: Shape-Customizable, Single-Layer, Inkjet Printable Patterns for 1D and 2D Flex Sensing.” In: *Proceedings of the Eleventh International Conference on Tangible, Embedded, and Embodied Interaction (TEI '17)*. Yokohama, Japan: ACM, Mar. 2017, pp. 153–162. DOI: [10.1145/3024969.3024989](https://doi.org/10.1145/3024969.3024989).
- [122] Alexander D. Valentine, Travis A. Busbee, John William Boley, Jordan R. Raney, Alex Chortos, Arda Kotikian, John Daniel Berrigan, Michael F. Durstock, and Jennifer A. Lewis. “Hybrid 3D Printing of Soft Electronics.” In: *Advanced Materials* (Sept. 2017), p. 1703817. DOI: [10.1002/adma.201703817](https://doi.org/10.1002/adma.201703817).
- [123] Nicolas Villar, James Scott, and Steve Hodges. “Prototyping with Microsoft .NET Gadgeteer.” In: *Proceedings of the Fifth International Conference on Tangible, Embedded, and Embodied Interaction (TEI '11)*. ACM, Jan. 2011, pp. 377–380. DOI: [10.1145/1935701.1935790](https://doi.org/10.1145/1935701.1935790).
- [124] *Voxel8*. 2017. URL: <http://www.voxel8.com/>.
- [125] Guanyun Wang, Tingyu Cheng, Youngwook Do, Humphrey Yang, Ye Tao, Jianzhe Gu, Byoungkwon An, and Lining Yao. “Printed Paper Actuator: A Low-cost Reversible Actuation and Sensing Method for Shape Changing Interfaces.” In: *Proceedings of the 2018 CHI Conference on Human Factors in Computing Systems (CHI '18)*. ACM, 2018, 569:1–569:12. DOI: [10.1145/3173574.3174143](https://doi.org/10.1145/3173574.3174143).
- [126] Michael Wehner, Ryan L. Truby, Daniel J. Fitzgerald, Bobak Mosadegh, George M. Whitesides, Jennifer A. Lewis, and Robert J. Wood. “An integrated design and fabrication strategy for entirely soft, autonomous robots.” In: *Nature* 536:7617 (Aug. 2016), pp. 451–455. DOI: [10.1038/nature19100](https://doi.org/10.1038/nature19100).
- [127] Chris Woodford. *Thermostats*. 2018. URL: <https://www.explainthatstuff.com/thermostats.html>.
- [128] Lining Yao, Jifei Ou, Chin-Yi Cheng, Helene Steiner, Wen Wang, Guanyun Wang, and Hiroshi Ishii. “bioLogic: Natto Cells As Nanoactuators for Shape Changing Interfaces.” In: *Proceedings of the 33rd Annual ACM Conference on Human Factors in Computing Systems (CHI '15)*. CHI '15. Seoul, Republic of Korea: ACM, Apr. 2015, pp. 1–10. DOI: [10.1145/2702123.2702611](https://doi.org/10.1145/2702123.2702611).

- [129] Ming-Yao Yen, Ming-Hung Chiang, Hsu-Hsin Tai, Hsien-Chang Chen, Kwok-Wai Yee, Crystal Li, Elie Najjar, Mark Lefebvre, and Betty Xie. "Advanced Thin Copper Electroplating Process for HDI Microvia Filling Application." In: *Proceedings of the 8th International Microsystems, Packaging, Assembly and Circuits Technology Conference (IMPACT)*. IEEE, Oct. 2013, pp. 245–250. DOI: [10.1109/IMPACT.2013.6706698](https://doi.org/10.1109/IMPACT.2013.6706698).
- [130] Takenobu Yoshiki, Shigeki Shino, and Kazuhisa Kobayashi. "Process for preparing conductive material." Pat. Sept. 2011.
- [131] Mei Zhen and Aravinthan D. T. Samuel. "*C. elegans* locomotion: small circuits, complex functions." In: *Current Opinion in Neurobiology* 33 (Aug. 2015), pp. 117–126. DOI: [10.1016/j.conb.2015.03.009](https://doi.org/10.1016/j.conb.2015.03.009).
- [132] Liangliang Zhu, Yunteng Cao, Yilun Liu, Zhe Yang, and Xi Chen. "Architectures of soft robotic locomotion enabled by simple mechanical principles." In: *Soft Matter* 13.25 (June 2017), pp. 4441–4456. DOI: [10.1039/c7sm00636e](https://doi.org/10.1039/c7sm00636e).